UNIVERSITAT POLITÈCNICA DE VALÈNCIA

Programa de Doctorado en Infraestructuras de Transporte y Territorio

PhD Thesis

EFFECTS OF HIGH TEMPERATURES IN THE PHYSICAL, MECHANICAL, AND DRILLING FEATURES OF PRADA LIMESTONE

Author:

Víctor Martínez Ibáñez

Advisors:

Dr Roberto Tomás Jover

Dr Carlos Hidalgo Signes

Valencia, May 2021

Table of Contents

Acknowledgements xi
Abstract xv
Resumen xvii
Resum xix
Chapter 1. Introduction 1
1.1. Presentation 1
1.2. Background 3
1.3. Research objectives 5
1.4. Hypotheses 6
1.4.1. Effects of high temperatures in the physical and mechanical properties of Prada limestone 6
1.4.2. Thermal damage mechanisms on pyrite-bearing limestones 6
1.4.3. Thermal effects on the drilling performance of rocks 6
1.4.4. Prediction of mechanical and drillability parameters using correlations 7
1.5. Rationale 7
1.6. Methodology 8

1.6.1. Rock samples preparation....8
1.6.2. Testing plan....9
1.6.3. Thermal treatment on samples....10
1.6.4. Laboratory tests....11
1.7. Scientific publications presented in this PhD thesis and its relationship with the research topic....15
1.8. Dissertation structure....18
Chapter 2. Micro and macro-structural effects of high temperatures in Prada limestone: key factors for future fire-intervention protocols in Tres Ponts Tunnel (Spain).21
Abstract....22
Keywords....22
2.1. Introduction....23
2.2. Materials and methods....26
2.2.1. Sample preparation....26
2.2.2. Heating and cooling procedures....27
2.2.3. Laboratory tests....28
2.2.4. Statistical analysis....29
2.3. Results....29
2.3.1. Geochemical and microstructural characterisation....29
2.3.2. Variation of physical properties....32
2.3.3. Variation of mechanical properties....34
2.3.4. Influence of sample position on the variability of physical and mechanical properties....37
2.3.5. Correlations between physical and mechanical properties....38
2.4. Discussion....39
2.5. Conclusions....46
Chapter 3. Temperature-induced explosive behaviour and thermo-chemical damage on pyrite-bearing limestones: causes and mechanisms....49
Abstract....50
Keywords....50
3.1. Introduction....51
3.2. Materials and methods....52

3.3. Results 56
3.3.1. Chemical, mineralogical, petrographic and microstructural characterisation 56
3.3.2. Variation of physical properties by thermal treatment 61
3.4. Discussion 67
3.5. Conclusions 71
Chapter 4. Thermal effects on the drilling performance of a limestone: relationships with physical and mechanical properties 75
Abstract 76
Keywords 76
4.1. Introduction 77
4.2. Materials and methods 79
4.3. Results 85
4.3.1. Effects of temperature on the micro- and macro-structural features 85
4.3.2. Drillability variation with temperature 86
4.3.3. Correlations between parameters 89
4.4. Discussion 95
4.5. Conclusions 98
Chapter 5. Discussion 101
5.1. Research Question Q1 101
5.2. Research Question Q2 104
5.3. Research Question Q3 106
5.4. Research Question Q4 107
Chapter 6. Conclusions 111
6.1. Effects of high temperatures on the physical and mechanical properties of Prada limestone 111
6.2. Thermal damage mechanisms on pyrite-bearing Prada limestones 112
6.3. Thermal effects on the drilling performance of Prada limestone 113
6.4. Prediction of mechanical parameters in Prada limestone using correlations 114
6.5. Future lines 115
References 117

List of Figures

Figure 1.1. Location of the Tres Ponts Tunnel in the Congost de Tresponts area. Image modified from Institut Cartogràfic i Geològic de Catalunya (www.icc.cat). 2

Figure 1.2. Core samples taken from horizontal survey boreholes (a) and cut samples with a slenderness of 2.5 (b). Slight changes in the grey tone and very thin veins of calcite observed in the tested samples (c). Heating of the samples at 105ºC for the determination of the intact rock properties (d). 9

Figure 1.3. Methodological scheme of the laboratory tests and the number of cylindrical and irregular samples tested to accomplish the first and second research stages. The tests performed at each temperature (T) are: unit weight (UW); open porosity (OP); ultrasound wave velocity (US); uniaxial compression strength (UCS); microstructure by scanning electron microscopy (SEM); pore distribution by mercury intrusion porosity (MIP); Siever's J drillability value (SJ); and brittleness value (S_{20}). 10

Figure 1.4. Intact samples placed in the furnace (a); screenshot from PicoLog data register showing temperatures from thermocouples in the furnace (b); samples after being heated exhibiting cracking, splitting and explosive behaviour (c); samples cooled at a rapid rate by water immersion (d). 12

Figure 1.5. Rock samples were prepared and placed in holders (a). SEM image of texture and fissures of a sample after thermally treated at 600 ºC (an increase of 1000x was used) (b). 13

Figure 1.6. Piezoelectric sensors (a) were covered with a shear wave transmitting gel (b). 14

Figure 1.7. Detail of a sample thermally treated at 400 ºC with longitudinal and lateral gauges installed before (a) and after failure at 250 kN (b). 14

Figure 2.1. Laboratory tests and the number of cylindrical and irregular samples tested at each temperature (T) to determine: unit weight (UW); open porosity (OP); ultrasound wave velocity (US); uniaxial compression strength (UCS); microstructure by scanning electron microscopy (SEM); and pore distribution by mercury intrusion porosity (MIP).....27

Figure 2.2. SEM images showing pores (p) and fissures (f) for different temperatures and cooling methods. An increase of 2000x was used for all figures. 31

Figure 2.3. Cumulative mercury intrusion and pore size distribution for samples heated at different temperatures and cooled by (a) air; and (b) water immersion. 32

Figure 2.4. Open porosity (normalised values) for air and water-cooled samples. 33

Figure 2.5. Volume and dry total weight (normalised values) for air and water-cooled samples. 34

Figure 2.6. P- (a) and S-wave (b) velocities (normalised values) for air and water-cooled samples. 34

Figure 2.7. UCS values for air and water-cooled samples. 35

Figure 2.8. Stress-strain curves for samples heated at different temperatures and then air- (a) or water-cooled (b).....35

Figure 2.9. Elastic modulus (a) and Poisson's ratio (b) values for air and water-cooled samples. 36

Figure 2.10. Dynamic elastic modulus (normalised values) for air and water-cooled samples. 36

Figure 2.11. Simple regression analysis of P-wave velocity and sample position. 38

Figure 2.12. Correlation between UCS and normalised values of volume variation (a), open porosity (b) and P-wave velocity (c) using potential functions. 42

Figure 2.13. Correlations between static elastic modulus and normalised: (a) volume variation; (b) open porosity; and (c) P-wave velocity. 43

Figure 3.1. Cylindrical cores from Prada limestones before thermal treatment. Samples with a dark grey texture are identified in the figure. 53

Figure 3.2. Optical microphotographs of intact Prada limestone. (A) Grain-supported texture composed of bioclasts, angular and sub-angular grains of quartz and sub-rounded grains of iron sulphides. Details of (B) molluscs, (C) foraminifera and (D)

red algae. (E-F) Bioclasts and micritic matrix cut by calcite veins. Microphotographs were taken under (A-E) parallel-nicols and (F) crossed-nicols 57

Figure 3.3. Images from scanning electron microscope of a dark grey sample (a) and a light grey sample (b) before thermally treated, showing different content of pyrites, quartz, and fissure distribution. Well-formed pyrite framboids appeared in dark grey samples heated to 105 ºC (c). Pyrite framboids showed uncomplete when heated to 500 ºC (d) 58

Figure 3.4. TG-DTA-DSC curves for the dark limestone (a) and MS curves for H_2O (b), SO_2 (c) and CO_2 (d) 60

Figure 3.5. Cumulative mercury intrusion and pore size distribution curves of dark (a) and light grey (b) textures before thermally-treated. 60

Figure 3.6. (a) Dark samples exploded or fractured when heated at 400 ºC. (b) Detail of the fragment embedded in the furnace chamber due to the violence of the event shown in (a). Dark samples before (c) and after (d) heating at 400ºC. Note the protection grid used to preserve the furnace. Dark and light grey cores before (e) and after (f) heating at 500 ºC. Note that only dark cores exploded, and their fragments overturned and damaged the surrounding light grey samples and the furnace chamber. A new set of dark samples before (g) and after (h) heating at 500 ºC using the protection grid. The temperatures were being registered using thermocouples when one sample exploded. 62

Figure 3.7. Variation of normalised (a) open porosity; (b) P-wave velocity; and (c) S-wave velocity of dark and light grey samples after heat treatment. Reference values used for the normalization are given in Table 3.4. 65

Figure 3.8. Compared images of the flat and polished face from one sample heated to 105 ºC (a), and later to 400 ºC (b), and from one sample heated to 105 ºC (c), and later to 500 ºC (d). A transition from dark grey and bluish tones to light red and increased lightness with temperature could be observed. Colour variation with temperature, expressed using CIELAB variables (e) 66

Figure 4.1. Location of the Tres Ponts Tunnel in the Congost de Tresponts area. Borehole coordinates are expressed in meters in the UTM 31N/ETRS 89 reference system. Image modified from Institut Cartogràfic i Geològic de Catalunya (www.icc.cat). 80

Figure 4.2. Changes in the grey tone and very thin veins of calcite observed in the intact samples. A dark grey texture was separated from the rest of samples and does not form part of this research. 81

Figure 4.3. Optical microphotographs of intact Prada limestone. Bioclasts and micritic matrix cut by calcite veins (a). Detail of molluscs (b). Microphotographs were taken under parallel-nicols. 82

Figure 4.4. Methodological scheme of the laboratory tests and the number of samples tested. The tests performed at each temperature (T) are: Siever's J drillability value (SJ); brittleness value (S_{20}); and microstructure by scanning electron microscopy (SEM). 83

Figure 4.5. Laboratory equipment for Sievers' J-miniature drill test (a) and miniature drill bit (b) used in this research. 84

Figure 4.6. Crushing of the aggregate in the mortar (a) and determination of the percentage of material passing through the 11.2 mm sieve (b). 85

Figure 4.7. SEM images showing fissures (f) for samples heated to 400 °C (a) and 600 °C (b) and then water-cooled. An increase of 2000× was used for all figures. 86

Figure 4.8. Samples before (a) and after (b) heated to 600 °C. Effects of temperature involve visible fissure growth, splitting, and cracking. 86

Figure 4.9. Variation with temperature of Siever's J miniature drillability SJ (a), brittleness S_{20} (b), and drilling rate index (c) for air- and water-cooled samples. Categories have been represented for Sj and S_{20} according to Dahl et al. (Dahl et al. 2012), and for DRI according to Bruland (2000). 88

Figure 4.10. Correlations between variation of SJ and: (a) UCS; (b) elastic modulus; and (c) Poisson's ratio for air- and water-cooled samples. 92

Figure 4.11. Correlations between variation of S_{20} and: (a) UCS; (b) elastic modulus; and (c) Poisson's ratio for air- and water-cooled samples. 94

Figure 4.12. Correlations between variation of SJ and (a) P- wave velocity; and (b) S-wave velocity for air- and water-cooled samples. 94

Figure 4.13. Correlations between variation of S_{20} and P- (a) and S-wave velocity (b) for air- and water-cooled samples. 95

List of tables

Table 2.1. Mineral element content of Prada limestone at different temperatures..... 30

Table 2.2. Mineral composition of Prada limestone before and after heating. 30

Table 2.3. Reference values for samples forming Prada limestone, heated at 105 ºC. . 33

Table 2.4. Results from ANOVA analysis. 37

Table 2.5. Coefficients of determination (R^2) for simple regression curves studied to predict UCS and elastic modulus (E) from normalised (N) physical parameters (volume, open porosity, and P-wave velocity). 40

Table 2.6. UCS values from laboratory tests and predicted from normalised values (N) of physical parameters for each temperature, based on potential functions. Residuals have been also represented. 40

Table 2.7. Elastic modulus (E) values from laboratory tests and predicted from normalised values (N) of physical parameters for each temperature, based on potential functions except for P-wave velocity, where exponential functions enabled the best predictions. Residuals have been also represented. 41

Table 3.1. Number of samples tested for each group (dark or light grey). All samples were first heated at 105 ºC, then treated at 300, 400 and 500 ºC. Additional 4 cylindrical samples from each group were used to determine UCS for the intact rock (at 105ºC). 53

Table 3.2. Compounds registered on light and dark grey samples. 58

Table 3.3. Number of samples that showed different grades of damage for each temperature. 63

Table 3.4. Reference values for dark and light grey samples forming Prada limestone, heated at 105 ºC. 63

Table 4.1. Reference values for intact samples heated at 105 °C. 82

Table 4.2. Variation with temperature of Siever's J miniature drillability test (SJ), brittleness test (S_{20}), and drilling rate index (DRI) final value and for air- and water-cooled samples. 87

Table 4.3. Coefficients of determination (R^2) for simple regression curves studied to predict SJ and S_{20} from mechanical and normalised (N) physical parameters (UCS, elastic modulus, Poisson's ratio, P- and S-wave velocities). 89

Table 4.4. Average residuals and relative errors for predictions of SJ and S_{20} from physical and mechanical variables at the highest temperatures (400, 500, and 600 °C). 90

Acknowledgements

First and foremost, I would like to express my sincere gratitude to my advisors Dr Roberto Tomás and Dr Carlos Hidalgo. Thank you for your guidance, contribution of ideas, instructive revisions, and for your availability at any time. Your humanity and working example have become a goal to me. I also want to thank coordinator Dr Eugenio Pellicer for his valuable advice from the very beginning of my career. Dr Tiago Miranda, for his guidance during my stay in ISISE. I would also extend my gratitude to María Elvira Garrido for her valuable contribution as a co-author in the articles presented in this PhD, and for her priceless guidance and support throughout these years. Dr David Benavente for guiding me in the microstructural characterisation and thermal analysis of the pyrite-bearing limestones, and for his contribution as a co-author in the related article. José Bernardo Serón for his excellent advice from the very beginning of my universitary studies and academic career. Dr Isidro Cantarino and Dr Miguel Ángel Carrión for welcoming me into their research team, and for their continuous guidance. Dr Rafael Cortés, Dr José Luis Denia, Manuel Ángel Morilla, Carlos Alonso, Salvatore Di Biase, Aniello Basco, and Asunta Cabanes for their help on laboratory and administrative tasks, support, and inspiring comments. Dr Julio Company Rodríguez from the Universitat Politècnica de València and Professor Juan Carlos Cañaveras from the University of Alicante, for their valuable help on mineralogical and petrographic description of rock, respectively. Isidro Sánchez Martín from the Departamento de Ingeniería Civil of the Universidad de Alicante for his kind help on MIP analyses. I also want to thank Jordi Calvís, Verònica Monné, and Daniel Cuit from KREUM SA for their confidence during all these years in Kreum SA and for getting me involved in the Tres Ponts Tunnel project. Kreum SA, Ayesa SA, Infraestructures.cat, and the Lleida regional road authority (Servei Territorial de Carreteres de Lleida, Generalitat de Catalunya) for providing rock samples. Finally, I want to express my deep gratitude to my parents for their relentless support and personal sacrifice. I wish to specially thank Marian, for her generosity and support (life is even brighter since I walk it by your side).

This research was partially supported by the Spanish Government [grant number RTI2018-099052-B-I00], also the Vice-Rectorate of Research and Knowledge Transfer at the University of Alicante through projects UAUSTI19-25 and UAUSTI20-20, and by the Departamento de Ingeniería del Terreno at the Universitat Politècnica de València.

To Marian

Abstract

This research is focused on Prada limestone, a lower Cretaceous formation located in the Catalan south Pyrenean zone (Spain). Rock samples were taken from boreholes drilled during the design stage of the Tres Ponts Tunnel. The work presented here explores different aspects related to the thermal behaviour of Prada limestone and the derived consequences on the Tres Ponts Tunnel. Firstly, this work reports the variation in the textural, physical, and mechanical properties of Prada limestone after being heated at temperatures of between 105 and 600 ºC and then cooled at a slow rate or by quenching and determines key temperatures and cooling methods that would most affect stability in case of a fire in the Tres Ponts Tunnel. Secondly, this research focuses on the causes and mechanisms involved in the explosive behaviour and release of sulphurous gas observed on a dark grey fraction of samples from Prada limestone. Implications of such dark grey samples are critical in underground infrastructure and mining engineering works, as the explosive potential of that sample represents risk of mass fracturing and dramatic strength decay. Moreover, the sulphurous gas released has harmful health effects and may form acid compounds that corrode materials, shorten their durability, and increase maintenance costs. Later, this work determines if thermal treatment on Prada limestone has a significant effect on improving its drillability. Understanding the variation in the drilling performance of the thermally treated Prada limestone would help improve the efficiency of mechanical excavation means. Finally, some correlations are proposed to indirectly determine the strength, deformational, and drillability features of Prada limestone after being thermally treated from simple, quick and non-destructive tests.

Resumen

Esta investigación se centra en la caliza de Prada, una formación del Cretácico inferior ubicada en la zona sur pirenaica de Cataluña (España). Se tomaron muestras de roca de sondeos perforados durante la etapa de diseño del túnel de Tres Ponts. El trabajo aquí presentado explora diferentes aspectos relacionados con el comportamiento térmico de la caliza de Prada y las consecuencias derivadas en el túnel de Tres Ponts. En primer lugar, este trabajo describe la variación en las propiedades texturales, físicas y mecánicas de la caliza de Prada después de ser sometida a temperaturas de entre 105 y 600 ºC, y luego enfriada a un ritmo lento o mediante templado, y determina las temperaturas clave y los métodos de enfriamiento que afectan más la estabilidad en caso de incendio en el túnel de Tres Ponts. En segundo lugar, esta investigación se centra en las causas y mecanismos implicados en el comportamiento explosivo y la liberación de gas sulfuroso observado en una fracción gris oscuro de muestras de caliza de Prada. Las implicaciones de tales muestras de color gris oscuro son críticas en infraestructuras subterráneas y en minería, ya que el potencial explosivo de esas muestras conlleva el riesgo de fracturación masiva y de disminución brusca en la resistencia. Además, el gas sulfuroso liberado tiene efectos nocivos sobre la salud de las personas y el potencial de formar compuestos ácidos que corroen los materiales, acortando su durabilidad y aumentando los costes de mantenimiento. Posteriormente, este trabajo determina si el tratamiento térmico sobre la caliza de Prada tiene un efecto significativo en facilitar su perforabilidad. Comprender la variación en el rendimiento de perforación de la caliza de Prada tratada térmicamente ayudaría a mejorar la eficiencia de los medios mecánicos de excavación. Finalmente, se proponen algunas correlaciones para determinar indirectamente las características de resistencia, deformación y perforabilidad de la caliza de Prada tras ser tratada térmicamente, a partir de pruebas simples, rápidas y no destructivas.

Resum

Aquesta investigació es centra en la calcària de Prada, una formació del Cretaci inferior situada a la zona sud pirinenca de Catalunya (Espanya). Es van prendre mostres de roca de sondejos perforats durant l'etapa de disseny del túnel de Tres Ponts. El treball aquí presentat explora diferents aspectes relacionats amb el comportament tèrmic de la calcària de Prada i les conseqüències derivades al túnel de Tres Ponts. En primer lloc, aquest treball descriu la variació en les propietats texturals, físiques i mecàniques de la calcària de Prada després de ser tractada a temperatures d'entre 105 i 600 ºC, i després refredada a un ritme lent o ràpid, i determina les temperatures clau i els mètodes de refredament que afecten més l'estabilitat en cas d'incendi al túnel de Tres Ponts. En segon lloc, aquesta investigació es centra en les causes i mecanismes implicats en el comportament explosiu i l'alliberament de gas sulfurós observat en una fracció gris fosc de mostres de calcària de Prada. Les implicacions de tals mostres de color gris fosc són crítiques en infraestructures subterrànies i en mineria, ja que el potencial explosiu d'aquestes mostres comporta el risc de fracturació massiva i de disminució brusca en la resistència. A més, el gas sulfurós alliberat té efectes nocius sobre la salut de les persones i el potencial de formar compostos àcids que corroeixen els materials, retallant la seua durabilitat i augmentant els costos de manteniment. Posteriorment, aquest treball determina si el tractament tèrmic sobre la calcària de Prada té un efecte significatiu en facilitar la seua perforabilitat. Comprendre la variació en el rendiment de perforació de la calcària de Prada tractada tèrmicament ajudaria a millorar l'eficiència dels mitjans mecànics d'excavació. Finalment, es proposen algunes correlacions per determinar indirectament les característiques de resistència, deformació i perforabilitat de la calcària de Prada després de ser tractada tèrmicament, a partir de proves simples, ràpides i no destructives.

Chapter 1. Introduction

1.1. Presentation

This PhD thesis is focused on the Prada limestone, a lower Cretaceous formation located in the Serra de Prada, a range of mountains in the Catalan south Pyrenean zone (Spain). The stratigraphy of the Prada formation has been widely studied in a narrowing of the Segre river as it passes next to the Serra de Prada, in an area known as the Congost de Tres Ponts (García Senz 2002). Rock samples studied in this PhD thesis were taken from two horizontal survey boreholes drilled during the design stage of the Tres Ponts Tunnel, which is planned to be entirely excavated in Prada limestone in the municipalities of Organyà and Fígols, close to Congost de Tres Ponts. The tunnel will be oriented north-south on the C-13 road, measures 1273 m in length, and its maximum depth from ground surface will be of 285 m. Figure 1.1. shows the area of study including the Serra de Prada, Congost de Tres Ponts, and the Tres Ponts Tunnel.

The work presented here explores different aspects related to the thermal behaviour of Prada limestone and the derived consequences on the Tres Ponts Tunnel. Firstly, this work reports the variation in the textural, physical, and mechanical properties of Prada limestone after being heated and determines key temperatures and cooling methods that would most affect stability in case of a fire in the Tres Ponts Tunnel. Secondly, this research focuses on the causes and mechanisms involved in the explosive behaviour and

release of sulphurous gas observed on a dark grey fraction of samples from Prada limestone. This work then determines if thermal treatment of Prada limestone has a significant effect on improving its drillability. Finally, to help make initial decisions if the Tres Ponts Tunnel is affected by a fire, several correlations using quick, simple, and non-destructive tests are proposed to predict key strength, deformational, and drillability features of Prada limestone after being thermally treated.

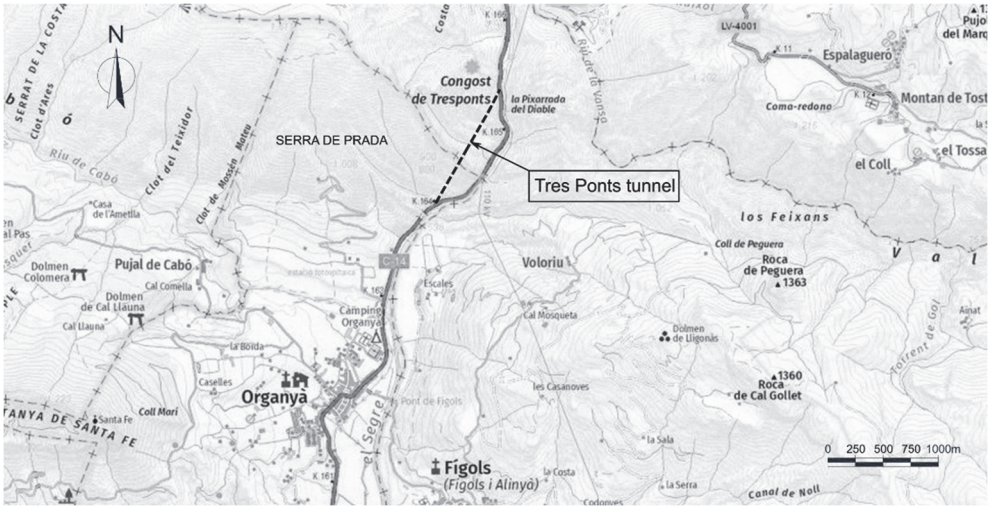

Figure 1.1. Location of the Tres Ponts Tunnel in the Congost de Tresponts area. Image modified from Institut Cartogràfic i Geològic de Catalunya (www.icc.cat).

This PhD thesis is presented as a compendium of publications in accordance with the regulations for doctorate studies at the Universitat Politècnica de València, approved by the Governing Council in its session of 15 December, 2011, published in the Official Bulletin of the Universitat Politècnica de València No. 54, modified by agreement of the Doctoral Commission on 9 April, 2013, and approved by the Governing Council on 25 April, 2013. In accordance with the above, a post-print (author's version) of the published articles, and a general discussion of the results are included as individual chapters.

The PhD presented here opts for an International Doctorate Mention, as conditions have been accomplished according to Spanish regulation 'Real Decreto 99/2011, de 28 de enero, por el que se regulan las enseñanzas oficiales de doctorado'. During the training period for the doctorate, the student completed a visit of three months outside Spain in the Institute for Sustainability and Innovation in Structural Engineering (ISISE, www.isise.net), in the Universidade do Minho, Guimaraes (Portugal). Given the existing mobility restrictions due to Covid-19, the stay was made in a virtual modality in accordance with the provision of the Permanent Commission of the Doctoral School of the Universitat Politècnica de València of 20 May, 2020. The visit and activities have been

endorsed by the supervisor, Dr Tiago Filipe Silva Miranda, and approved by the Academic Committee of the Doctorate Programme. Research carried out during the stay focused on the study of the variation in the drillability of Prada limestone after being subjected to high temperatures, and its relationship with the variation in the physical and mechanical properties of the material. This research resulted in an article included as Chapter 4 in this PhD thesis. The required language requirement has been also accomplished as the complete document is presented in a language for scientific communication in the field of knowledge (i.e. English), other than Spanish or another official language in Spain.

1.2. Background

Fires in road tunnels are not rare events and although most are relatively small, such fires can become more serious events. Dramatic tunnel fires that occurred in the Mont Blanc (France-Italy 1999), the Tauern (Austria 1999), and the Gotthard (Switzerland 2001) gave rise to international regulations and recommendations. Various factors that fully condition fire safety were identified (PIARC 2016): tunnel design; location of the tunnel; geometry of the road; monitoring; technical standard of the vehicles; traffic regulation; and speed limits or driving culture. Huge heat rates are released in pool fires of burnable liquids and in fully developed fires in the cargo of heavy goods vehicles (ITA 2004). Therefore, temperatures measured in the ceiling and wall surfaces of a tunnel can reach 1400 ºC in the early stages of a fire, and persist for hours (Keski-Rahkonen et al. 1986; PIARC 1999). Such elevated heat release may cause dramatic cracking and spalling in the concrete lining (Prochazka and Peskova 2008; Bamonte et al. 2016) and heat transfer through the lining to the rock mass according to existing bi-layer models (Ferreira et al. 2014). Rock mass is quickly exposed to high temperature in a tunnel fire if there is no lining, or a thin layer of shotcrete exists. Smith and Pells (2008) studied the effects of high temperatures in tunnels excavated from sandstone in Australia and observed a decrease in uniaxial compression strength and elastic modulus. Substantial explosive spalling events were also reported at relatively low temperatures (little more than 100 ºC) with real fire and in a real accident (Smith and Pells 2009). Studies on tunnels in igneous rocks in Sweden (Nordlund et al. 2014) identified key temperatures causing severe variations in the mineralogical, physical, and mechanical properties of rocks, and a strong dependence of micro-cracking on the reduction in compression strength. Nevertheless, case-studies focused on the thermal performance of rock in which tunnels are made are still scarce.

The study of the variation in textural, mineralogical, physical, and mechanical properties of limestones, not specifically focused on tunnel engineering, points to heating as a cause for decay in rock integrity. A decrease in strength limit due to microcracking at relatively low temperatures (up to 250 ºC) was described for a limestone from Anstrude (France) (Lion et al. 2005). In Yavuz et al. (2010) marked decreases in bulk density, ultrasound wave velocities, and effective porosity were registered at 400ºC. Andriani and

Germinario (2014) observed a clear reduction in uniaxial compressive strength (UCS) from 500 ºC on calcareous and dolomitic rocks from Apulia in Italy. Temperatures above 600 ºC usually mark a dramatic decline in UCS (Mao et al. 2009; Sengun 2014). Zhang et al. (2017b) indicated that from 500 to 600 °C the maximum strength slowly decreased, while peak strain continuously increased, elastic modulus declined quickly, and Poisson's ratio dropped. Zhang and Lv (2020) found a strong relationship between the mineral content and limestone properties under the effect of temperature for limestones from Shandong Province (China). Brotóns et al. (2013) reported a greater variation in the physical and mechanical features of carbonate rocks when cooled by water immersion. Thus, existing research points to heating and cooling methods as causes for decay in rock integrity. Magnitude and key temperatures strongly depend on the physical and mineralogical properties of the limestone considered.

Different mechanisms control property variation in limestones, temperature, heating/cooling rate, and mineral and textural composition play key roles. Cooling at a high rate (quenching) provokes tensile stresses that result in crack formation (Mallet et al. 2014), causing a reduction in resistance and deformational properties and an increase in permeability (Kumari et al. 2018) even at temperatures below 300 ºC (Kim et al. 2014). This effect can also be observed when using high local heating rates (i.e. greater than 5 ºC/s) (Nordlund et al. 2014; Rossi et al. 2018). Low heating rates cause thermal damage in carbonate rocks, and this is linked to the anisotropic expansion of calcite, since local thermal stress concentrations occur between mineral particles that lead to microcracking (Sippel et al. 2007; Yavuz et al. 2010). Mismatches in thermal expansion coefficients between mineral particles lead to local thermal stress concentrations that increase microcracking (Liu and Xu 2013; Zhang et al. 2017b; Villarraga et al. 2018; Yang et al. 2019). The loss of constitution water leads to the destruction of the mineral lattice, causing increased porosity and rock expansion (Ranjith et al. 2012). Finally, thermo-chemical damage involves some specific chemical reactions in limestones, such as the thermal decomposition of calcite that starts at 500 ºC, exhibits the highest decomposition rate at around 700 ºC, and is complete near 900 ºC. The presence of pyrites may be common in limestones with organic content (Berner 1985) and heating pyrite-bearing natural materials produce severe problems in various productive processes. For example, oxidation of pyrites is one of the main sources of SO_2 emission from various industrial activities, such as cement production (Hansen et al. 2003; Cheng et al. 2014), coal conversion (Seehra and Jagadeesh 1981), and power production (Lv et al. 2015). Pyrite oxidation is harmful to the corrosion kinetics of metallic engineered components (Verron et al. 2019). It is also a destabilising factor in different industrial processes such ceramic production, where sulphur emissions produce defects in the final product (Gómez-Tena et al. 2014). Oxidation of pyrites is an exothermic reaction that destabilises the fabrication process of explosive products (Xu et al. 2015). A research gap exists in the thermo-chemical damage in pyrite-bearing limestones, and that could explain the explosive behaviour and release of sulphurous gas in a fraction of the samples from Prada limestone when heated.

There is little research on the effects of high temperatures and cooling methods in the drilling performance of rocks. Rossi et al. (2018) explored the effects of using a flame jet to achieve high local heating rates, and determined a severe decay of 30% in rock strength for temperatures up to 600 ºC. Rossi et al. (2020) studied a combined thermo-mechanical drilling (CTMD) technique and stated that thermal treatment of rocks causes extensive thermally induced cracks in the rocks, which significantly enhances the penetration performance of the cutting tool. Jamali et al. (2019) used high powered laser technology to decrease rock strength, drilling resistance, and fracture toughness. Existing research is still scarce on the drilling performance of thermally treated rocks, even when that would help improve the efficiency of mechanical excavation.

Understanding the thermal effects on physical, mechanical, and drilling properties of limestones would enable predicting the resistance and deformational parameters from other physical properties, whose determination is quicker and easier. Existing research is mostly centred on correlating properties for intact rocks, and few authors have focused on thermally treated samples. Thus, multivariate regression analysis enabled the prediction of thermal changes in strength from density, porosity, thermal expansion coefficients, and ultrasonic waves on sandstones (Gautam et al. 2016). Predictions for the same type of rock improved when using artificial neural network and adaptive neuro-fuzzy inference systems (Sirdesai et al. 2017).

1.3. Research objectives

The main objective of this PhD thesis is to explore the effects of high temperatures on Prada limestone. In view of the research context, some questions shall be raised in relation to the thermal effects on Prada limestone and the consequences derived for the Tres Ponts Tunnel.

Q1. What are the micro and macro-structural effects of high temperatures in Prada limestone?

Q2. What mechanisms are behind thermal damage and explosive behaviour registered in a dark fraction of the Prada limestones?

Q3. Could temperature and cooling methods improve the drilling of Prada limestone?

Q4. Do significant correlations exist between properties in the thermally treated Prada limestone? Would correlations be useful to indirectly predict the final values of strength, elasticity, and drillability after a fire in the Tres Ponts Tunnel affecting Prada limestone?

To give an appropriate response to such questions, the following specific objectives are established for this PhD thesis:

1. Review the existing literature regarding the effects on the stability of rock masses derived from fires in tunnels, and the effects of high temperatures on the physical, mechanical, and drilling properties of limestones.

2. Determine key temperatures that play an important role in the thermo-mechanical behaviour of Prada limestone, and evaluate the influence of cooling methods.
3. Explore the mechanisms involved in the thermo-chemical damage of a dark grey fraction of the Prada limestone.
4. Determine key temperatures and the influence of cooling methods on the drillability of Prada limestone.
5. Propose correlations between properties following from simple, quick, and non-destructive tests on thermally treated Prada limestone that are useful to indirectly predict final values of strength, elasticity, and drillability.

1.4. Hypotheses

1.4.1. Effects of high temperatures in the physical and mechanical properties of Prada limestone

According to existing research, high temperatures are expected to induce a marked decay in the physical and mechanical properties of Prada limestone. Pore growth and micro-cracking are supposed to develop during the heating process, resulting in a generalised cracking of the samples at the maximum target temperature (600 ºC). Key temperatures are expected to be critical for severe variation in physical and mechanical features. Differences between cooling methods are also expected to be relevant: samples cooled by quenching would show a more severe variation of mechanical and physical properties. Consequently, it is expected that micro-cracking will be greater in water-cooled samples than in those cooled in air.

1.4.2. Thermal damage mechanisms on pyrite-bearing limestones

The presence of pyrites may be common in limestones with organic content (Berner 1985) and providing them a dark tone. Such pyrites could experiment thermal oxidation when limestones are heated. Thermal oxidation of pyrites is a well-known process that involves the release of SO_2 and the formation of Fe_2O_3 (hematite) at temperatures above 400 ºC (Hong and Fegley 1997; Gazulla et al. 2009). Such gas releases might increase the pore pressure and could explain, at least in part, the explosive behaviour of dark grey samples of Prada limestone, and the sulphurous gas released into the atmosphere.

1.4.3. Thermal effects on the drilling performance of rocks

Rock properties influencing drillability have been discussed by various authors for non-thermally treated rocks. The strength of the intact rock exhibits a strong influence in the efficiency of the drilling process (Altindag 2010; Yarali and Soyer 2011, 2013; Yaşar et al. 2011). Elastic and plastic deformations also occur in the drilling (Jamshidi et al. 2013; Ataei et al. 2015; Su et al. 2016). Therefore, it is expected that strength and elastic parameters exhibit significant variations when samples are thermally treated, and so the

drilling performance of rock would vary with temperature. In addition, the Drilling Rate Index (DRI) is related to ultrasound wave velocity, and this is a parameter closely linked with the texture (porosity and fissures) in the rock. The thermal treatment of Prada limestone is supposed to result in pore growth and micro-crack progression, and that would lead to an increase in the ability to indent represented by Sievers' J-value (SJ), and a drop in the strength of rock to withstand crushing represented by brittleness (S_{20}). For these reasons, an improvement in the drillability of Prada limestone is expected in terms of the DRI, and its variation is estimated to be more significant for the water-cooled samples.

1.4.4. Prediction of mechanical and drillability parameters using correlations

Previous research is mainly focused on carbonate rocks at room temperature. Estimations of rock strength from predictors such density, porosity, and ultrasound wave velocity have been proposed by many authors using simple regression analysis (Yasar and Erdogan 2004; Baykasoğlu et al. 2008; Dehghan et al. 2010; Yagiz et al. 2012; Aboutaleb et al. 2018). Research on strength and drillability prediction from temperature and physical properties (such as density, porosity, thermal expansion coefficients, and ultrasound ultrasonic waves) for thermally-treated rocks is scarce and the existing research is mainly focused in sandstones (Gautam et al. 2016). For these reasons, correlations are expected to determine the variation in strength, deformational and drillability features with temperature, from other physical and mechanical properties of Prada limestone.

1.5. Rationale

The reasoning that underpins this research follows:

This study aims to provide an in-depth insight into the changes induced by temperature and cooling methods on the chemical, textural, physical, and mechanical properties of Prada limestone. The obtained results will enable an evaluation of the degree of damage in this limestone if affected by fire in the Tres Ponts Tunnel – and the subsequent determination of the new physical and mechanical properties of this rock after a fire event.

Investigations describing thermo-chemical damage on pyrite-bearing rocks are scarce, although this type of rock is common in civil and mining engineering works. The practical relevance in underground engineering works is critical since high temperatures can lead to strength decay in the rock. In addition, sulphurous gases released into the atmosphere can harm the health (ATSDR 1998) of people involved in tunnel construction works, users, or emergency intervention teams in case of a fire event. Additionally, sulphurous gases can react with other atmospheric chemical elements forming acid compounds (sulphurous or sulphuric acid) that corrode metals, concrete, limestone, and other materials (Kumar and Imam 2013), shortening the service life of underground structures and increasing maintenance costs.

Modern mechanical excavation strongly depends on the efficiency of the means involved in order to optimise investment costs, and so, understanding the variation in the drilling performance of thermally treated Prada limestone will help improve the efficiency of mechanical excavation means.

Different phases can be defined in the development of a fire inside a tunnel that are important for the integrity of the structure (CETU 2005): a) the structural stability that fully conditions the time available for evacuation; b) the safety conditions during post-fire inspection; and c) the scope of the repair and the time during which traffic will be disrupted after a fire. The use of correlations will enable predicting the strength and deformational features from other parameters whose determination is quicker and easier. Additionally, correlations enable easily performed and quick evaluations of drillability based on basic geomechanical parameters to support the Tres Ponts Tunnel excavations. This research fills a gap on correlating parameters for thermally treated limestones.

1.6. Methodology

The materials and methods used in this thesis are briefly described in this section. For the sake of completeness, the reader is referred to the methodology sections of the articles that form the compendium of this thesis, included in Chapters 2, 3 and 4.

1.6.1. Rock samples preparation

Samples (Figure 1.2a) were taken from two horizontal survey boreholes drilled during the design stage of the Tres Ponts Tunnel, which is planned to be entirely excavated from Prada limestone. Boreholes 1 and 2 were in the southern and northern mouths of the tunnel and reached prospection depths of 65.30 m and 91.45 m, respectively. Borehole cores with a diameter of 65 mm were cut with a slenderness of 2.5 (Figure 1.2b) to perform uniaxial compressive strength (UCS) tests according to International Society for Rock Mechanics (ISRM) standards (Fairhurst and Hudson 1987). Samples were very homogeneous and only presented slight changes in the grey tone and very thin veins of calcite (Figure 1.2c). A temperature of 105 ºC was initially applied to remove moisture from the rock samples for the determination of the intact rock properties (Figure 1.2d).

Figure 1.2. Core samples taken from horizontal survey boreholes (a) and cut samples with a slenderness of 2.5 (b). Slight changes in the grey tone and very thin veins of calcite observed in the tested samples (c). Heating of the samples at 105ºC for the determination of the intact rock properties (d).

1.6.2. Testing plan

The testing plan followed to meet the objectives established for this PhD thesis is structured into three stages. The first stage aims to identify key temperatures for rock weakening and the influence of the cooling method on the variation in the geomechanical properties of rock. Thus, a total of 55 cylindrical samples of 63 mm in diameter and a slenderness of 2.5 were randomly selected from both horizontal boreholes to perform ultrasound and uniaxial compression strength tests. In addition, 55 irregular fragments were selected to determine unit weight and open porosity variation with temperature, mercury intrusion porosimetry tests, and scanning electron microscopy observations. Samples were then heated at 105, 200, 300, 400, 500 and 600 ºC, and then cooled using one of two methods to simulate different modes of fire intervention: air-cooling or water-cooling. Variations in chemical composition and microstructure, physical (open porosity, volume, dry total weight, P- and S-wave velocities), and mechanical (uniaxial compressive strength, elastic modulus, and Poisson's ratio) properties were then analysed. To study the influence of the natural location of the samples (borehole and

depth) on property variation, statistical techniques (ANOVA and linear regression) were used. Finally, a set of correlations were proposed to indirectly determine the variation in strength and elasticity from physical properties.

Second stage explores the variation in the drilling performance of Prada limestone with temperature. Therefore, the Sievers J drillability test and the brittleness S_{20} tests were performed on samples thermally treated in the first stage. The variation in Drilling Rate Index (DRI) with temperature was obtained from Siever's J (SJ) and S_{20} values at each temperature. The results were compared and correlated with that from physical and mechanical properties at various temperatures obtained in the first stage. Figure 1.3 illustrates the number of laboratory tests performed for each temperature and the number of samples used for the first and second stages in this research methodology.

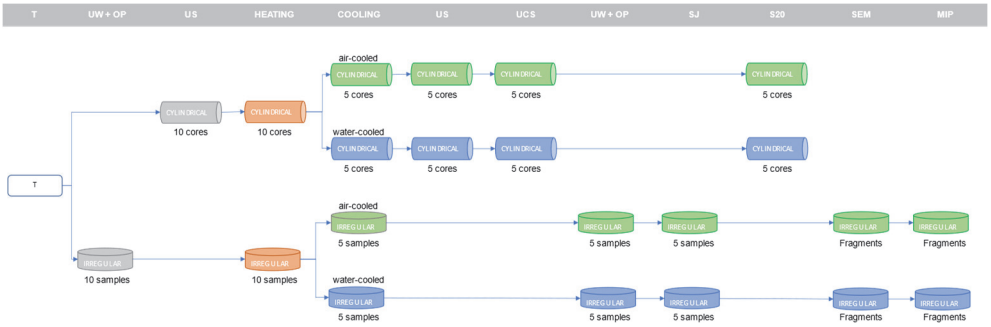

Figure 1.3. Methodological scheme of the laboratory tests and the number of cylindrical and irregular samples tested to accomplish the first and second research stages. The tests performed at each temperature (T) are: unit weight (UW); open porosity (OP); ultrasound wave velocity (US); uniaxial compression strength (UCS); microstructure by scanning electron microscopy (SEM); pore distribution by mercury intrusion porosity (MIP); Siever's J drillability value (SJ); and brittleness value (S_{20}).

Finally, the third stage is focused on exploring the causes and mechanisms of the explosive behaviour of a dark grey fraction of the Prada formation. For this aim, the variation in physical properties (colour, open porosity, P and S-wave velocities) at temperatures of 105, 300, 400 and 500 ºC is studied. Moreover, chemical, mineralogical, and microstructure changes are determined; and special attention is paid to the thermal reactions involved and the gases released.

1.6.3. Thermal treatment on samples

To accomplish the first and second stages of the testing plan described in the previous section, the samples were subjected to thermal treatment in a furnace at temperatures of 200, 300, 400, 500 and 600 ºC (Figure 1.4). Thermal treatment was limited to 600 ºC as the rock lost its integrity at higher temperatures due to mass cracking – and so preventing open porosity, ultrasonic, and UCS tests. A gradient of 5 ºC/min was applied to reach the target temperatures and once reached, it was maintained for one hour. Samples heated

at 400, 500, and 600 °C were cooled at a slow rate inside the furnace to 300 - 350 °C to ensure a safe manipulation, and then the furnace was opened. To simulate various modes of fire intervention equipment, samples were cooled in one of two ways: air-cooled at a slow rate to room temperature; or by rapid cooling using water immersion according to the procedure described by Brotóns et al. (Brotóns et al. 2013). A set of thermocouples registered the temperature inside the furnace every minute using a PicoLog 6 data logger. For the third stage of the research methodology described in the previous section, target temperatures were limited to 300, 400, and 500 ºC and samples were air-cooled.

1.6.4. Laboratory tests

Chemical composition

Rock fragments were pulverised after being heated to 105, 300, and 500 ºC. Total carbon and sulphur content was then determined using an Eltra CS IR spectrometer after heating in a furnace. The whole rock analysis was performed by X-ray fluorescence (XRF) using a XRF Panalytical Axios Fast equipment. The phase composition of samples was analysed by powder X-ray diffraction (XRD) on a Bruker D8-Advance diffractometer with a Goebel mirror (non-planar samples) using Cu Kα radiation and a setting of 40 kV and 40 mA. XRD data were collected and interpreted using the XPowder software package, which allows a quantitative analysis for the identified phases. Determination of oxidizable organic matter aims to explain the different coloration between light and dark grey textures. To do so, finely ground rock samples previously subjected to 105 ºC and 500 ºC were selected, and oxidizable organic matter contents were determined using potassium permanganate, according to Spanish standard (UNE-EN-103204 2019).

Thermo-chemical behaviour

Thermal analyses of dark grey samples were conducted using thermogravimetric (TG), differential thermal analysis (DTA), and differential scanning calorimetry (DSC), TG-DTA-DSC, and TG-DTA coupled to a mass spectrometer (MS). TG-DTA-MS and TG-DTA-DSC experiments were performed using a NETZSCH STA 449 Jupiter F5 thermal analyser. The NETZSCH Aeölos Quadro Mass Spectrometer was coupled to the TG-DTA analyser. Measurements were conducted under dynamic mode from 25 to 700 ºC at a heating rate of 10 ºC min^{-1} under air conditions (N_2:O_2 in 4:1) at 50 ml/min.

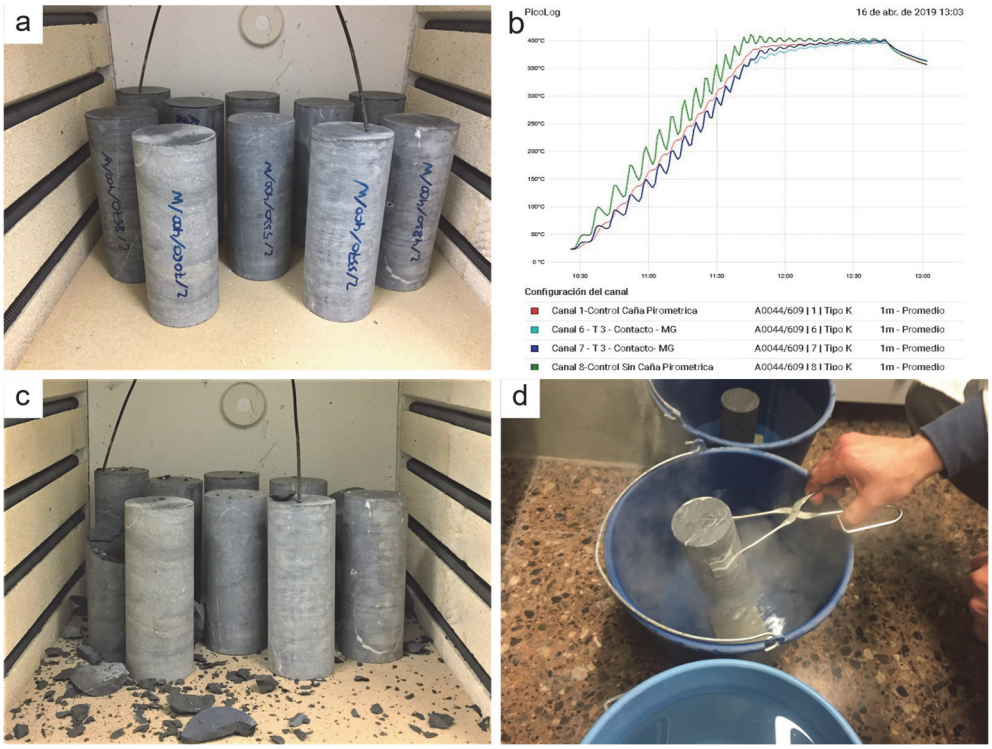

Figure 1.4. Intact samples placed in the furnace (a); screenshot from PicoLog data register showing temperatures from thermocouples in the furnace (b); samples after being heated exhibiting cracking, splitting and explosive behaviour (c); samples cooled at a rapid rate by water immersion (d).

Microstructure

Optical and scanning electron microscopy (SEM) in backscattered electron mode was used to study the petrographic features of Prada limestone. Sample surfaces were polished with alumina and diamond powder; the finest abrasive used was a 0.4 mm diamond powder. Uncovered polished surfaces were studied in a Hitachi S-3000 N variable pressure SEM working in a low vacuum, and salt tested surfaces were analysed in a high vacuum SEM in secondary electron mode (Figure 1.5). Mercury intrusion porosimetry (MIP) was used to obtain pore size distribution in samples thermally treated at 105, 300, and 600 ºC. Tests were developed with a PoreMaster 60 GT (Quantachrome Instruments). The employed surface tensions and contact angles of mercury were 480 mN/m and 130°, respectively.

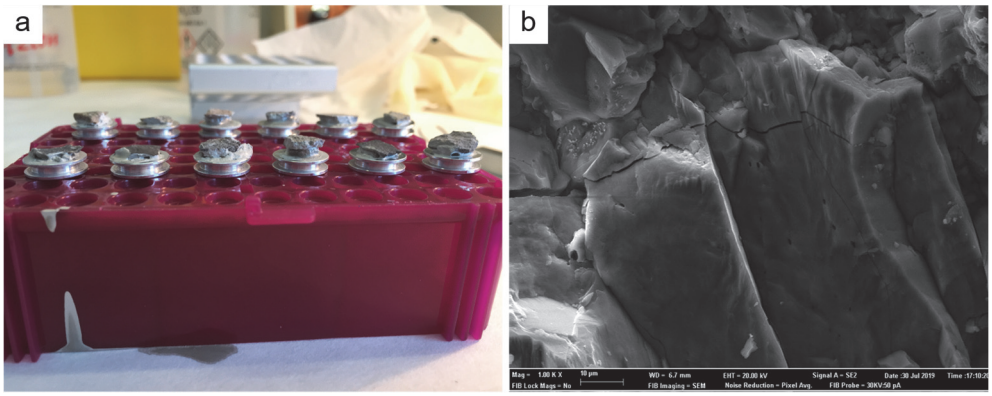

Figure 1.5. Rock samples were prepared and placed in holders (a). SEM image of texture and fissures of a sample after thermally treated at 600 ºC (an increase of 1000x was used) (b).

Physical properties

A preliminary colour classification of the intact rock was performed using Munsell soil colour charts (GLEY 2 chart for low chroma colours). To observe colour differences before and after heat treatment, both the faces of samples were polished and moistened, and their images were captured using an HP OfficeJetPro 7740 scanner with a resolution of 600 ppi. The average sRGB colour values of the pixels were obtained for representative regions of the material using software GIMP 2.10.12. The colour was described in terms of CIELAB space colour (CIE 1977) as used by many authors (Pospíšil et al. 2007; González-Gómez et al. 2015) where L* represents lightness (i.e. the darkest black at L* = 0, and the brightest white at L* = 100), and a* and b* chromaticity. The a* axis represents green in the negative direction and red in the positive direction, and b* axis represents blue in the negative direction and yellow in the positive direction.

Open porosity and unit dry weight values before and after thermal treatment were determined using irregular samples. To do so, saturation and buoyancy techniques were applied according to the methods suggested by the ISRM (Franklin 1979). Ultrasonic measurements were carried out over cylindrical samples before and after thermal treatment, according to the method suggested by the ISRM (Aydin 2014). The transmission method consisted of two Olympus V1548 0.1 MHz piezoelectric sensors coupled to the sample at constant pressure. Compressive (P) and shear (S) waves were measured using polarised Olympus transducers videoscan V1548 (0.1 MHz) (Figure 1.6). An emitting-receiving equipment (Proceq Pundit lab +) was used to acquire and digitalise the waveforms to be displayed, manipulated, and stored.

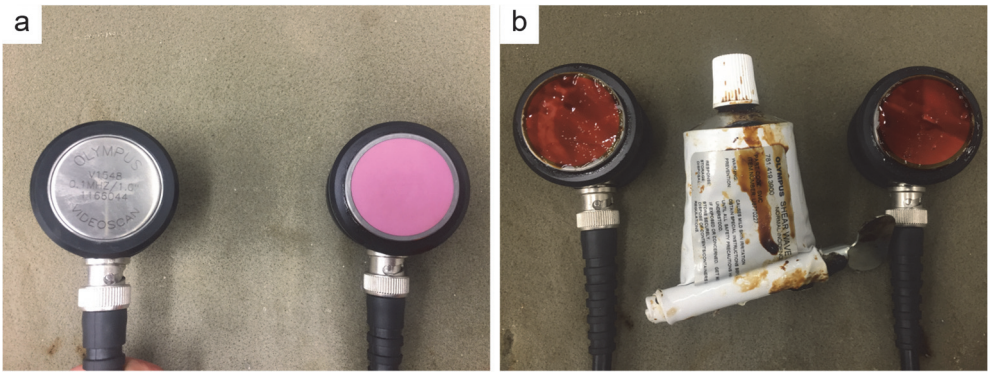

Figure 1.6. Piezoelectric sensors (a) were covered with a shear wave transmitting gel (b).

Mechanical properties

UCS tests were performed on cylindrical samples with a slenderness of 2.5 according to the method suggested by the ISRM (Fairhurst and Hudson 1987) (Figure 1.7). Core faces were polished to ensure flatness and perpendicularity relative to the axis. A four-column press machine (Mecánica Científica SA model 28.5200) with a capacity of 2000 kN was used, and a compression rate of 0.5 MPa/s was applied until the ultimate load. Strain gauges (Tokyo Measuring Instruments Lab PF-30-11) measuring 30 mm in length (120.3±0.5 Ω, k=2.13±1) were used for longitudinal and lateral strains. Values were registered for each loading cycle using MecaSoft software v.1.3.8. Young's tangent modulus and the corresponding Poisson ratio were determined from values of 50% of the ultimate sample load according to the method suggested by the ISRM mentioned above.

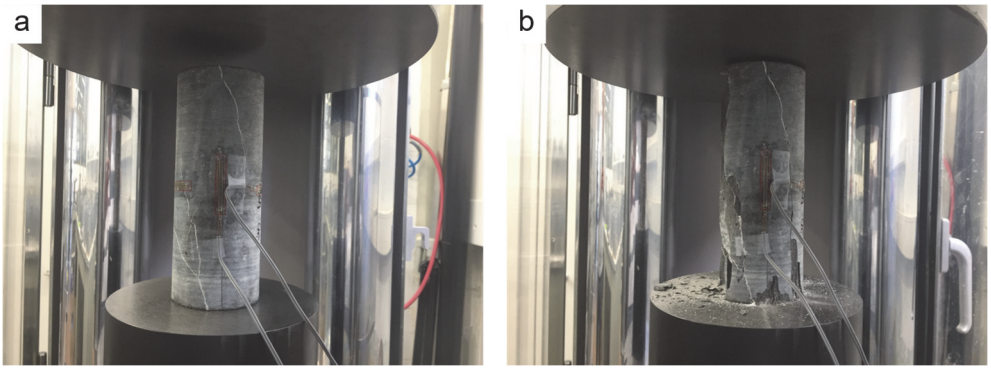

Figure 1.7. Detail of a sample thermally treated at 400 ºC with longitudinal and lateral gauges installed before (a) and after failure at 250 kN (b).

Drilling properties

Sievers' J-miniature drill test constitutes a measure of rock surface hardness or resistance to indentation, and is defined as the measured drillhole depths after 200 revolutions of

an 8.5 mm miniature drillbit acting with a vertical load of 20 kg (Figure 4.5). The test was repeated five times on each rock sample, and the Sievers' J-value was calculated as the mean value of the depth of the miniature drill holes, measured in 1/10 mm according to Bruland (2000). The brittleness test gives a good measure of the ability of rocks to resist crushing by repeated impacts. The test was conducted according to Bruland (2000), and so a total of 500 g of aggregate in the fraction 11.2 - 16.0 mm was prepared from each sample. Then, the aggregate was crushed by 20 impacts in the mortar and then the value S_{20} was expressed as the percentage of material passing the 11.2 mm sieve (Figure 4.6).

1.7. Scientific publications presented in this PhD thesis and its relationship with the research topic

The main results of this PhD thesis have been published in journals indexed in the Journal Citation Reports of Clarivate Analytics in the year 2021. A post-print (author's version) of these articles are included as individual chapters in this PhD thesis:

Journal Article #1. Published in the journal Construction and Building Materials, and included as Chapter 2 in this PhD tesis:

Martínez-Ibáñez V, Garrido M, Hidalgo Signes C, Tomás R (2021). Micro and macro-structural effects of high temperatures in Prada limestone: key factors for future fire-intervention protocols in Tres Ponts Tunnel (Spain). Construction and Building Materials 286:122960. https://doi.org/10.1016/j.conbuildmat.2021.122960

This article was published in the journal Construction and Building Materials, an international reference in the field of construction and building materials and their application in new works and repair practice. This journal is published by Elsevier and identified as ISSN 0950-0618. Impact Factor (IF) is of 4.419, and this journal is ranked 10/63 (Q1) in the field of construction & building technology, 11/134 (Q1) in the field of civil engineering, and 86/314 (Q2) in the field of multidisciplinary materials science, according to the most recent statistics published by JCR (2019).

In this article, samples of Prada limestone are heated at temperatures of 105, 200, 300, 400, 500 and 600 ºC, and later cooled with air or water to simulate fire extinguishing interventions. Analysis of changes in the thermally treated samples are focused in the chemical composition and microstructure, physical (i.e. open porosity, volume, dry total weight, and ultrasound wave velocities) and mechanical properties (i.e. uniaxial compressive strength, elastic modulus, and Poisson's ratio). Results point to a rock weakening even at low temperatures (200 ºC). Initial trans-granular fissures and porosity could be appreciated when heating to 400 ºC, and samples cooled using water showed greater property variation at 300-400 ºC. A trans-granular micro-crack progression is observed at 500 ºC using scanning electron microscope (SEM), and this leads to a dramatic thermal decay in terms of an increase in porosity and decrease in P- and S-wave

velocities under both cooling methods. Water-cooled samples show micro-crack coalescence and growing fissures that produce a greater loss in uniaxial compressive strength (UCS). Well-formed fissures are perceived at 600 ºC, with samples almost losing their integrity due to mass cracking, and thermal damage is also greater when samples are quickly cooled. Statistical analyses are performed to discard the influence of the natural location of the borehole samples in the variability of the experimental results, and this enables correlations to be proposed for predicting UCS and elastic modulus from volume, open porosity, and P-wave velocity after thermal treatment.

Journal Article #2. Published in the journal Rock Mechanics and Rock Engineering, and included as Chapter 3 in this PhD thesis.

Martínez-Ibáñez, V., Benavente, D., Hidalgo Signes, C., Tomás, R., & Garrido, M. E. E. (2021). Temperature-Induced Explosive Behaviour and Thermo-Chemical Damage on Pyrite-Bearing Limestones: Causes and Mechanisms. Rock Mechanics and Rock Engineering, 54(1), 219–234. https://doi.org/10.1007/s00603-020-02278-x

This article was published in the journal Rock Mechanics and Rock Engineering, an international reference in the experimental and theoretical aspects of rock mechanics, including laboratory and field testing, methods of computation and field observation of structural behaviour. This journal is published by Springer and identified as ISSN 0723-2632, has an impact factor (IF) of 4.140, and is ranked 5/39 (Q1) in the field of geological engineering, and 25/200 (Q1) in the field of multidisciplinary geosciences, according to the most recent statistics published by JCR (2019).

In this research, two different varieties of Prada limestone are compared: a dark grey texture, bearing quartz, clay minerals, organic matter and pyrites; and a light grey texture with little or no presence of such components. The explosion of some samples was observed when heating the dark texture from 400 ºC, and it is remarkable that the violence of the explosive events was clear and cannot be confounded with ordinary splitting or cracking on thermally treated rocks. To evaluate the causes and mechanisms behind such differences in the dark and light grey samples, chemical and mineralogical composition, texture, microstructure, and physical properties (i.e. colour, open porosity, ultrasound wave velocity) are evaluated at temperatures of 105, 300, 400 and 500 ºC. Thermal oxidation of pyrites releasing SO_2 is identified in the dark texture from 400 ºC by means of thermogravimetric analysis, as a cause for the dramatic increase in pore-pressure, leading to a rapid growth and coalescence of microcracks and a catastrophic decay in rock integrity. Apart from the explosive events, variations in ultrasound wave velocities and open porosity are greater in the dark texture than in the light grey. Results in this research point towards a significant contribution of oxidation of pyrites for the thermo-chemical damage to the rock, among other factors such as the pre-existence of micro-fissures and a thermal expansion coefficient mismatch between minerals.

Journal Article #3. Published in the journal Applied Sciences, and included as Chapter 4 in this PhD thesis.

Martínez-Ibáñez V, Garrido M, Hidalgo Signes C, Basco A, Miranda T, Tomás R (2021). Thermal effects on the drilling performance of a limestone: relationships with physical and mechanical properties. Applied Sciences 11:3286. https://doi.org/10.3390/app11073286

This article was published in the Special Issue 'Effects of Temperature on Rock and Rock Masses' in the journal Applied Sciences, an international publication covering all aspects of applied physics, applied chemistry, engineering, environmental and earth sciences, and applied biology. This journal is published by MDPI and identified as ISSN 2076-3417. Impact Factor (IF) is of 2.474, and this journal is ranked 88/177 (Q2) in the field of multidisciplinary chemistry, 32/91 (Q2) in the field of multidisciplinary engineering, 63/155 (Q2) in the field of applied physics, and 161/314 (Q3) in the field of multidisciplinary materials science, according to the most recent statistics published by JCR (2019).

In this article, samples of Prada limestone are subjected to temperatures of 105, 200, 300, 400 and 600 ºC, and then cooled at a slow rate or by quenching. Sievers' J value and brittleness S_{20} are then evaluated for each temperature and the drilling rate index (DRI) was calculated. Thermal treatment implied a sustained increase in the drillability of rock. At 600 ºC, SJ and S_{20} tripled and doubled, respectively, and the DRI increased by 40% on the initial values obtained for the intact rock. Results are inconclusive in the influence on the cooling method on the drilling performance of Prada limestone for the tested range of temperatures. Strong correlations are observed between most of the physical, mechanical, and drillability variables on the thermally treated samples. This is attributed to thermal damage in the rock, especially at certain temperatures, affecting proportionally all the studied properties of the Prada limestone – and so coefficients of determination are high.

In addition to the articles published in journals, partial results derived from this research were accepted to be presented in the ISRM International Symposium Eurock 2020 – Hard Rock Engineering, initially planned for the 14-19 June in Trondheim, Norway. However, this event was cancelled due to Covid-19 pandemic, and consequently, the articles were not orally presented. The conference proceedings were finally published digitally via Onepetro.org:

Conference Article #1. *Martínez-Ibáñez, V., Garrido, M. E., Signes, C. H., & Tomás, R. (2020). Indirect Evaluation of Strength for Limestones Subjected to High Temperatures. In ISRM International Symposium - EUROCK 2020. Trondheim, Norway. Available in https://onepetro.org/ISRMEUROCK/proceedings/EUROCK20/All-EUROCK20/ISRM-EUROCK-2020-110/447352*

Conference Article #2. *Martínez-Ibáñez, V., Garrido, M. E., Signes, C. H., & Tomás, R. (2020). Study of Explosive Behaviour at High Temperatures on Limestones from a Road Tunnel in Spain. In ISRM International Symposium - EUROCK 2020. Trondheim, Norway. Available https://onepetro.org/ISRMEUROCK/proceedings/EUROCK20/All-EUROCK20/ISRM-EUROCK-2020-184/447430*

Finally, the following conference articles, which will be presented in forthcoming national and international conferences to be held in 2021 and 2022, have been accepted:

Conference Article #1 (accepted). *Martínez-Ibáñez V, Garrido M, Hidalgo Signes C, Basco A, Miranda T, Tomás R. Variation of Drilling Rate Index (DRI) with temperature and its relationship with thermal damage on 'Prada' limestone. In: ISRM International Symposium - EUROCK 2021*

Conference Article #2 (accepted). *Martínez-Ibáñez V, Garrido M, Hidalgo Signes C, Tomás R. Determination of thermal conductivity variation through Modified Transient Plane Source (MTPS), and its relationship with porosity variation on thermally treated Prada limestone. In: ISRM International Symposium - EUROCK 2021*

Conference Article #3 (abstract accepted). *Martínez-Ibáñez V, Garrido M, Hidalgo Signes C, Seron J, Basco A, Miranda T, Tomás R. Variación del valor de perforabilidad Sj de Sievers con la temperatura y su relación con el factor de daño de una roca caliza. In: XI Simposio Nacional de Ingeniería Geotécnica (Mieres, Spain) 2022*

1.8. Dissertation structure

The dissertation presented in this document is structured in six chapters. This PhD thesis is presented as a compendium of publications in accordance with the regulations for doctorate studies at the Universitat Politècnica de València, and so a post-print (author's version) of the published articles, and a general discussion of the results are included as individual chapters.

- **Chapter 1. Introduction.** This section provides a research context, states the objectives, hypothesis, rationale, and briefly describes the research methodology used in this work. It also presents the published journal articles derived from this research, and justifies their concordance with the research topic of this PhD thesis.
- **Chapter 2. Micro and macro-structural effects of high temperatures in Prada limestone: key factors for future fire-intervention protocols in Tres Ponts Tunnel (Spain).** This is journal article #1, published in Construction and Building Materials. This research identifies key temperatures for severe decay on physical and mechanical properties of Prada limestone, and relates them with the variation in microstructure. Moreover, it explores correlations to predict

strength and deformational features to perform an initial evaluation of the integrity of rock and may help in making the initial decisions after a fire in the Tres Ponts Tunnel.

- **Chapter 3. Temperature-induced explosive behaviour and thermo-chemical damage on pyrite-bearing limestones: causes and mechanisms.** This is journal article #2, published in Rock Mechanics and Rock Engineering. This novel research points to a significant contribution of oxidation of pyrites on the thermo-chemical damage of pyrite-bearing Prada limestones, involving the explosion of certain samples.
- **Chapter 4. Thermal effects on the drilling performance of a limestone: relationships with physical and mechanical properties.** This is journal article #3, published in Applied Sciences journal. This research describes an appreciable increase in the drilling ability of the thermally-treated Prada limestone. In addition, correlations are presented for variations in the drilling, mechanical, and physical properties with temperature.
- **Chapter 5. Discussion.** This is a global discussion about the significance of the results, and of the contribution of the articles presented in the previous chapters.
- **Chapter 6. Conclusions.** The main conclusions derived from the published articles are presented in this section. This work has opened new lines of research that will be presented in this chapter.

Chapter 2. Micro and macro-structural effects of high temperatures in Prada limestone: key factors for future fire-intervention protocols in Tres Ponts Tunnel (Spain)

Authors:	Víctor Martínez-Ibáñez, María Elvira Garrido, Carlos Hidalgo Signes, Roberto Tomás		
Status:	Manuscript published		
Journal:	Construction and Building Materials, 2021		
DOI	https://doi.org/10.1016/j.conbuildmat.2021.122960		
JCR IF (2019)	4.419		
	JCR Category	Ranking	Quartile
	Construction & Building Technology	*10/63*	*Q1*
	Civil Engineering	*11/134*	*Q1*
	Multidisciplinary Materials Science	*86/314*	*Q2*
Presentation:	Post-print (Author version)		

Abstract

Temperature and cooling methods strongly affect the stability of tunnels drilled in rock masses and so condition interventions for fire emergencies. Samples from two horizontal boreholes drilled in Prada limestone during the design stage of the Tres Ponts Tunnel in the Catalan south Pyrenean zone (Spain) are heated from 105 to 600 ºC, and subsequently cooled with air or water to simulate fire extinguishing interventions. Changes in chemical composition and microstructure, physical properties (open porosity, volume, dry total weight, P and S-wave velocity), and mechanical properties (uniaxial compressive strength, elastic modulus, and Poisson's ratio) are analysed. Rock weakening is observed even at low temperatures (T<300 ºC). The influence of the cooling method appeared at intermediate temperatures of 300-400 ºC and open porosity, P and S-wave velocities, and elastic modulus show greater variation for water-cooled samples. A temperature of 500 ºC is of paramount importance for Prada limestone as it leads to a dramatic increase in porosity and a notable decrease in P and S-wave velocities under both cooling methods. Trans-granular micro-crack progression is observed at 500 ºC using scanning electron microscope (SEM), and water-cooled samples show a greater loss in uniaxial compressive strength (UCS), and this is due to micro-crack connections and growing fissures. Thermal damage at 600 ºC is also greater when samples are quickly cooled. An ANOVA and a simple regression analysis are performed to discard the influence of the natural location of the borehole samples in the obtained experimental results. Finally, correlations to predict UCS and elastic modulus from volume, open porosity, and P-wave velocity after thermal treatment are proposed using simple exponential and potential functions to help make preliminary decisions after a tunnel fire. These predictive results on the effects of fire on Prada limestone will be considered for the definition of future fire intervention protocols in the Tres Ponts Tunnel.

Keywords

thermal damage; physical and mechanical properties; cracks; tunnel fire; limestone; correlations

2.1. Introduction

Vehicle fires in road tunnels are not very rare events and their consequences may be far greater than fires in open spaces (Ingason 2012). The extreme events that occurred in the Mont Blanc tunnel (France-Italy 1999), the Tauern tunnel (Austria 1999) (Leitner 2001), and the Gotthard tunnel (Switzerland 2001) dominated discussion of tunnel fires in the early 21st century and gave rise to international regulations and recommendations. Although the majority of tunnel fires are relatively small events, they nevertheless have the potential to evolve into more serious events depending on various factors: tunnel design; location of the tunnel; geometry of the road; monitoring; technical standard of the vehicles; traffic regulation; and speed limits or driving culture (PIARC 2016). Fully developed fires in the cargo of heavy goods vehicles and pool fires of burnable liquids can develop very high heat release rates (ITA 2004). Temperatures in the ceiling and wall surfaces can reach from 400 ºC (private car) to 1400 ºC (heavy goods vehicle) in the early stages of a fire, and persist for hours (PIARC 1999) with dramatic consequences for tunnel structure.

Different phases can be defined in the development of a fire inside a tunnel that are important for the integrity of the structure (CETU 2005): a) the structural stability fully conditions the time available for evacuation; b) the safety conditions during post-fire inspection; and c) the scope of repair and the time during which traffic will be disrupted after a fire. The effect of high temperature on tunnel lining has been studied using full-scale tests (PIARC 1999). The heat generated during a major fire may cause a dramatic drop in concrete strength and spalling that exposes reinforcement to high temperatures and accelerating structural degradation. Even fire-resistant advances for lining protection can never completely prevent concrete weakening and spalling due to high temperatures, and so heat will transfer through the lining to the rock mass. Obviously, rock mass will be quickly exposed to high temperature in a tunnel fire if there is no reinforced concrete or only a thin layer of shotcrete.

Some studies are specifically focused on the evaluation of the performance of the rock mass of a tunnel affected by fire. Smith and Pells (2008) used real fire to register substantial explosive spalling events at relatively low temperatures (little more than the boiling point of water) on sandstone tunnels in Australia. Moreover, these authors observed a decrease in uniaxial compression strength and elastic modulus in sandstone samples when using an electrical furnace. Conclusions on rock spalling were later confirmed in a real accident (Smith and Pells 2009), and the generation of steam pressure was recognised as the main mechanism causing spalling. Studies on tunnels in igneous rocks in Sweden (Nordlund et al. 2014) enabled the identification of ranges of temperatures causing key variations in the mineralogical, physical, and mechanical properties of rocks. These authors generated high temperature gradients to simulate standard time-temperature curves. The results showed a strong dependence of micro-

crack formation on the mineralogy, as well as a direct influence on the reduction in compression strength.

The study of the variation in physical, mineralogical, and mechanical properties of rocks with temperature, not specifically focused on tunnel engineering, is an issue of current interest among the scientific community due to its application in various fields such as mining (Li et al. 2017), cultural heritage (Koca et al. 2006; Brotóns et al. 2013), geothermal energy (Pei et al. 2018), or underground storage of radioactive waste (Zhang et al. 2017a). Research points to heating as the cause for decay in rock integrity, and where magnitude and key temperatures strongly depend on the type of rock and their diverse physical and mineralogical properties. Some of the above mentioned works are focused on limestones, one of the most common types of sedimentary rocks. Lion et al. (2005) described a decrease in strength due to microcracking at low temperatures (T<250 ºC) in a limestone from Anstrude (France). Yavuz et al. (2010) observed that microcracking does not seem to occur below 150 ºC on limestones from Turkey; while marked decreases in bulk density, P-wave velocity, and effective porosity were registered at 400ºC. Andriani and Germinario (2014) observed a clear reduction in uniaxial compression strength (UCS) from 500ºC on calcareous and dolomitic rocks from Apulia in Italy. Temperatures above 600ºC usually mark a dramatic decline in UCS (Mao et al. 2009; Sengun 2014). Zhang et al. (2017b) studied limestones from Linyi (China) noting that from 200 to 500 °C the porosity and pore volume rapidly increased, and from 500 to 600 °C the maximum strength, elastic modulus, Poisson's ratio, and hardness decreased – while peak strain continuously increased. Crosby et al. (2018) observed a lowering of peak strength at confining pressures up to 10 MPa on triaxial tests caused by microcracking that did not affect the strength of the heated Salem limestone at greater pressures. Induced microcracking by thermal treatment lowered peak strength at confining pressures up to 10 MPa on triaxial tests, and did not affect the strength of limestone at greater pressures. Zhang and Lv (2020) found a strong relationship between the mineral content and limestone properties under the effect of temperature for limestone from Shandong Province (China).

Valuable general knowledge about the thermal performance of limestone has been produced. Nevertheless, case-studies focused on the thermal performance of rock where future tunnels are to be drilled are still scarce. Therefore, we consider that certain features could be found in the thermal performance of limestone formations that fully condition fire emergency interventions, as it is known that certain temperature ranges and cooling methods usually compromise the stability of rock. Understanding the thermal performance of rock enables predicting mechanical parameters by using non-destructive tests on heated limestone and correlations whose determination is quick and easy. Previous research mainly focused on rocks at room temperature and estimated the UCS using simple regression analysis, multivariate regression analysis, or soft-computing tools such as neural networks and adaptive neuro-fuzzy inference systems. Predictors in most cases were physical properties such as mineral grain characteristics (Singh et al. 2001; Sonmez et al. 2004, 2006; Zorlu et al. 2008; Cevik et al. 2011), density, porosity,

and wave velocity (Gokceoglu and Zorlu 2004; Singh et al. 2013, 2017; Yesiloglu-Gultekin et al. 2013; Armaghani et al. 2016; Sharma et al. 2017). Such correlations strongly depend on the type of rock, so several studies are focused on carbonate specimens (Yasar and Erdogan 2004; Baykasoğlu et al. 2008; Dehghan et al. 2010; Yagiz et al. 2012; Aboutaleb et al. 2018). Little research is available on strength prediction for thermally-treated rocks. Multivariate analysis enabled the prediction of thermal damage on Dholpur sandstone (India) from temperature and mechanical parameters (i.e. compressive strength, failure strain, and elastic modulus) (Gautam et al. 2016). Dholpur sandstone was also studied after thermal treatment using multivariate regression analysis to predict changes in strength from temperature and physical properties (such as density, porosity, thermal expansion coefficients, and ultrasonic waves). These predictions improved when using artificial neural network and adaptive neuro-fuzzy inference systems (coefficients of determination were close to 1) (Sirdesai et al. 2017). Such techniques and predictors were used to improve the prediction of thermal damage (Sirdesai et al. 2018).

In this research, laboratory tests have been made on samples from two horizontal boreholes drilled during the design stage of the Tres Ponts Tunnel, which will be entirely excavated from Prada limestone in the Catalan south Pyrenean zone (Spain). Samples were thermally-treated at temperatures of 105, 200, 300, 400, 500 and 600 ºC, then cooled using two methods: air-cooling (slow rate) and water-cooling (rapid rate) to simulate different modes of fire intervention. Variations in chemical composition and microstructure, physical (open porosity, volume, dry total weight, P- and S-wave velocities), and mechanical (uniaxial compressive strength, elastic modulus, and Poisson's ratio) properties were analysed. Various Prada formation features were observed such as key temperatures for rock weakening, and the influence of the cooling method. Statistical techniques (ANOVA and linear regression) were used to study the influence of the natural location of the samples (borehole and depth) on property variation and so explore the viability of comparing results between different samples and generalising the results throughout the tunnel. Finally, several correlations have been proposed to indirectly determine the variation in strength and elasticity from the variation in physical properties (such as volume, open porosity, and P-wave velocity) with temperature. This research fills a gap on correlating parameters for thermally-treated limestone. The results also provide a valid approach to predict the effects of a fire in the Tres Ponts Tunnel by helping in planning intervention protocols for emergency response teams, predicting times available for evacuation, evaluating safety conditions during post-fire inspections, as well estimating the extent of the damage and the time needed for repair.

2.2. Materials and methods

2.2.1. Sample preparation

The Tres Ponts Tunnel is planned on the C-13 road near Organyà in the Catalan south Pyrenean zone (Spain). The tunnel is oriented north-south, measures 1273 m in length, and will have a maximum depth of 285 m. It will be entirely excavated from Prada limestone, a lower Cretaceous limestone formation with a mudstone-wakestone texture and fossil fauna (García Senz 2002). Rock samples were taken from two horizontal survey boreholes drilled during the design stage. Boreholes 1 and 2 were in the southern and northern mouths of the tunnel and reached prospection depths of 65.30 m and 91.45 m, respectively. The planning and performance of the survey works was led by an independent engineering consultancy in charge of tunnel design. Therefore, the position and depth of the boreholes were decided according to tunnel design criteria.

Borehole cores with a diameter of 65 mm were cut with a slenderness of 2.5 to perform uniaxial compression strength tests according to International Society for Rock Mechanics (ISRM) standards. Samples were very homogeneous and only presented small changes in the grey tone and very thin veins of calcite. Furthermore, no changes were observed in the material composition throughout the length of the boreholes. Five cylindrical samples and five irregular fragments were used for the determination of rock properties for each temperature and cooling method. This number of samples was defined by the limited availability of borehole rock cores, and the minimum number of specimens recommended by the ISRM standard for the uniaxial compression strength test (Fairhurst and Hudson 1987). Thus, a total of 55 cylindrical samples of 63 mm in diameter and a slenderness of 2.5 were randomly selected from both horizontal boreholes to perform ultrasound and uniaxial compression strength tests. In addition, 55 irregular fragments were selected to determine unit weight and open porosity variation with temperature, mercury intrusion porosimetry tests, and scanning electron microscopy observations. Figure 2.1 illustrates the number of laboratory tests performed for each temperature and the number of samples used.

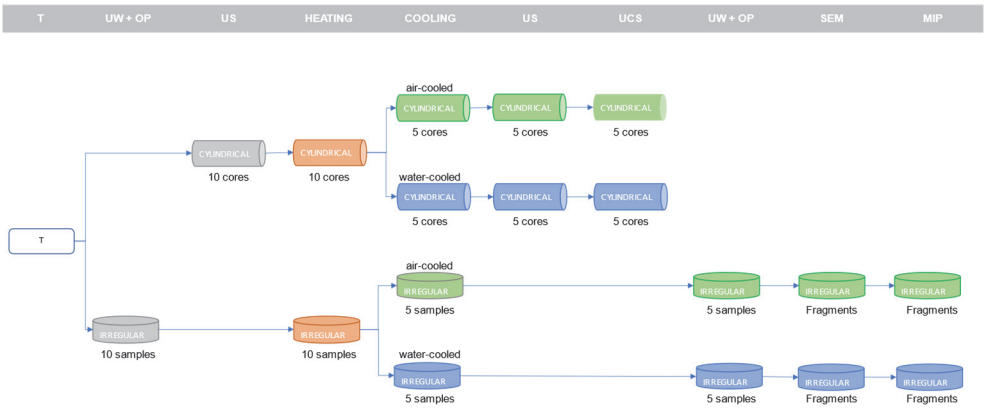

Figure 2.1. Laboratory tests and the number of cylindrical and irregular samples tested at each temperature (T) to determine: unit weight (UW); open porosity (OP); ultrasound wave velocity (US); uniaxial compression strength (UCS); microstructure by scanning electron microscopy (SEM); and pore distribution by mercury intrusion porosity (MIP).

2.2.2. Heating and cooling procedures

Research reveals that water content can play a key role in the determination of UCS and the deformational features of the intact rock, even for small variations in the moisture content due to changes in the relative humidity of the air (Rabat et al. 2020b, a). Natural moisture in rocks is also related to spalling events at temperatures lower than 200 ºC (Smith and Pells 2008, 2009; Nordlund et al. 2014). Even when water absorption in Prada limestone is extremely low (0.45±0.20 %), we decided to study its properties after moisture was completely removed by pre-heating the samples. Although such initial heating may induce micro-structural effects on the rock, we are interested in the micro and macro-structural effects of high temperatures and its implications for Tres Ponts Tunnel fire-intervention protocols. Thus, a temperature of 105 ºC was initially applied to remove moisture from the rock samples for the determination of the intact rock properties and in line with other authors (Yavuz et al. 2010; Brotóns et al. 2013; Sengun 2014). Subsequently, the samples were subjected to thermal treatment in a furnace at temperatures of 200, 300, 400, 500 and 600 ºC. Thermal treatment was limited to 600 ºC as the rock lost its integrity at higher temperatures due to mass cracking, and so preventing open porosity, ultrasonic, and UCS tests. A gradient of 5 ºC/min was applied to reach the target temperatures and once reached, it was maintained for one hour. Samples heated at 400, 500, and 600 °C were cooled at a slow rate inside the furnace to 300 °C to ensure a safe manipulation of the rock, and then the furnace was opened. To simulate different modes of fire intervention equipment, samples were cooled in one of two ways: air-cooled at a slow rate to room temperature; or by rapid cooling using water immersion according to the procedure described by Brotóns et al. (2013). A thermocouple registered the temperature inside the furnace every minute using a PicoLog 6 data logger.

2.2.3. Laboratory tests

Rock fragments were pulverised after being heated to 105, 300, and 500 ºC. Total carbon and sulphur content was then determined using an Eltra CS IR spectrometer after heating in a furnace. The whole rock analysis was performed by fusion and X-ray fluorescence (XRF) using XRF Panalytical Axios Fast. Optical and scanning electron microscopy (SEM) in backscattered electron mode was used to study the petrographic features of Prada limestone. Sample surfaces were polished with alumina and diamond powder; the finest abrasive used was a 0.4 mm diamond powder. Uncovered polished surfaces were studied in a Hitachi S-3000 N variable pressure SEM working in a low vacuum, and salt tested surfaces were analysed in a high vacuum SEM in secondary electron mode. Mercury intrusion porosimetry (MIP) was used to obtain pore size distribution in samples thermally-treated at 105, 300, and 600 ºC. Tests were developed with a PoreMaster 60 GT (Quantachrome Instruments). The employed surface tensions and contact angles of mercury were 480 mN/m and 130°, respectively.

Open porosity and unit weight values before and after thermal treatment were determined using irregular samples. To do so, saturation and buoyancy techniques were applied according to the methods suggested by the ISRM (Franklin 1979). Ultrasonic measurements were made over cylindrical samples before and after thermal treatment, according to the ISRM suggested method (Aydin 2014). The transmission method consisted of two Olympus V1548 0.1 MHz piezoelectric sensors coupled to the sample at constant pressure. Compressive (P) and shear (S) waves were measured using polarised Olympus transducers videoscan V1548 (0.1 MHz). Emitting-receiving equipment (Proceq Pundit lab +) was used to acquire and digitalise the waveforms to be displayed, manipulated, and stored.

UCS tests were performed on cylindrical samples with a slenderness of 2.5 according to the ISRM suggested method (Fairhurst and Hudson 1987). Core faces were polished to ensure flatness and perpendicularity relative to the axis. A four-column press machine (Mecánica Científica SA model 28.5200) with a capacity of 2000 kN was used, and a compression rate of 0.5 MPa/s was applied until the ultimate load. Strain gauges (Tokyo Measuring Instruments Lab PF-30-11) of 30 mm long (120.3±0.5 Ω, k=2.13±1) were used for longitudinal and lateral strains. Values were registered for each loading cycle using MecaSoft software v.1.3.8. Young's tangent modulus and the corresponding Poisson ratio were determined from values of 50% of the ultimate sample load according to the ISRM suggested method mentioned above.

2.2.4. Statistical analysis

A variance analysis (ANOVA) was performed to determine the potential influence of the sample position on the results. P-wave velocity normalised to the same samples at a reference temperature of 105 ºC was chosen to study the influence of the sample's position on results before thermal treatment, since it is a parameter closely linked with other properties such as porosity, elastic modulus, or the Poisson ratio. Normalised P-wave velocity and uniaxial compression strength were chosen to study the influence of sample position on results after heating. The variables described above were compared with other factors to evidence relative influence (such as the position of the samples in the boreholes, the borehole from which they were extracted, the temperature variation, and the cooling method). F-tests enabled the identification of the main factors in the variability of each studied property, and the verification of the null hypothesis (i.e., no difference between means for F=1). P-values tested the statistical significance of each factor (statistical significance for F<0.05). Additionally, a simple regression analysis was performed as an alternative method to study the dependence between P-wave velocity for intact samples, the depth of extraction of the sample in the boreholes, and the borehole from which the samples were extracted.

Finally, several correlations have been proposed to predict the variation in peak strength and elastic modulus from the variation in physical properties (such as volume, open porosity, and P-wave velocity) as a useful, simple, and quick method to estimate the mechanical properties of the rocks after a tunnel fire. Mean values of peak strength, elastic modulus, and normalised physical variables for each temperature have been used, and the best-fitting linear, exponential, logarithmic, or potential curves (fitted using the least squares method) have been adopted. The coefficient of determination (R^2) and the residuals (the difference between predicted and observed values) have been used to evaluate the goodness-of-fit of the data to the curve.

2.3. Results

2.3.1. Geochemical and microstructural characterisation

Mineral elements in Prada limestone before and after heating were obtained using XRF analysis (Table 2.1). The analysis showed that CaO was the most abundant element at all temperatures, followed (by far) by MgO. Clay minerals such as SiO_2, Al_2O_3, and Fe_2O_3 appeared in proportions of less than 1 %. SiO_2 was the dominant compound and this is related to the presence of quartz. Thermal treatment enabled the identification of an important proportional decrease in MgO with temperature, while CaO remained almost constant. Indicative mineral composition of Prada limestone in terms of the proportion of calcite, dolomite, and argillaceous material was deduced following the procedure described by Meng et al. (2020) and based on the chemical affinity of compounds to mineral elements (obtained by XRF) and the ratio of molecular weight. Results show that the primary mineral component of the intact rock is calcite (Cc) with a proportion

above 93% that increased with temperature Table 2.2). The content of dolomite (Cd) was above 6% for the intact rock and this proportion decreased with temperature. Argillaceous material (Ca) showed a proportion of around 1% for all temperatures.

Table 2.1. Mineral element content of Prada limestone at different temperatures.

Temperature (ºC)	CaO (%)	MgO (%)	Al_2O_3 (%)	SiO_2 (%)	Fe_2O_3 (%)
100	54.30	1.34	0.11	0.65	0.19
300	54.40	0.78	0.16	0.95	0.21
500	54.15	0.47	0.12	0.83	0.11

Table 2.2. Mineral composition of Prada limestone before and after heating.

Temperature (ºC)	Cd (%)	Cc (%)	Ca (%)
100	6.11	92.95	0.95
300	3.57	95.13	1.31
500	2.16	96.76	1.07

SEM enabled the identification of micro-defects of increasing magnitude in Prada limestone when heated. Initial trans-granular fissures and porosity could be appreciated when heating to 400 ºC, with no significant differences between air- (Figure 2.2a) and water-cooled samples (Figure 2.2b). Pore-size increase and fissure growth could be clearly appreciated at 500 ºC. When that temperature was reached, isolated fissures were observed in air-cooled samples (Figure 2.2c), and fissures were larger and more connected in water-cooled samples (Figure 2.2d). Well-formed fissures could be observed at 600 ºC for both air (Figure 2.2e) and water-cooled samples (Figure 2.2f). MIP analysis reflected dual porosity features on samples heated at 105 ºC (Figure 2.3). A small size pore family is recognised (in the range of 0.006-0.02 μm) that represents the interparticle porosity defined by grain minerals, cements, and fine-grains. A second pore family representing micro-fissures, which are more abundant and appear in larger sizes (4-10 μm) can also be recognised. Samples heated at 300 ºC and then air-cooled show an increase in the number of pores and large micro-fissures (> 200μm) that MIP cannot measure completely. Results show differences when samples are heated to 300 ºC and cooled with water, where pores smaller than 10 μm almost disappear (attributable to a disaggregation of the samples induced by the effect of water immersion). It is remarkable that retained mercury was maximum in samples heated at 300 ºC (Hg retained 89%) probably due to a growth in pore size and a lack of connections that leads to an accumulation of mercury in the sample. Finally, samples heated to 600 ºC show new pores in a wide range of sizes

that seem to be more connected than in those samples heated to lower temperatures due to a smaller volume of retained mercury (Hg retained 74%).

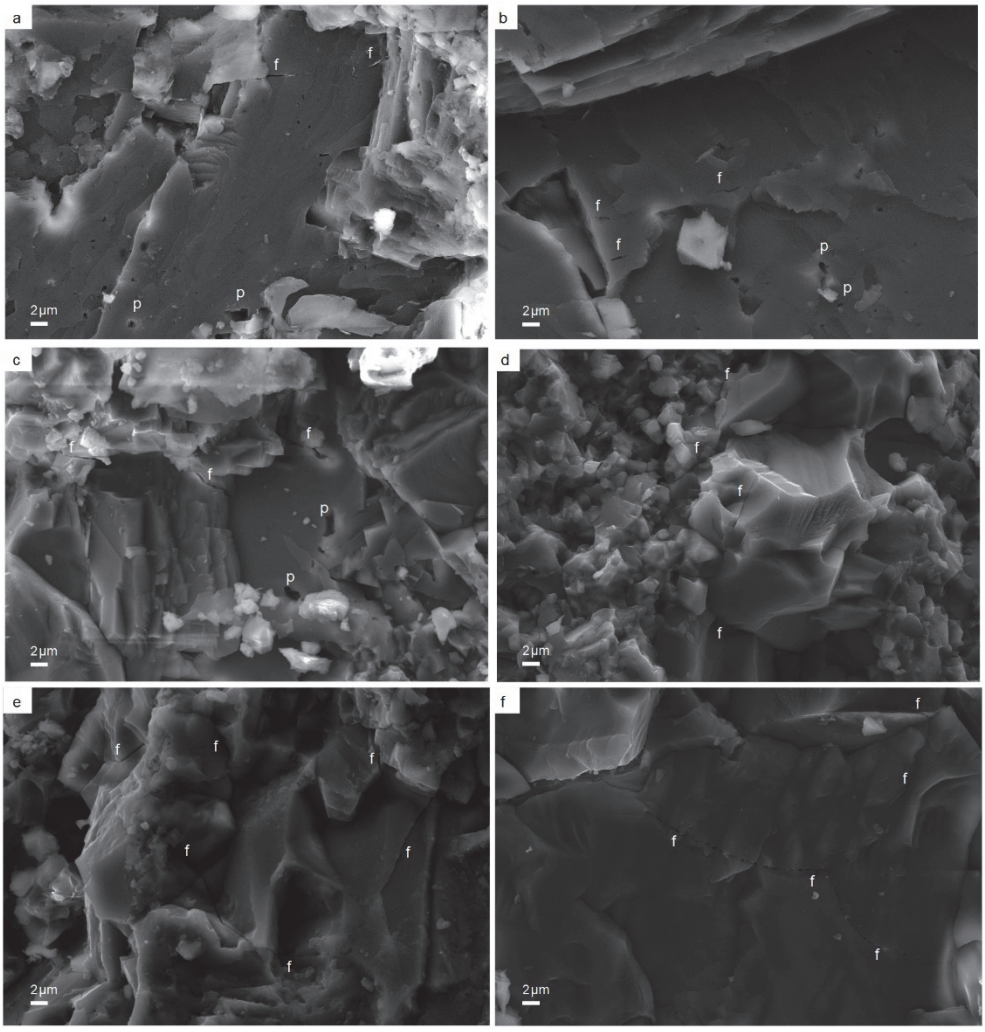

Figure 2.2. SEM images showing pores (p) and fissures (f) for different temperatures and cooling methods. An increase of 2000x was used for all figures.

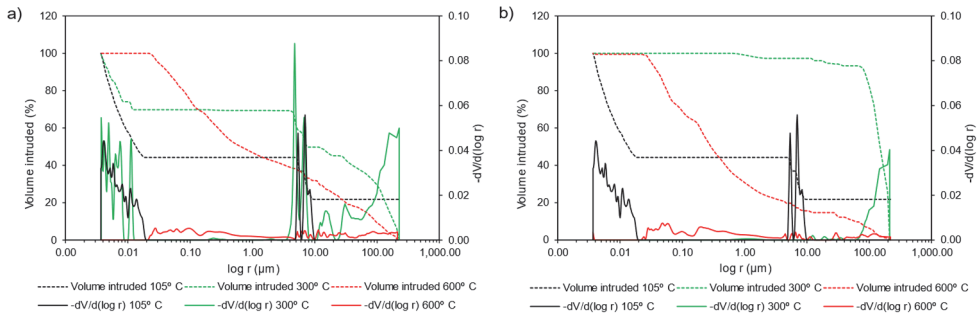

Figure 2.3. Cumulative mercury intrusion and pore size distribution for samples heated at different temperatures and cooled by (a) air; and (b) water immersion.

2.3.2. Variation of physical properties

The average initial values for physical and mechanical properties were initially determined for the intact rock (defined at a reference temperature of 105 ºC) and are summarised in Table 2.3. Variations in physical properties (open porosity, volume, dry total weight, P- and S-wave velocities) with temperature were studied using normalised values (i.e., results after heating were divided by those of the same samples obtained at the reference temperature of 105 ºC).

The variation in open porosity was small at low and intermediate temperatures (Figure 2.4). A marginal reduction in open porosity (slightly greater for water-cooled samples) was reported at 200 ºC. A gentle increase with temperature was then observed at up to 400 ºC (a slightly greater increase is observed at 300 ºC for water-cooled samples). For all cooling methods, appreciable changes appeared at 500 ºC, where open porosity tripled the initial porosity. Moreover, an appreciable rise in standard deviation was observed as the temperature increased. Additionally, differences are noticeable at 600 ºC according to the cooling method as samples cooled by water immersion and air exhibit dramatic increases in mean total porosity of up to 5.68 and 3.82, respectively. Therefore, open porosity showed the greatest variation with temperature among all the studied physical parameters. The variation of volume with temperature exhibited a similar trend to open porosity (Figure 2.5). Variation in volume was of two orders of magnitude smaller than that observed for open porosity. It is worth noting that dry total weight showed almost negligible variations with the temperature, suggesting that volume change is mainly responsible for the observed variation in dry density. The ultrasound wave velocity decreased with temperature (Figure 2.6). Differences between cooling methods appeared at 400 ºC, since water-cooled samples exhibited a significant reduction. At 500 ºC a considerable decrease in ultrasound velocities for both air and water-cooled samples was observed. Finally, the lowest values of P- and S-wave velocities were reached at 600 ºC, and this was mostly noticeable for water-cooled samples.

Table 2.3. Reference values for samples forming Prada limestone, heated at 105 ºC.

Parameter	Value
Dry unit weight, ρ_d (kN/m³)	26.84±0.25
Water absorption (%)	0.45±0.20
Unit weight of solids, γ_s (kN/m³)	27.21±0.01
Thermal conductivity, k (W/mk)	3.50±0.01
Open porosity, n_e (%)	1.21±0.54
Total porosity, n (%)	1.46±0.91
P-wave velocity, V_p (km/s)	5.35±0.06
S-wave velocity, V_s (km/s)	2.65±0.02
Uniaxial compressive strength, σ_{ci} (MPa)	164.63±23.77
Elastic modulus, E (GPa) (from mechanical tests)	77.69±6.54
Poisson's ratio, ν (from mechanical tests)	0.31±0.05

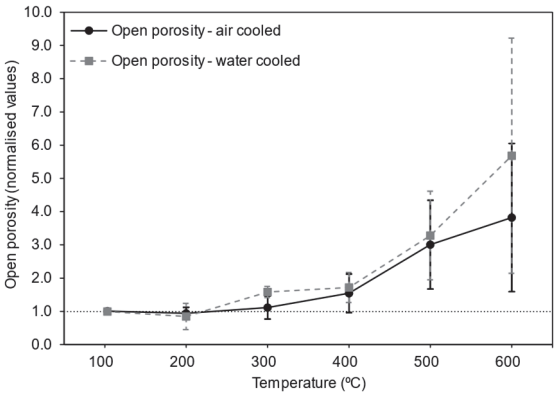

Figure 2.4. Open porosity (normalised values) for air and water-cooled samples.

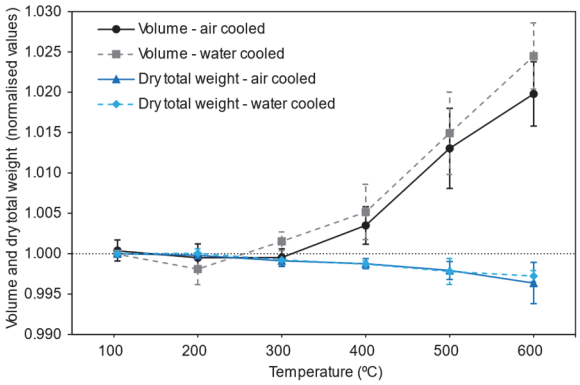

Figure 2.5. Volume and dry total weight (normalised values) for air and water-cooled samples.

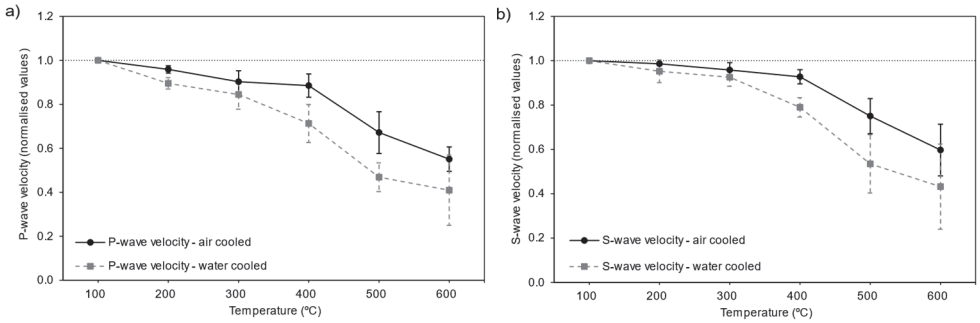

Figure 2.6. P- (a) and S-wave (b) velocities (normalised values) for air and water-cooled samples.

2.3.3. Variation of mechanical properties

Given the destructive nature of the UCS test, it was not possible to obtain values before and after heating for a single sample. Therefore, changes in UCS, elastic modulus, and Poisson's ratio with temperature were studied using absolute values instead of normalised values. UCS results exhibited significant values of standard deviation at certain temperatures which hampered the identification of local changes (Figure 2.7). However, the general trend showed a steady decrease in UCS (even at a low temperature of 200ºC) and final value at 600 ºC was of above 20 % that for the intact rock. The mean values and the small standard deviations at 400 and 500 ºC in the air-cooled samples are consistent with a slight increase in the values of UCS, or at least a stabilisation in the variable. Values showed a more substantial reduction of UCS at 500 ºC in those samples cooled by water immersion. Finally, mean values at 600 ºC reached minimum values for both cooling methods, and the considerable standard deviations prevent a full confirmation that samples cooled with water achieve a lower strength than those cooled in air for

the studied range of temperatures. During the mechanical tests, the axial and lateral deformations and the axial load were recorded. Figure 2.8 shows the stress-strain diagram for representative air- (a) and water-cooled (b) samples. The features of the stress-axial strain curve for air-cooled samples did not present significant changes up to 300 ºC, and then an abrupt increase in ductility is observed for both 400 and 500 ºC. In the case of water-cooled samples, the increase in ductility was more progressive except for an abrupt increase at 400 ºC. We observe a marked elastic axial deformation after the compression phase and a lack of brittle deformation for both cooling methods. Axial stress-lateral strain curves show a progressive increase in the transverse ductility of the samples.

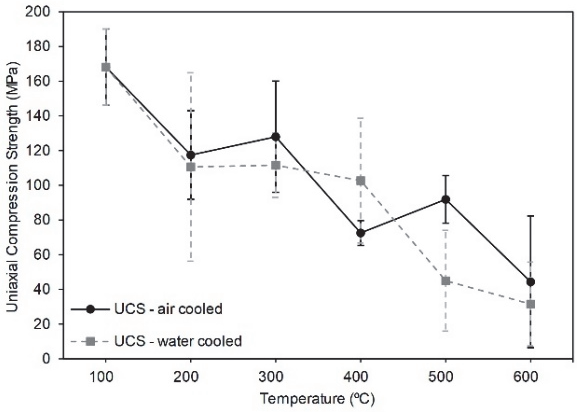

Figure 2.7. UCS values for air and water-cooled samples.

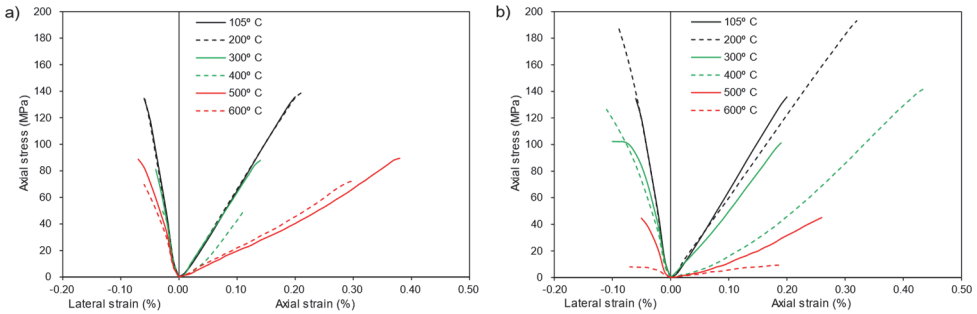

Figure 2.8. Stress-strain curves for samples heated at different temperatures and then air- (a) or water-cooled (b).

Elastic modulus (E) also showed a sustained decrease with temperatures up to about a quarter of the values obtained for the reference samples heated at 105 ºC (Figure 2.9a). The influence of cooling methods was clearly noticeable at 400 ºC, where water-cooled

values registered an abrupt decrease. Final values at 600 ºC were above 25 % of the intact rock at 105 ºC for air-cooled samples, and 11 % in water-cooled samples. Although a slight increase in the mean value could be observed at 600 ºC for air-cooled samples, standard deviations reported at 500 and 600 ºC are not negligible. Therefore, we conclude that the observed trend is consistent with a stabilisation in the variable. Poisson's ratio also showed a clear reduction with temperature (Figure 2.9b). Final values at 600 ºC were near one-third of the values obtained for the intact rock at 105 ºC for both cooling methods. Finally, normalised values for dynamic elastic modulus (Figure 2.10) were computed following the ISRM suggested method (Aydin 2014) using ultrasonic wave velocity and density variation. The trends were similar to those obtained for P- and S-wave velocities. The differences between air- and water-cooled samples mainly appeared at 400 ºC, as observed for the static elastic modulus.

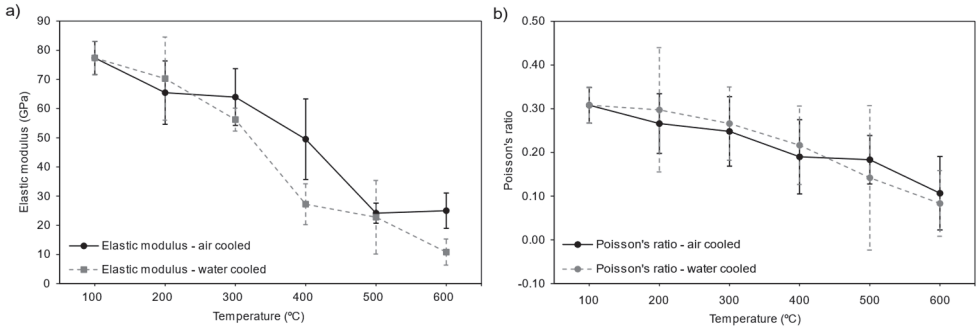

Figure 2.9. Elastic modulus (a) and Poisson's ratio (b) values for air and water-cooled samples.

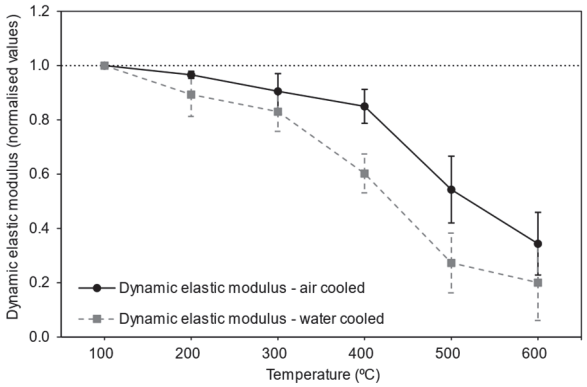

Figure 2.10. Dynamic elastic modulus (normalised values) for air and water-cooled samples.

2.3.4. Influence of sample position on the variability of physical and mechanical properties

The results from the performed ANOVA analysis are summarised in Table 2.4. They enable discarding statistical significance for the depth of samples and number of boreholes on the variation of P-wave velocity for intact samples, and of P-wave velocity and UCS for heated samples (since F-test values were around 1 and P-values were greater than 0.05). Moreover, ANOVA analysis enabled the identification of temperature and cooling method as factors with statistical significance. Depth in the horizontal borehole cannot explain the variability of P-wave velocity for intact samples for both boreholes, since the coefficient of determination of simple regression analysis (Figure 2.11) was extremely low. These results agreed with the ANOVA analysis and enabled discarding a significant influence of sample location on experimental results obtained in this study. As a conclusion, the laboratory results of the different samples can be compared regardless of the borehole from which they were obtained and their location within the borehole. This enables generalising laboratory results throughout the tunnel and opens the door for using correlations to determine variation in mechanical parameters from other physical variables.

Table 2.4. Results from ANOVA analysis.

Variable	Factor	F-test	P-value	Significance
P-wave velocity for intact samples (m/s)				
	Depth of samples (m)	0.87	0.5365	NO
	Number of borehole (1 or 2)	1.06	0.3070	NO
Normalised P-wave velocity for heated samples				
	Depth of samples (m)	0.90	0.5109	NO
	Temperature (ºC)	54.63	0.0000	YES
	Cooling method (air or water)	13.32	0.0000	YES
Normalised UCS for heated samples				
	Depth of samples (m)	2.10	0.0625	NO
	Temperature (ºC)	12.32	0.0000	YES
	Cooling method (air or water)	3.43	0.0406	YES

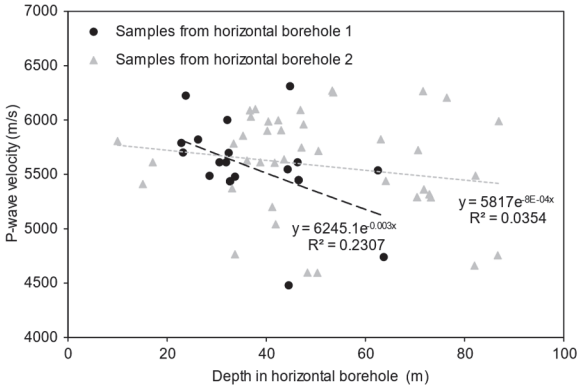

Figure 2.11. Simple regression analysis of P-wave velocity and sample position.

2.3.5. Correlations between physical and mechanical properties.

As described above, some correlations have been proposed in this work to predict the variation of UCS and elastic modulus (E) from the variation in physical properties (volume, open porosity, and P-wave velocity) for both air and water-cooled samples. With this aim, simple regression curves and their respective coefficient of determination (R^2) were calculated (Table 2.5). The best coefficients of determination were found when using exponential and potential curves. To discuss predictions of mechanical properties from physical parameters in detail, we have calculated the difference between the estimated and the observed values (i.e. the residuals) of UCS (Table 2.6) and E (Table 2.7). Potential functions were used in all cases, except to predict E from P-wave velocity, where exponential functions exhibited the best coefficients of determination.

The proposed functions for the prediction of UCS from normalised volume are represented in Figure 2.12a. Calculated values for air-cooled samples were greater than observed for intermediate temperatures of 200, 400 and 600º C, and smaller than observed at 500º C. The average residual for all temperatures was 20 MPa, and 21 MPa for the highest temperatures (400 to 600º C). The fitting was better for water-cooled samples, especially for intermediate and higher temperatures (300 to 600º C). The average residual for all temperatures was 16 MPa, and 6 MPa for the highest temperatures. Predicted values using normalised open porosity (Figure 2.12b) were greater for air-cooled samples than those observed for temperatures of 200, 400 and 600º, and smaller at 500º C. The average residual for all temperatures and the highest temperatures was 21 MPa. The obtained function showed better predictions for water-cooled samples, since the average residual for all temperatures was 20 MPa, and 7 MPa for the highest temperatures. The correlation between UCS and normalised P-wave velocity was represented (Figure 2.12c). The average residuals for air-cooled samples were 22 MPa for all data, and 25 MPa for the highest temperatures. The fitted function was close to linear for water-cooled samples, and residuals were minimum for almost every temperature, since the average

residual was 9 MPa for all the dataset and 7 MPa for the highest temperatures. Correlation functions exhibited good predictions for E for all physical parameters and cooling methods, and the residuals were in all cases lower than those obtained for UCS predictions. Predicted values for normalised volume are represented in Figure 2.13a, and for air-cooled samples were greater than those observed for intermediate temperatures of 400 and 500º C, and smaller than those observed at 600º C. The average residual for all temperatures and the highest temperatures was 5 GPa. The fitting was better for water-cooled samples for temperatures of 300, 500, and 600º C, although predicted values for 400º C were clearly greater than observed. The average residual for all the dataset and for the highest temperatures was 6 GPa. Predicted values using normalised open porosity (Figure 2.13b) were greater for air-cooled samples than for those observed at 500º C, and smaller at 600º C. The average residual for all temperatures was 4 GPa, and 3 GPa for the highest temperatures. Predicted values for water-cooled samples were greater than observed at 400º C and slightly lower at 500º C. The average residual for all temperatures was 8 GPa, and 5 MPa for the highest temperatures. Finally, the correlation between E and normalised P-wave velocity (Figure 2.13c) exhibited greater predicted values than those observed at 400 and 500º C, and smaller at 600º C. Average residuals for air-cooled samples were 4 GPa for all data, and 5 GPa for the highest temperatures. For water-cooled samples, the predicted values were smaller than those observed at 200 and 500º C, and greater than those observed at 400 and 600º C. The average residual was 5 MPa for all the dataset and for the highest temperatures.

2.4. Discussion

Chemical analysis showed that Prada limestone was mainly formed by calcite (92.95 %) and a small fraction of dolomite (6.11 %). Thermal treatment led to a gradual decomposition of the latter as previously reported by different authors (Crosby et al. 2018; Meng et al. 2020). Slight or non-perceptible changes in calcite are considered normal for the range of temperatures between 105 and 600 ºC, because target temperatures were much lower than that for carbonate dissociation, that exhibit the highest decomposition rate at around 700 ºC, and is complete near 900 ºC (Ferrero and Marini 2001). The content of oxides remained almost unchanged with temperature and showed no clear trend. Thus, different mechanisms seem to be behind the observed variation for Prada limestone. Thermal damage is linked to the anisotropic expansion of calcite, since local thermal stress concentrations occur between mineral particles that lead to microcracking (Sippel et al. 2007; Yavuz et al. 2010). The loss of constitution water leads to the destruction of the mineral lattice, causing microstructural changes (including increased porosity) and rock expansion (Ranjith et al. 2012). Such microstructural changes could be directly observed for Prada limestone using SEM and MIP techniques, and the consequent rock expansion was registered in terms of an increase in open porosity and volume.

Table 2.5. Coefficients of determination (R^2) for simple regression curves studied to predict UCS and elastic modulus (E) from normalised (N) physical parameters (volume, open porosity, and P-wave velocity).

		R^2 for UCS predictions				R^2 for E predictions			
Parameter (N)	Cooling	Linear	Exponential	Logarithmic	Potential	Linear	Exponential	Logarithmic	Potential
Volume	air	0.61	0.69	0.61	0.69	0.86	0.90	0.86	0.90
	water	0.78	0.91	0.78	0.91	0.78	0.91	0.78	0.91
Open porosity	air	0.60	0.67	0.64	0.68	0.88	0.92	0.93	0.96
	water	0.75	0.89	0.79	0.88	0.71	0.87	0.84	0.91
P-wave velocity	air	0.61	0.64	0.60	0.65	0.90	0.94	0.87	0.92
	water	0.93	0.95	0.91	0.97	0.91	0.92	0.86	0.91

Table 2.6. UCS values from laboratory tests and predicted from normalised values (N) of physical parameters for each temperature, based on potential functions. Residuals have been also represented.

		Volume (N)			Open porosity (N)			P-wave velocity (N)		
Temperature (º C)	Cooling	Predicted UCS (MPa)	Measured UCS (MPa)	Residual (MPa)	Predicted UCS (MPa)	Measured UCS (MPa)	Residual (MPa)	Predicted UCS (MPa)	Measured UCS (MPa)	Residual (MPa)
105	air	124.80	168.09	-43.29	130.71	168.09	-37.38	133.89	168.09	-34.20
	water	126.64	168.09	-41.45	137.60	168.09	-30.49	156.33	168.09	-11.76
200	air	127.78	117.46	10.32	136.09	117.46	18.63	125.49	117.46	8.03
	water	141.86	110.57	31.28	157.84	110.57	47.27	129.51	110.57	18.93
300	air	127.64	128.01	-0.37	121.83	128.01	-6.17	114.33	128.01	-13.67
	water	115.54	111.57	3.97	94.03	111.57	-17.54	117.14	111.57	5.58
400	air	106.20	72.49	33.71	98.62	72.49	26.12	110.94	72.49	38.45
	water	93.17	102.68	-9.51	87.93	102.68	-14.75	87.70	102.68	-14.98
500	air	68.57	91.92	-23.35	63.98	91.92	-27.95	66.29	92.53	-26.24
	water	52.31	45.02	7.30	51.51	45.02	6.49	42.80	45.02	-2.21
600	air	29.92	31.58	-1.66	32.70	31.58	1.12	34.00	31.58	2.42
	water	50.46	44.40	6.06	54.75	44.40	10.35	53.28	44.40	8.88

Table 2.7. Elastic modulus (E) values from laboratory tests and predicted from normalised values (N) of physical parameters for each temperature, based on potential functions except for P-wave velocity, where exponential functions enabled the best predictions. Residuals have been also represented.

		Volume (N)			Open porosity (N)			P-wave velocity (N)		
Temperature (º C)	Cooling	Predicted E (MPa)	Measured E (MPa)	Residual E (MPa)	Predicted E (MPa)	Measured E (MPa)	Residual E (MPa)	Predicted E (MPa)	Measured E (MPa)	Residual E (MPa)
105	air	64.41	77.37	-12.96	67.42	77.37	-9.94	73.13	77.37	-4.23
	water	60.45	77.37	-16.92	67.49	77.37	-9.88	82.28	77.37	4.91
200	air	66.32	65.48	0.84	71.01	65.48	5.53	65.54	65.48	0.06
	water	69.37	70.29	-0.92	79.91	70.29	9.62	60.49	70.29	-9.79
300	air	66.22	63.96	2.26	61.59	63.96	-2.37	56.42	63.96	-7.54
	water	54.08	56.22	-2.15	42.24	56.22	-13.99	54.73	56.22	-1.50
400	air	52.79	49.52	3.27	46.92	49.52	-2.60	57.66	49.52	8.14
	water	41.65	27.23	14.42	38.89	27.23	11.66	34.24	27.23	7.01
500	air	30.78	24.15	6.63	26.89	24.15	2.74	28.20	24.15	4.05
	water	20.68	22.76	-2.08	20.13	22.76	-2.62	16.22	22.76	-6.53
600	air	21.08	25.00	-3.92	22.01	25.00	-3.00	22.04	25.00	-2.97
	water	10.50	10.82	-0.32	11.51	10.82	0.69	13.54	10.82	2.73

Although the visual appearance of Prada limestone was very homogeneous, samples presented the slight variations that are typical of such natural materials (including changes in the grey tone and the presence of calcite veins) in contrast to manufactured materials whose composition and texture can be controlled. In our study, standard deviation (SD) on UCS for all temperatures was 23.07 MPa with a maximum value of 37.94 MPa at 600 ºC. These values are similar to those reported by Sengun (2014) (mean SD 25.28 MPa; and maximum SD 31.7 MPa). For elastic modulus, we registered mean SD for all temperatures of 8.21 GPa with a maximum of 13.80 GPa at 400 ºC, which are of the same order of magnitude as those obtained by González-Gómez et al. (2015) (mean SD 10.17 GPa; maximum SD 15 GPa). We state that accuracy in our results can be considered normal for a natural material such as the studied rock. Trends have been discussed in view of mean values and also considering standard deviation at each temperature. This leads us to make conclusions based on general trends and to dismiss variations based on mean values when SD is high.

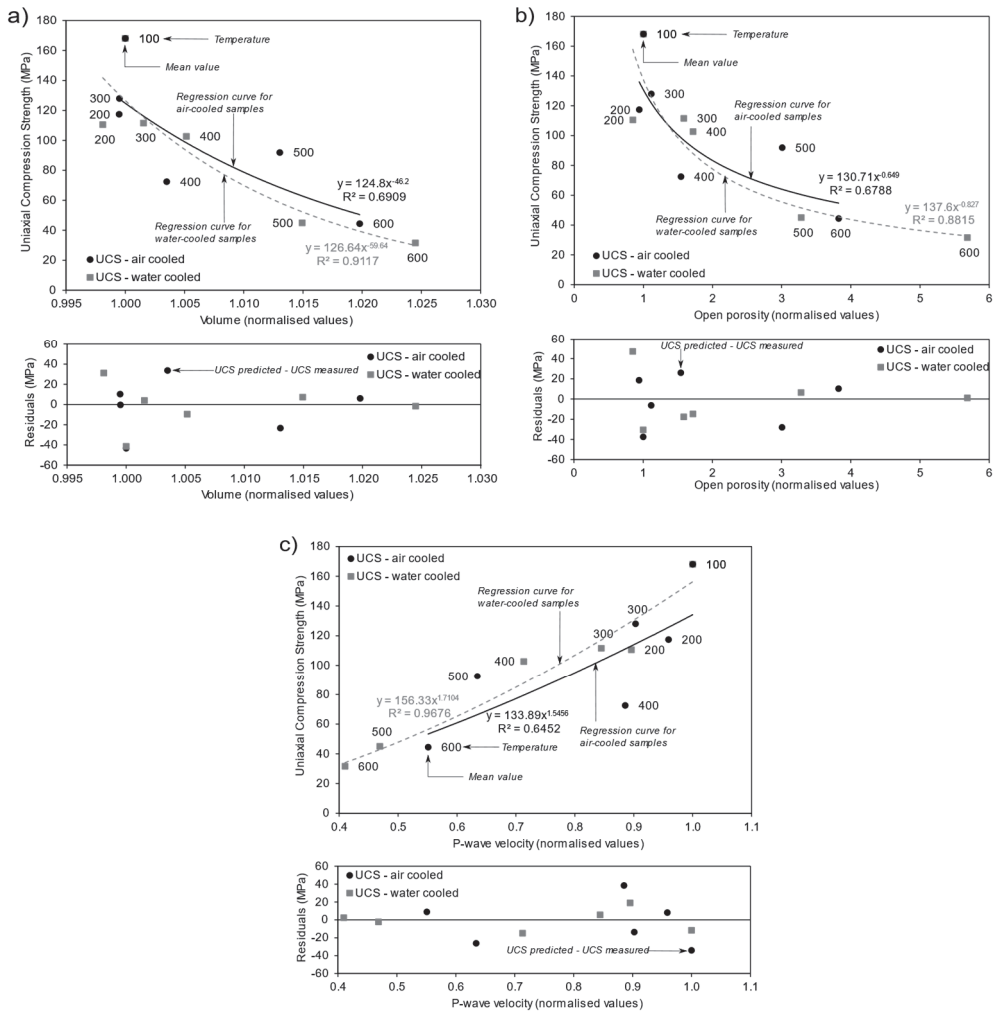

Figure 2.12. Correlation between UCS and normalised values of volume variation (a), open porosity (b) and P-wave velocity (c) using potential functions.

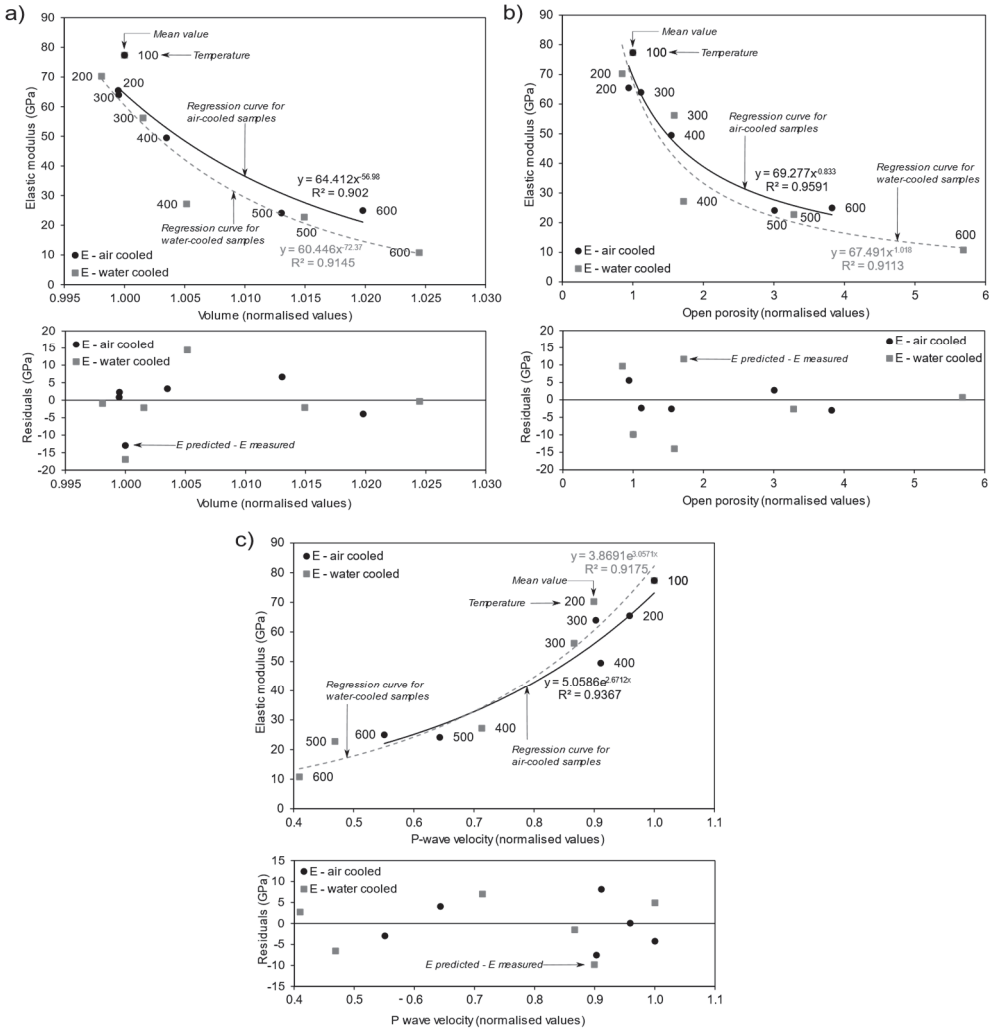

Figure 2.13. Correlations between static elastic modulus and normalised: (a) volume variation; (b) open porosity; and (c) P-wave velocity.

Thermal effects on Prada limestone at lower temperatures (105 to 200 ºC) refer to a dramatic drop in UCS of more than 30% for all cooling methods (Figure 2.7) which were previously reported at low temperatures by Lion et al. (2005). Thus, structural resistance within the Tres Ponts Tunnel may be affected from the initial stages of a fire. A decrease in elastic modulus at 300 ºC coincided with an increase in open porosity for water-cooled samples, and this points to an influence of the cooling method at intermediate temperatures. Furthermore, when open porosity increases, elastic modulus also decreases

at 400 ºC, as observed for low-porosity limestones (such as Prada) in previous research (Yavuz et al. 2010; Sengun 2014). Such variation in open porosity and elastic modulus is explained by means of an expansion of fissures with temperature that leads to a considerable deformation (as observed on stress-strain plots on Figure 2.8). This is consistent with other works (Lion et al. 2005; González-Gómez et al. 2015), and produces a gradual decrease in the elastic modulus (Zhang et al. 2017b). A decrease in ultrasound velocity was registered at 400 ºC due to thermal cracking, as reported for limestone by different authors (Yavuz et al. 2010; Andriani and Germinario 2014; Sengun 2014; Yang et al. 2019). This fact is consistent with initial trans-granular fissures and porosity observed using SEM at 400 ºC (Figure 2.2b). P- and S-wave velocities decrease and elastic modulus drops were greater for water-cooled samples, so the induced micro-structural changes are a function of the maximum temperature as deduced by Crosby et al. (2018) and the cooling method. The dynamic elastic modulus trend was similar to that observed for P- and S-wave since ultrasound velocities describe similar trends and dry unit weight showed little variation. It is worth noting that dynamic and static elastic modulus showed similar differences for air- and water-cooling methods for temperatures equal to and greater than 400 ºC. The temperature of 500 ºC marked a key point for Prada limestone. Samples showed a sharp increase in open porosity for both cooling methods, as well as a decrease in P- and S-wave velocities. This threshold temperature also exhibited a significant growth in the density of trans-granular fissures observed by SEM (Figure 2.2c), as previously reported by Chen et al. (2009). For these reasons, 500 ºC is a threshold temperature from which severe physical damage develops in Prada limestone. Differences induced by the cooling method were perceived for mechanical resistance, since samples cooled by water immersion exhibited a steep drop in the compressive strength of the rock, probably related to the enlargement, coalescence, and connectivity of the trans-granular fissures observed by SEM (Figure 2.2d) in water-cooled samples. The trends at 600 ºC showed slight variations after the abrupt changes observed at up to 500 ºC, in agreement with the work published by Zhang et al. (2017b). Porosity was an exception and continued exhibiting a significant increases for water-cooled samples. It is remarkable that final values at 600 ºC showed greater variations for water-cooled samples for most parameters, and this indicates greater thermal damage when samples are cooled by water immersion – which is consistent with the results published by Brotóns et al. (2013).

A controversial issue arises in the variation of Poisson's ratio for high temperature. Some authors did not report any induced effect of temperature on the rocks (Heuze 1983; Zhang et al. 2018) or describe a decreasing trend (Lion et al. 2005; Brotóns et al. 2013; Zhang et al. 2017b). However, Yang et al. (2019) suggest that the different instrumental devices, methods, or even the diversity of samples, could lead to such scattered results. This study throws light on this aspect and advances in the analysis of this mechanical parameter using both slow and rapid cooling methods. A continuous decrease in Poisson's ratio can be observed in all cases. This trend is related to a greater transverse

ductility in the sample in view of the axial stress-lateral strain curves determined in our study.

The performed ANOVA (Table 2.4) and simple regression analyses (Figure 2.11) confirmed the negligible impact of the sample positions (meaning their location in the borehole) in the variability of physical and mechanical properties. As a conclusion, the laboratory results for the different samples can be compared regardless of the borehole from which they were obtained and their location within the borehole. This fact opens the door to the possibility of generalising laboratory results throughout the tunnel to determine variation in mechanical parameters (UCS and elastic modulus) from other physical parameters (normalised volume, open porosity, and P-wave velocity) in the event of a fire. Consequently, simple correlations can be fitted to indirectly obtain reference values for the rock affected by temperature in order to make initial decisions after a fire in the tunnel, since previous experiments show that simple regression can provide good predictions for intact carbonate rocks (Yasar and Erdogan 2004).

In this research, the best predictions were achieved using exponential and potential functions. Focusing on UCS predictions for air-cooled samples, the coefficients of determination varied depending on the physical property studied (between 0.65 and 0.69), that is, fitting-quality and average residuals (between 20 and 25 MPa) were similar for all the predictors studied. Samples cooled with water showed better determination coefficients between 0.88 and 0.97, the latter being for correlations with P-wave velocity, and average residuals were calculated between 9 and 20 MPa, being minimal when using P-wave velocity. Predictions for water-cooled samples were more accurate for the highest temperatures (between 400 and 600 ºC), with residuals of 6 – 7 MPa, with P-wave velocity being the best predictor in the analysis. In the case of elastic modulus predictions, coefficients of determination varied from 0.87 to 0.96 and average residuals for the highest temperatures were calculated between 3 and 6 GPa for all predictors and cooling methods. Predictions of elastic modulus by means of potential and exponential functions were more accurate than those of UCS, with little difference between predictors and cooling methods. The influence in data accuracy has also been evaluated. Predictions of UCS and elastic modulus using normalised volume requires the observation of changes in the third decimal, and the accepted accuracy in volume determination using buoyancy techniques is 0.1 g (Franklin 1979) and this implies a variation in the fourth decimal in the calculated normalised volume. This makes such correlation little sensitive to the accuracy of the data determination. In the case of predictions made from normalised open porosity, an accuracy of 0.1% is accepted in open porosity determination (Franklin 1979). This means that variation in the third decimal could be expected in the normalised values, and so predictions using open porosity would be little sensitive to data accuracy. Accuracy in ultrasound P-wave time is 0.1 μs, and consequently, variation in the third decimal could be expected in the P-wave normalised values, and so that correlation is insensitive to data accuracy. For these reasons, such correlations enable predicting mechanical parameters from non-destructive tests on limestone affected by high temperatures.

2.5. Conclusions

In this research, samples from Prada limestone were taken from two horizontal boreholes in the design stage of the Tres Ponts Tunnel. Samples were thermally treated at temperatures of 105, 200, 300, 400, 500 and 600 ºC, and subsequently air or water-cooled. Variation in chemical composition and microstructure, as well as physical (open porosity, volume, P- and S-wave velocities) and mechanical (uniaxial compressive strength, elastic modulus, and Poisson's ratio) properties were analysed. The following are the primary conclusions:

1. Prada limestone is a rock formed by calcite (92.95 %) and a small fraction of dolomite (6.11 %). Thermal cracking is mainly associated with anisotropic expansion of calcite. A clear increase in cracking and porosity with temperature was observed using SEM and MIP and this leads to the loss of physical and mechanical properties.
2. Rocks showed severe weakening in terms of a drop in UCS even at low temperatures (T<200ºC). Therefore, the structure might be threatened in the initial stages of a fire. Thermal Tres Ponts Tunnel damage (open porosity increase, as well as P- and S-wave velocity decay) increased in the range of temperatures between 300 and 400 ºC according to porosity and micro-fissure progression, and damage was greater in water-cooled samples.
3. The temperature threshold of 500 ºC is of paramount importance in Prada limestone and is linked to a dramatic increase in porosity and a decrease in P- and S-wave velocity, and this is associated with the trans-granular fissure progression observed using SEM. Such fissures are larger and more connected in water-cooled samples, which lead to appreciable loss in UCS. Consequently, emergency intervention plans in the Tres Ponts Tunnel should consider such effects when deciding on fire-extinction methods.
4. A final temperature of 600 ºC confirmed greater thermal damage due to water-cooling, as values showed greater variation for most parameters. UCS was of above 20 % that for the intact rock and higher temperatures led to samples losing their integrity due to mass cracking.
5. ANOVA and simple regression analyses enabled discarding a significant influence of the natural sample position in the variability of physical and mechanical properties, therefore results can be compared between different samples, and conclusions can be generalised throughout the tunnel.
6. Predictions for elastic modulus were more accurate than those for UCS, with little difference between predictors and cooling methods. Calculated values of UCS after thermal treatment were better for water-cooled samples, especially when using P-wave velocity as a predictor. Exponential and potential functions exhibited best coefficients of determination, are easy to use, and provide quick indicative values to make the initial decisions after a tunnel fire.

This study provides an in-depth insight into the changes induced by temperature in the properties of Prada limestone. The obtained results enable evaluation of the degree of damage and any changes produced in the Tres Ponts Tunnel excavated in this limestone if it is affected by a fire that produces thermal effects.

Chapter 3. Temperature-induced explosive behaviour and thermo-chemical damage on pyrite-bearing limestones: causes and mechanisms

Authors:	Víctor Martínez-Ibáñez, David Benavente, Carlos Hidalgo Signes, Roberto Tomás, María Elvira Garrido		
Status:	Manuscript published		
Journal:	Rock Mechanics and Rock Engineering, 2021		
DOI	https://doi.org/10.1007/s00603-020-02278-x		
JCR IF (2019)	4.140		
	JCR Category	Ranking	Quartile
	Geological Engineering	*5/39*	*Q1*
	Multidisciplinary Geoscience,	*25/200*	*Q1*
Presentation:	Post-print (Author version)		

Abstract

In this investigation, two different varieties of Prada limestones were studied: a dark grey texture, bearing quartz, clay minerals, organic matter and pyrites, and a light grey texture with little or no presence of such components. We have observed two effects of different intensity when heating the dark texture from 400 ºC: i) the explosion of certain samples and ii) greater thermal damage than in the light grey texture. Chemical and mineralogical composition, texture, microstructure, and physical properties (i.e. colour, open porosity, P and S-wave velocity) have been evaluated at temperatures of 105, 300, 400 and 500 ºC in order to identify differences between textures. The violence of the explosive events was clear and cannot be confounded with ordinary splitting and cracking on thermally treated rocks: exploded samples underwent a total loss of integrity, displacing and overturning the surrounding samples, and embedding fragments in the walls of the furnace, whose impacts were clearly heard in the laboratory. Thermogravimetric results allowed the identification of a process of oxidation of pyrites releasing SO_2 from 400 ºC. This process jointly with the presence of micro-fissures in the dark texture, would cause a dramatic increase in pore-pressure, leading to a rapid growth and coalescence of microcracks that leads to a process of catastrophic decay in rock integrity. In addition to the explosive events, average ultrasound velocities and open porosity showed a greater variation in the dark grey texture from 400 ºC. That results also points towards a significant contribution of oxidation of pyrites on the thermo-chemical damage of the rock, among other factors such as the pre-existence of micro-fissures and the thermal expansion coefficient mismatch between minerals. Implications in underground infrastructure and mining engineering works are critical, as the explosive potential of pyrite-bearing limestones bear risk for mass fracturing and dramatic strength decay from 400 ºC. Moreover, SO_2 released has harmful effects on health of people and the potential to form acid compounds that corrode materials, shortening their durability and increasing maintenance costs.

Keywords

limestone; pyrite oxidation; thermal treatment; explosive behaviour; thermo-chemical damage

3.1. Introduction

The variation in physical, mineralogical, and mechanical properties of rock with temperature is an issue of current interest among the scientific community, due to its applicability in different fields of engineering and architecture – such as mining (Behnia et al. 2017), geothermal energy (Pei et al. 2018), underground storage of radioactive waste (Zhang et al. 2017a), building materials (Brotóns et al. 2013; Fioretti et al. 2018), tunnelling (Nordlund et al. 2014), and rock drilling (Rossi et al. 2018). As a general overview, an increase in temperature leads to a growth in pores and fissures, and a decrease in ultrasonic wave propagation, uniaxial compression strength, and elastic modulus. Altogether, a temperature increase points to a decay in rock integrity, whose magnitude and key temperatures strongly depend on the type of rocks, and their diverse physical and mineralogical properties.

Limestone is one of the most common types of sedimentary rocks. Its mineralogical composition is mostly calcite, which presents an anisotropic thermal expansion. A decrease in strength limit due to microcracking at relatively low temperatures (up to 250 ºC) was described for a limestone from Anstrude (France) (Lion et al. 2005). Below 150 ºC, microcracking does not seem to occur according to Yavuz et al. (2010), who observed a marked decay in physical properties (i.e. bulk density, P-wave velocity, and effective porosity) above 400ºC. A clear reduction in uniaxial compression strength (UCS) from 500ºC, and a tendency to redden when heating, were described for calcareous and dolomitic rocks from Apulia in Italy (Andriani and Germinario 2014). Temperatures above 600ºC usually mark a dramatic decline in UCS (Sengun 2014). Subsequent research contributed by accurately setting the temperature variation ranges for limestones from Linyi, China (Zhang et al. 2017b). These authors indicated that from 200 to 500 °C the porosity and pore volume rapidly increased, and from 500 to 600 °C the porous parameters were relatively stable. The maximum strength slowly decreased while peak strain continuously increased, elastic modulus declined quickly, Poisson's ratio dropped suddenly, and the hardness decreased from mid-hard to soft. Recently, research correlated physical and mechanical properties to define a thermal damage factor (Yang et al. 2019).

Different mechanisms control thermal damage of rocks, where the heating/cooling rate plays a fundamental role. On the one hand, a sharp variation of temperature when cooling (quenching) leads to tensile stresses that nucleate cracks (Mallet et al. 2014) even at temperatures below 300 ºC (Kim et al. 2014), causing a reduction on strength and elastic properties and enhancing permeability (Kumari et al. 2018). Such effect can be observed after high local heating rates (i.e. greater than 5 ºC/s), where thermal cracking is dominated by the stress concentrations caused by high thermal gradients (Nordlund et al. 2014; Rossi et al. 2018). On the other hand, low heating rates cause thermal cracking in carbonate rocks mainly controlled by the anisotropic expansion of calcite (Sippel et al. 2007; Yavuz et al. 2010). Finally, thermo-chemical damage involves some specific

chemical reactions, such as thermal decomposition of calcite that starts at 500 ºC, exhibiting the highest decomposition rate at around 700 ºC, and being complete near 900 ºC.

Presence of pyrites may be common in limestones with organic content (Berner 1985), and that gives them a dark tone. Such pyrites could experiment thermal oxidation when limestones are heated. The investigation of pyrite thermal oxidation is important in a wide number of productive fields. The wide occurrence of pyrite in different minerals and coals makes it one of the main sources of SO_2 (acid rain precursor) emission from various industrial activities, such as coal conversion (Seehra and Jagadeesh 1981), power production (Lv et al. 2015), and cement production (Hansen et al. 2003; Cheng et al. 2014). Pyrite in auriferous and carbonaceous matters is usually found in association with valuable metallic elements such as Au, Ag, and Cu and their recovery includes the oxidative roasting of raw materials (Zhang et al. 2019). Pyrite is common in sedimentary rocks studied as a potential host rock for radioactive waste like claystone, and its oxidation is harmful to the corrosion kinetics of metallic engineered components (Verron et al. 2019). The oxidation reaction of pyrite is a destabilising factor in commercial emulsion explosive products, due to its exothermic reaction (Xu et al. 2015). In ceramic production, research focuses on reducing sulphur emissions produced when heating clays containing pyrites – which involve defects in the final product (Gómez-Tena et al. 2014).

However, investigations describing thermo-chemical damage on pyrite-bearing rocks are scarce, although this type of rocks is common in civil and mining engineering works. In this research, we study the thermal behaviour of a pyrite-bearing limestone from Prada formation (Spain) to explore the causes and mechanisms of induced thermal damage. To this aim, we evaluate the variation of physical properties (colour, open porosity, P and S-wave velocities) at different temperatures between 105 and 500 ºC; we determine chemical, mineralogical, and microstructure changes; and we pay special attention to the thermal reactions involved and the released gases.

3.2. Materials and methods

Rock samples were taken from two horizontal boreholes in Organyà, in the Catalan south Pyrenean zone (Spain). Both were drilled in a lower Cretaceous limestone formation locally named Prada limestone, widely described by García Senz et al. (2002). The depth explored in horizontal borehole 1 was of 65.30 m and 91.45 m in borehole 2. Intact rock showed a bluish grey colour, and two varieties of samples could be clearly distinguished according to their lightness: light and dark grey.

Dark and light grey samples forming Prada limestone were separated in two groups. A total of 20 irregular fragments, with an average volume of 113±36 cm³, were then randomly selected from each group to determine the physical properties of the intact rock (i.e. dry density, water absorption, unit weight of solids, total and open porosity) and to compare the variation of open porosity with increase of temperature. In addition, a total of 68 cylindrical samples of 63 mm in diameter and a slenderness of 1.0 and 2.5 were

chosen among both dark and light grey specimens to compare thermal damage between textures. Finally, four cylindrical samples were selected from each group to determine UCS for the intact rock. Table 3.1 depicts the number of samples tested for each group (dark or light grey) and their dimensions. All samples were identified by the borehole number and the depth at which they were extracted (Figure 3.1). A temperature of 105 ºC was applied to remove moisture content and are considered references for the determination of the intact rock properties.

Table 3.1. Number of samples tested for each group (dark or light grey). All samples were first heated at 105 ºC, then treated at 300, 400 and 500 ºC. Additional 4 cylindrical samples from each group were used to determine UCS for the intact rock (at 105ºC).

Temperature (ºC)	Dark grey limestones		Light grey limestones	
	Irregular samples	Cylindrical samples	Irregular samples	Cylindrical samples
105	15	34	15	34
300	5	10	5	10
400	5	10	5	10
500	5	10	5	10

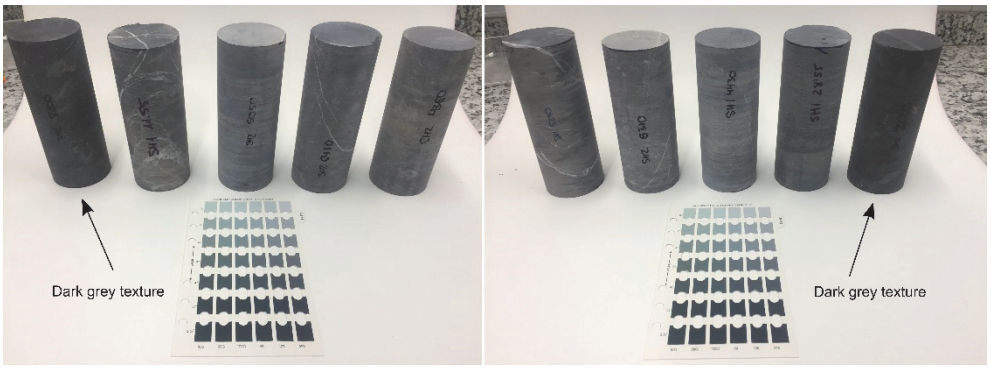

Figure 3.1. Cylindrical cores from Prada limestones before thermal treatment. Samples with a dark grey texture are identified in the figure.

Samples were subjected to thermal treatment, except those used for UCS tests. The heating process was performed in a furnace under air atmosphere and constant pressure. Temperatures of 300, 400, and 500 ºC were selected and a gradient of 5 ºC/min was applied. Once the target temperature was reached, it was maintained for one hour. Then, cooling stage started inside the furnace at a slow rate from 5 to 1 ºC/min. Once the temperature inside the furnace reached 300 ºC, limestones were then put outside the furnace and naturally cooled at air (at a slow rate) to room temperature (21 ºC). It is worth noting that during the heating process, one thermocouple registered the temperature inside the furnace, another thermocouple was in contact with the surface of one cylindrical sample,

and a third one was installed inside the sample, in a small drill made along its axis. The evolution of the temperature was registered every minute using a PicoLog 6 data logger. Special attention was paid to perceptible sounds through the furnace chamber indicating explosions of samples during heating, and the temperature at which that occurred. Once the furnace was opened, the explosive events of certain samples had already happened, and the visual damage were recorded.

Fragments from representative dark and light grey rock fractions were then pulverised. Total carbon, sulphur, and sulphides content were determined over pulverised rock samples using an IR spectrometer after heating in a furnace. The whole rock analysis was performed using fusion and X-ray fluorescence.

Determination of oxidizable organic matter aims to explain the different coloration between light and dark grey textures. To do so, finely ground rock samples previously subjected to 105 ºC and 500 ºC were selected, and oxidizable organic matter contents were determined using potassium permanganate, according to Spanish standard (UNE-EN-103204 2019).

Thermal analyses of dark grey samples were conducted using thermogravimetric, differential thermal analysis, and differential scanning calorimetry, TG-DTA-DSC, and TG-DTA coupled to a mass spectrometer. TG-DTA-MS and TG-DTA-DSC experiments were performed using a NETZSCH STA 449 Jupiter F5 thermal analyser. The NETZSCH Aeölos Quadro Mass Spectrometer was coupled to the TG-DTA analyser. Measurements were conducted under dynamic mode from 25 to 700 ºC at a heating rate 10 ºC min^{-1} under air conditions (N_2:O_2 in 4:1) at 50 ml/min.

The phase composition of samples was analysed by powder X-ray diffraction (XRD) on a Bruker D8-Advance diffractometer with a Goebel mirror (non-planar samples) using Cu Kα radiation and a setting of 40 kV and 40 mA. XRD data were collected and interpreted using the XPowder software package, which allows a quantitative analysis for the identified phases.

Optical and scanning electron microscopy (SEM) in backscattered electron mode was used to study the petrographic features of Prada limestone. Thin-section examination was performed under an optical polarising microscope (Model Zeiss Assioscop). For the SEM analysis, sample surfaces were polished with alumina and diamond powder; the finest abrasive was a 0.4 mm diamond powder. Uncovered polished surfaces were studied in a HITACHI S-3000 N variable pressure SEM working at low vacuum, and salt tested surfaces were analysed in a high vacuum SEM in secondary electron mode. The chemical analysis of the elements associated with the SEM images were accomplished using the energy dispersive X-ray (EDX) technique.

Mercury intrusion porosimetry (MIP) was used to obtain fine porosity results and pore size distribution in both dark and light grey samples. Tests were developed with a PoreMaster 60 GT (Quantachrome Instruments). The employed surface tensions and contact angles of mercury were 480 mN/m and 130°, respectively.

Physical properties of both dark and light grey limestones were determined using irregular samples. Dry density, water absorption, unit weight of solids, total and open porosity, were determined before and after thermal treatment using saturation and buoyancy techniques according to the suggested methods of the International Society for Rock Mechanics (ISRM) (Franklin 1979).

A preliminary colour classification of the intact rock was performed using Munsell soil colour charts (GLEY 2 chart for low chroma colours). To observe colour differences before and after heat treatment, both faces of samples were polished and moistened, and their image captured using an HP OfficeJetPro 7740 scanner with a resolution of 600 ppi. The average sRGB colour values of the pixels were obtained for representative regions of the material using software GIMP 2.10.12. The colour was described in terms of CIELAB space colour (CIE 1977), used by many authors (Pospíšil et al. 2007; González-Gómez et al. 2015) where L* represents lightness (i.e. the darkest black at L* = 0, and the brightest white at L* = 100), and a* and b* chromaticity. The a* axis represents green in the negative direction and red in the positive direction, and b* axis represents blue in the negative direction and yellow in the positive direction.

The presence of discontinuities such as pores and fissures, reduces the propagation velocity of the mechanical waves, and so it is a commonly used parameter to evaluate the evolution in rock deterioration. Thus, ultrasonic measurements were carried out over light and dark grey cylindrical samples before and after thermal treatment. The transmission method consists of two piezoelectric sensors coupled to the sample at constant pressure. Compressive (P) and shear (S) waves were measured using polarised Panametric transducers (1 MHz). Emitting-receiving equipment (Panametrics-NDT 5058PR) and an oscilloscope (TDS 3012B-Tektronix) were used to acquire and digitalise the waveforms to be displayed, manipulated, and stored. Every measurement of the P and S waves was repeated three times to test the reproducibility of the experiments and the corresponding results.

Finally, UCS tests were performed to determine mechanical properties for the intact rock (at 105 ºC) for both light and grey textures. A slenderness of 2.5 was decided to ensure their suitability according to ISRM suggested methods (Fairhurst and Hudson 1987). Core faces were polished to ensure flatness and perpendicularity relative to the axis. A four-column press machine Mecánica Científica SA model 28.5200 with a capacity of 2000 kN was used. A compression rate of 0.5 MPa/s was applied until the ultimate load and controlled by MecaTouch software v.1.1. Strain gauges of 30 mm long Tokyo Measuring Instruments Lab PF-30-11 (120.3±0.5 Ω, k=2.13±1) were used for longitudinal and transverse strains. Values were registered for each loading cycle using MecaSoft software v.1.3.8. The tangent Young's modulus and the corresponding Poisson's ratio were determined from values of 50% of the sample ultimate load

3.3. Results

3.3.1. Chemical, mineralogical, petrographic and microstructural characterisation

Prada limestone is a grainstone or biosparite with abundant bioclasts (0.2–2 mm): mainly planktonic foraminifera and minor amounts of molluscs, red algae, bryozoan, and frequently fragmented echinoderm (Figure 3.2). Some angular and sub-angular grains of monocristalline quartz (0.02–0.1 mm) are also present. Sub-rounded grains of iron sulphides (0.02–0.04 mm) are irregularly distributed in the limestone (Figure 3.2A). They can be found dispersed in the rock matrix and concentrated in grain borders, cement, or stylolites. Cement is abundant and mainly consists of micro and meso-crystalline mosaics of calcite spar. Cement fills interparticle (bioclasts) porosity. Syntaxial cement is related to fragmented echinoderms. Micritic matrix is minor (<5%) and irregularly distributed. Discontinuities are abundant and consist of fissures, calcite veins and a minor amount of stylolites (Figure 3.2E and Figure 3.2F).

Observations using SEM allowed identify two different textures on Prada limestones: dark and light grey. Samples with a dark grey texture showed a higher concentration of pyrite, quartz and fissures (Figure 3.3a) than those with a light grey aspect (Figure 3.3b). Fissures were mainly intergranular and did not show a preferred orientation. Pyrite appeared with both cubic and well-formed framboidal (raspberry like aggregates of pyrite spheres) geometries (Figure 3.3c) at 105 ºC with different sizes and distribution. Such structures evolved to incomplete framboids when heated to 500 ºC (Figure 3.3d). EDX analysis was performed over different framboidal structures. Thus, a structure heated to 105 ºC was formed mainly by Fe (30.97%) and S (34.48%), and a small fraction of O (4.78%), while another structure when heated to 500 ºC showed increased values for Fe (65.83%), a severe decrease in S (2.66%), and an appreciable increase in O (75.51%).

Chemical composition (expressed as weight percent) is different for both textures (Table 3.2). Dark grey texture presented SiO_2 (9.27 %), what is consistent with grains of monocristaline quartz referred above, and other oxide combinations such as Al_2O_3 (2.74 %), Fe_2O_3 (1.33 %) and K_2O (0.49 %) related to a clay fraction in the limestone. Sulphur was present in the dark texture (0.85 %), partly forming sulphide (0.60 %), and organic matter was also present (1.16 %). Moreover, light grey limestones showed residual or inexistent percentages of quartz and clay minerals, sulphide and organic matter, while percentages of CaO and C were slightly greater than in the dark texture. Results for dark grey limestones after calcination at 500 ºC revealed decreases in the total amount of sulphur, sulphide, total carbon and calcium, and an increase in quartz and clay compounds.

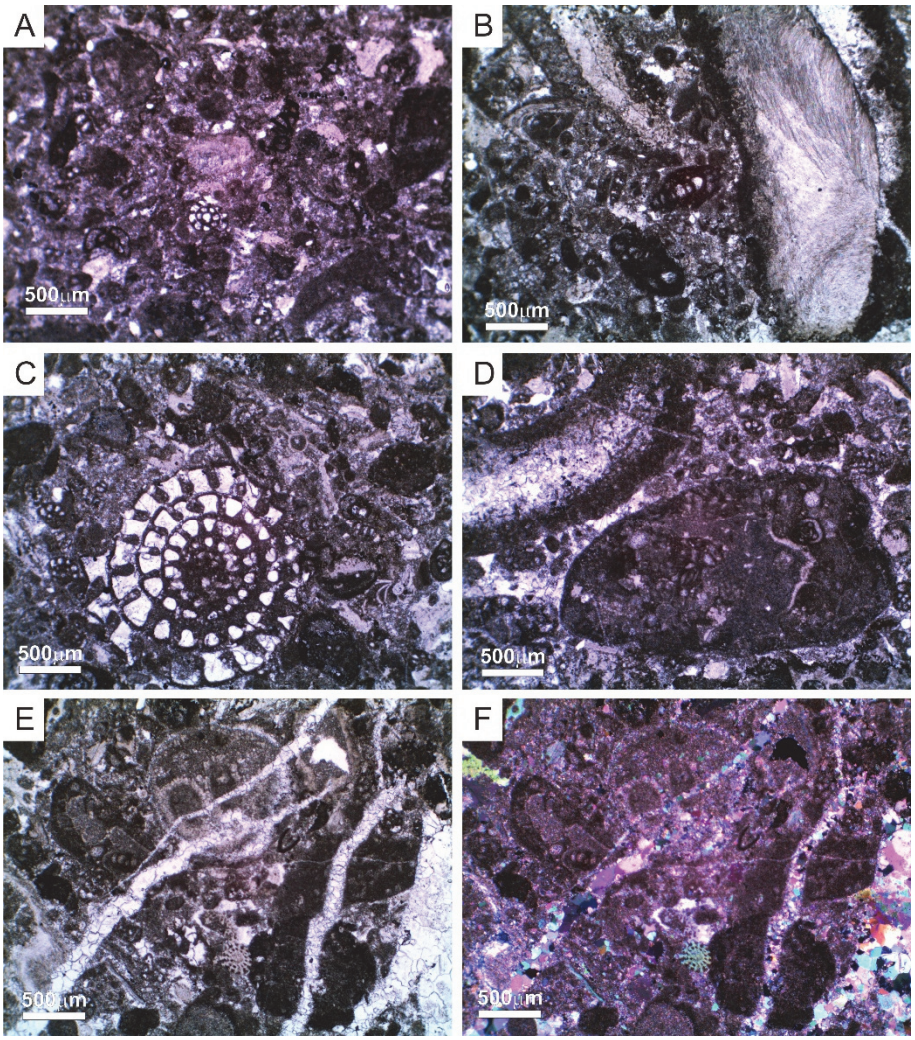

Figure 3.2. Optical microphotographs of intact Prada limestone. (A) Grain-supported texture composed of bioclasts, angular and sub-angular grains of quartz and sub-rounded grains of iron sulphides. Details of (B) molluscs, (C) foraminifera and (D) red algae. (E-F) Bioclasts and micritic matrix cut by calcite veins. Microphotographs were taken under (A-E) parallel-nicols and (F) crossed-nicols

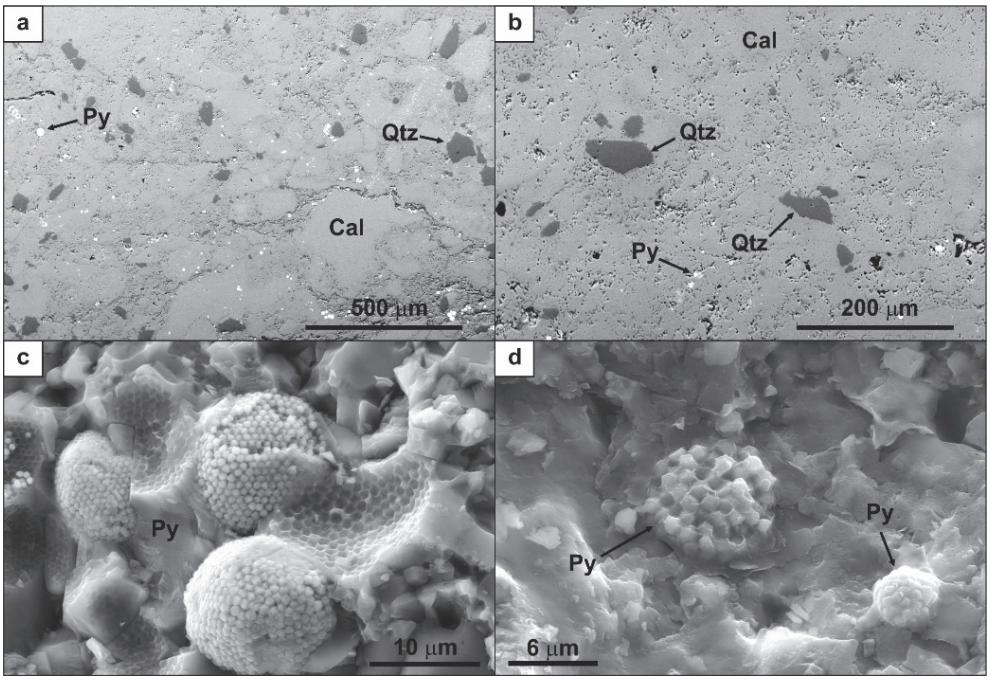

Figure 3.3. Images from scanning electron microscope of a dark grey sample (a) and a light grey sample (b) before thermally treated, showing different content of pyrites, quartz, and fissure distribution. Well-formed pyrite framboids appeared in dark grey samples heated to 105 ºC (c). Pyrite framboids showed uncomplete when heated to 500 ºC (d)

Table 3.2. Compounds registered on light and dark grey samples.

Compound (%)	Light grey samples	Dark grey samples	
	105 ºC	105 ºC	500 ºC
CaO	54.30	46.60	40.70
Al_2O_3	0.11	2.74	3.62
SiO_2	0.65	9.27	11.55
Fe_2O_3	0.19	1.33	1.52
K_2O	0.02	0.49	0.65
C_{total}	11.80	10.20	9.87
S_{total}	0.01	0.85	0.76
Sulphide	-	0.60	0.47
Organic matter	0.11	1.16	-

Results using XRD on dark grey samples before and after heat treatment enabled the determination of a greater proportion of pyrites (expressed as percentage by weight) in the intact rock (1.5%), and a decrease after heating to 500 ºC (1.2%). The presence of hematite was also registered after heat treatment on dark grey samples (0.6%). It is worth noting that XRD can only characterise crystalline solid phases and consequently any possible amorphous phase formed by the pyrite oxidation would be not detected using this technique.

TG-DTA-DSC and TG-DTA-MS experiments on dark grey samples were conducted up to 700 ºC, and allowed the identification of three different stages (Figure 3.4), involving the generation of different chemical compounds. Stage I (100 <T <200 ºC) showed an initial release of H_2O (Figure 3.4a). Stage II (400 <T <600 ºC) revealed a greater release of H_2O (Figure 3.4b), as well as of CO_2 (Figure 3.4d), with a peak at above 520 ºC. Also the release of SO_2 was recorded in a narrow range of temperatures, between 405 and 535 ºC, and showed a marked peak at 460 ºC (Figure 3.4c). Finally, stage III (T > 600 ºC) showed an increasing release of CO_2 with temperature (Figure 3.4d). Results on TG curve (Figure 3.4a) revealed a small weight loss in stages 1 and 2 (less than 0.5% in weight). DSC curve confirmed that reactions taking place on stage 2 are exothermic.

MIP analysis reflected dual porosity features on dark grey samples (Figure 3.5a), which is in concordance with the textural characterisation. The first pore family represents the interparticle porosity defined by grain minerals, cements, and fine-grains and shows a small pore size (in the pore range of 0.01-0.2 μm). A second pore family represents micro-fissures, which are more numerous, and appear in larger sizes (> 200μm) that MIP cannot measure completely. Otherwise, light grey samples showed interparticle porosity with greater pore size (lower than 1 μm), and very few micro-fissures (Figure 3.5b).

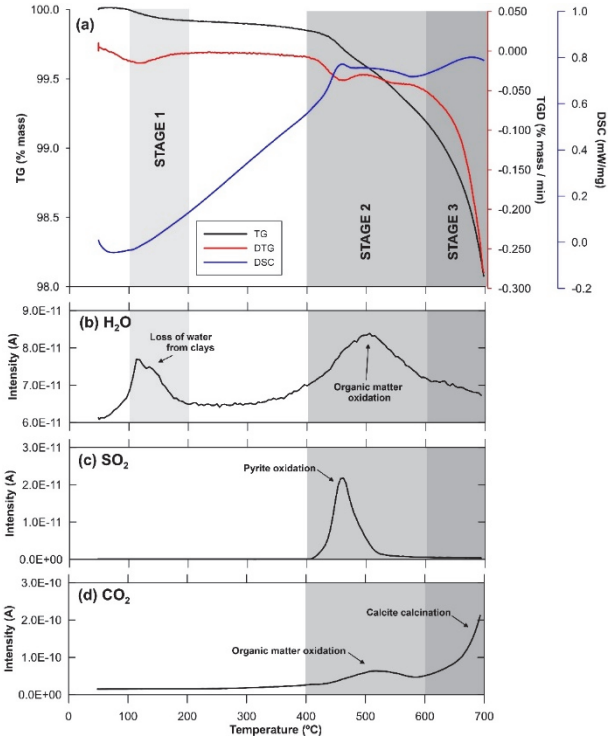

Figure 3.4. TG-DTA-DSC curves for the dark limestone (a) and MS curves for H_2O (b), SO_2 (c) and CO_2 (d)

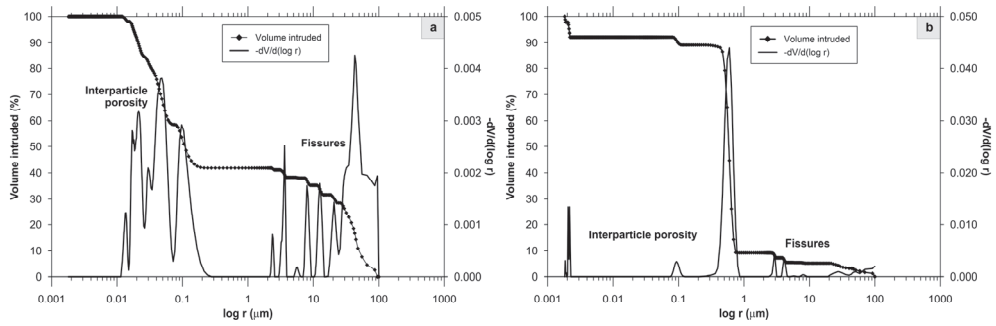

Figure 3.5. Cumulative mercury intrusion and pore size distribution curves of dark (a) and light grey (b) textures before thermally-treated.

3.3.2. Variation of physical properties by thermal treatment

Some dark grey samples exploded inside the furnace when heated at 400 ºC and 500 ºC exhibiting a total loss of structure and causing fragments spread over the furnace (Figure 3.6a, d, f, h), displacement, overturn or damage of the surrounding samples by fragments impacts (Figure 3.6f), and even the embedding of some rock pieces in the walls of the furnace (Figure 3.6a,b). We also perceived the sound of rock fragments impacting inside the furnace. It occurred instantly, and such impacts were violent enough to be clearly heard in the laboratory. Consequently, for the subsequent heating rounds the samples were covered with a metal protection grid to avoid further damage in the furnace (Figure 3.6c, d, g, h). The temperatures recorded by the thermocouples were 470 ºC inside the furnace, 438 ºC on the surface of an instrumented sample, and 390 ºC in its centre in the precise moment in which we heard the explosion of one sample. It is noteworthy that, after the explosion, the room was impregnated by an intense acrid smell attributed to the release of SO_2. That strong smell reached such intensity that a gas extraction system was needed, and we were forced to leave the room. We undoubtedly related such phenomenon with the explosive event, which due to its violence could not be confused with fracturing or splitting of the samples. Explosions were not registered for temperatures of 300 ºC, neither in the light grey samples. In addition to the exploded specimens, some dark samples fractured and clearly exhibited visible cracks. Table 3.3 summarizes the number of dark samples that showed differing grades of damage for each temperature. The maximum number of exploded samples was registered at 500 ºC, although the grade of fracturing of specimens was greater at 400 ºC, and not evident for temperatures lower than 300 ºC.

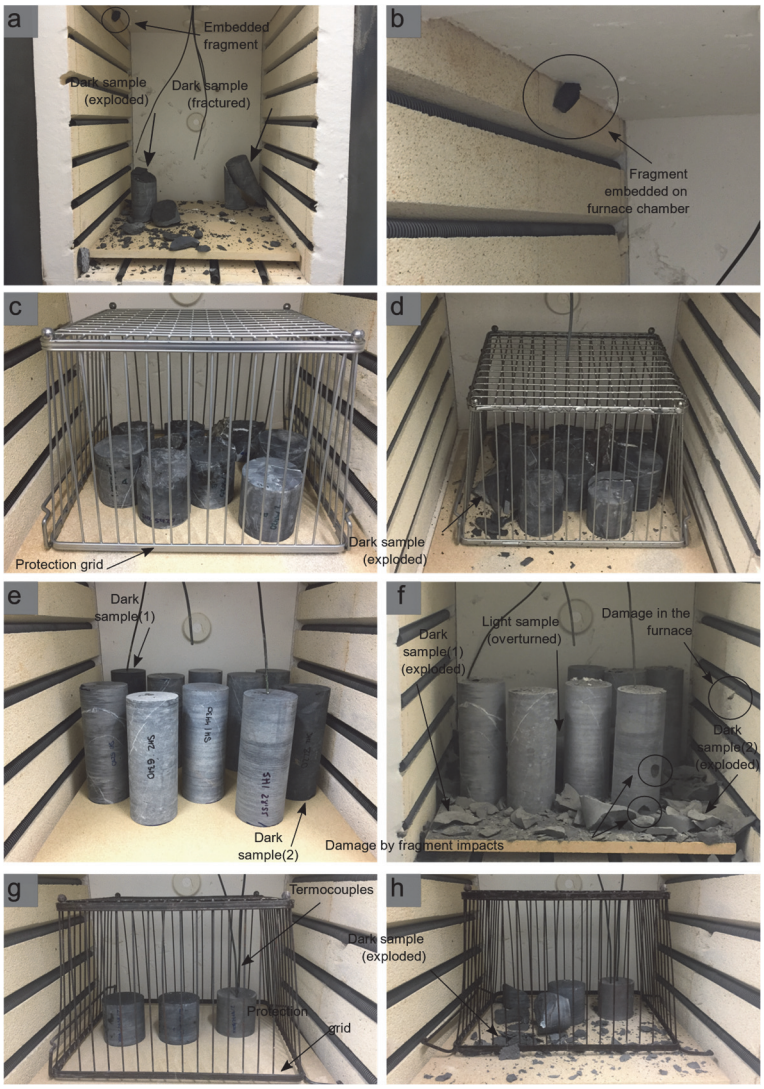

Figure 3.6. (a) Dark samples exploded or fractured when heated at 400 ºC. (b) Detail of the fragment embedded in the furnace chamber due to the violence of the event shown in (a). Dark samples before (c) and after (d) heating at 400 ºC. Note the protection grid used to preserve the furnace. Dark and light grey cores before (e) and after (f) heating at 500 ºC. Note that only dark cores exploded, and their fragments overturned and damaged the surrounding light grey samples and the furnace chamber. A new set of dark samples before (g) and after (h) heating at 500 ºC using the protection grid. The temperatures were being registered using thermocouples when one sample exploded.

Table 3.3. Number of samples that showed different grades of damage for each temperature.

Temperature	Grade of damage		
(ºC)	Explosion	Fracturing and visible fissures	No visible damage
300	0	0	10
400	2	4	4
500	4	2	4

Before discussing the evolution of physical and mechanical parameters with temperature of both textures, average values for the intact rock (defined at a reference temperature of 105 ºC) are depicted (Table 3.4). Values of physical parameters were in the same range for both textures, while mechanical parameters (UCS, Young's modulus, and Poisson's ratio) were smaller for the dark grey samples.

Table 3.4. Reference values for dark and light grey samples forming Prada limestone, heated at 105 ºC.

Parameter	Dark grey samples	Light grey samples
Dry density, ρ_d (kN/m^3)	26.80±0.24	26.84±0.25
Water absorption saturated (%)	0.46±0.36	0.45±0.20
Unit weight of solids, γ_s (kN/m^3)	27.23±0.01	27.21±0.01
Open porosity, n (%)	1.22±0.94	1.21±0.54
Total porosity, n (%)	1.60±0.89	1.46±0.91
P-wave velocity, V_p (km/s)	5.76±0.05	5.35±0.06
S-waves velocity, V_s (km/s)	3.11±0.02	2.65±0.02
Uniaxial compressive strength, σ_{ci} (MPa)	103.76±59.11	164.63±23.77
Young's modulus, E (GPa) (from mechanical tests)	50.65±20.44	77.69±6.54
Poisson's ratio, ν (from mechanical tests)	0.24±0.06	0.31±0.05

Open porosity trends were compared for both textures using normalised average values (i.e. results after heating were divided by those of the same samples obtained at the reference temperature of 105 ºC) (Figure 3.7a). The porosity showed little variation between 105 and 300 ºC, and then gradually increased from 300 ºC. Differences between textures appeared at 400 and 500 ºC. Normalised open porosity was greater on dark grey samples (2.61 at 400 ºC; 3.43 at 500 ºC) than on light grey (1.54 at 400 ºC; 3.01 at 500 ºC). Ultrasound wave velocity was also represented using normalised values. Values of P- (Figure 3.7b) and S-wave (Figure 3.7c) velocities progressively decreased with temperature for both textures, although the rate of decline accelerated between 400 and

500 ºC. Differences between both textures appeared at 400 and 500 ºC, since P-wave normalised velocity was smaller on dark grey samples (0.84 at 400 ºC; 0.57 at 500 ºC) than on light grey (0.89 at 400 ºC; 0.64 at 500 ºC); S-wave normalised velocity was also smaller on dark grey samples (0.87 at 400 ºC; 0.52 at 500 ºC) than on light grey (0.93 at 400 ºC; 0.75 at 500 ºC).

Intact rock showed a bluish grey colour, with different grades of lightness: Munsell colour values varied from light bluish grey (5B 6/1) to dark bluish grey (5B 3/1). Visual observation revealed colour variation when heating: one sample at 105 ºC (Figure 3.8a) evolved towards red and greater luminosity when heated at 400 ºC (Figure 3.8b); while reddening and lightness intensified when one sample was heated from 105 ºC (Figure 3.8c) to 500 ºC (Figure 3.8d). CIELAB values enabled the trend to be quantified: lightness L* and colour a*, b* increased with temperature, especially from 400 ºC, with maximum values at 500 ºC (Figure 3.8e). The most significant variation could be observed for L*, marking a clear trend towards lighter tones with higher temperatures, especially between 400 ºC and 500 ºC. In relation to colour parameter a *, a slight increasing trend could be observed at up to 400 ºC, and an accelerated reddening of the samples from 400 ºC to 500 ºC. The parameter b * marked lower values than a*, showing an increasing trend towards yellow with temperature.

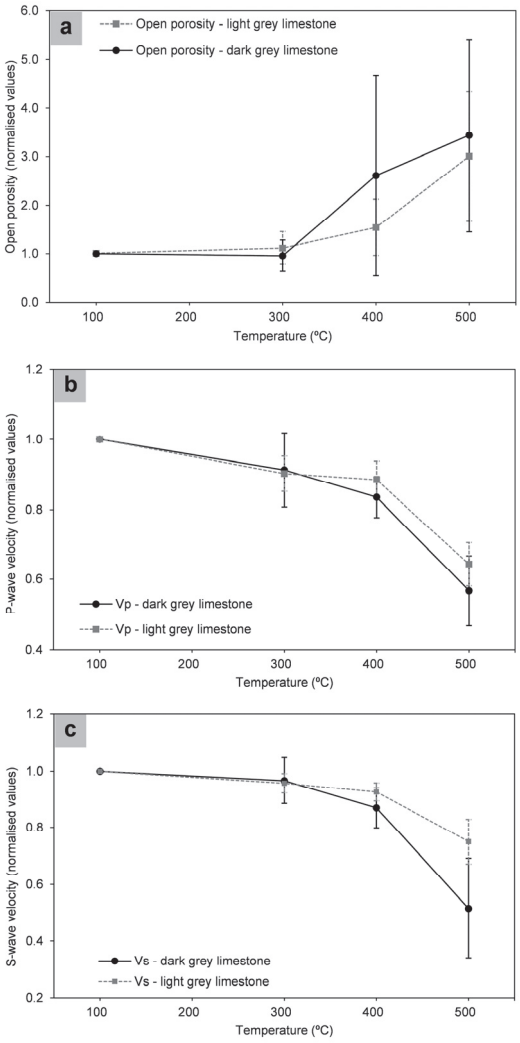

Figure 3.7. Variation of normalised (a) open porosity; (b) P-wave velocity; and (c) S-wave velocity of dark and light grey samples after heat treatment. Reference values used for the normalization are given in Table 3.4.

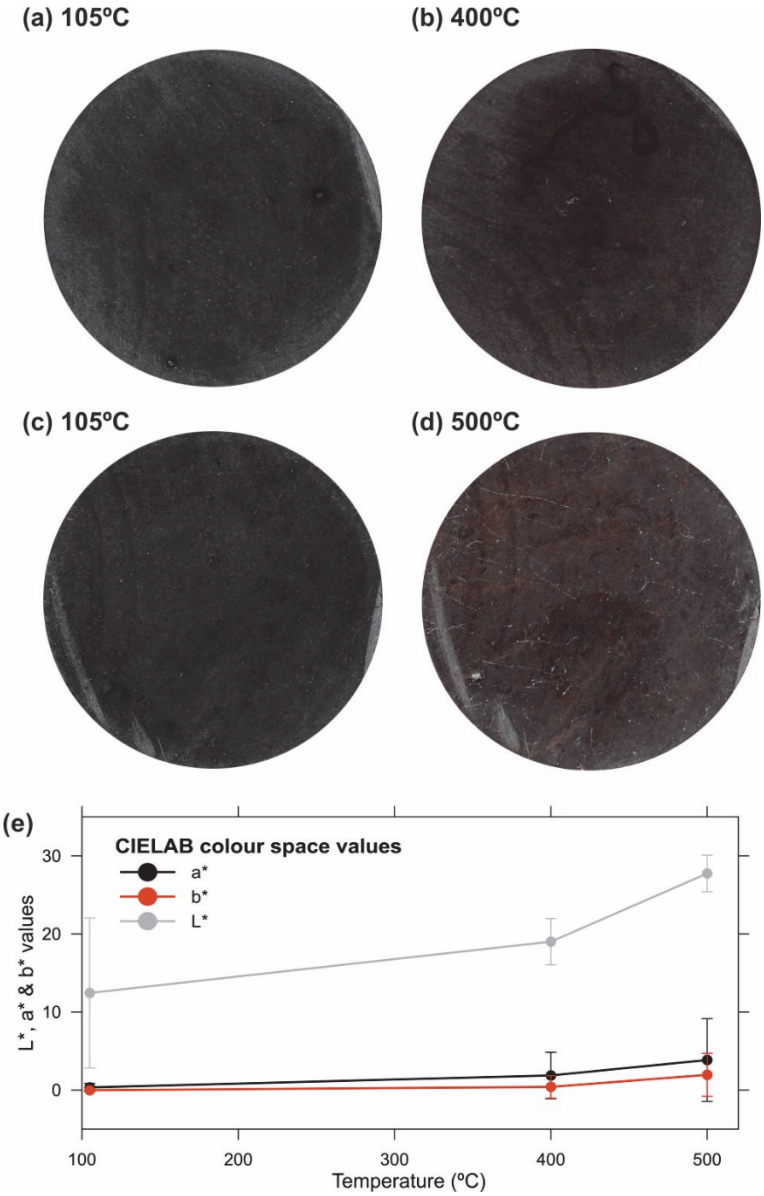

Figure 3.8. Compared images of the flat and polished face from one sample heated to 105 ºC (a), and later to 400 ºC (b), and from one sample heated to 105 ºC (c), and later to 500 ºC (d). A transition from dark grey and bluish tones to light red and increased lightness with temperature could be observed. Colour variation with temperature, expressed using CIELAB variables (e)

3.4. Discussion

In this investigation, we study two different varieties of Prada limestones: (a) a dark grey texture, bearing quartz, clay, organic matter, and pyrites, and (b) a light grey texture with little or no presence of such components. Dark grey texture showed micro-porosity and microcracks, while light grey samples showed greater pore size and few microcracks. We have observed two negative effects of different intensity when heating the dark texture over 400 ºC, not reported in the light grey texture. On the one hand, the explosion of certain samples and, on the other hand, a greater thermal damage in terms of open porosity and ultrasound wave velocity variation.

Dry density reference values are similar for dark and light grey samples, and values of open porosity at 105 ºC classify the samples as low-porosity rocks, compared to other limestones (e.g. Sengun 2014; Yavuz et al. 2010; W. Zhang et al. 2017). A growing trend in open porosity that accelerated between 400 and 500 ºC was previously reported by other authors (e.g. Yavuz et al. 2010), although values are smaller than those reported for low-porosity rocks (e.g. Sengun 2014; W. Zhang et al. 2017). Samples showed typical initial ultrasonic wave velocity values for low porous limestones (e.g. Sengun 2014; Yavuz et al. 2010), and the scatter is consistent with the observed microstructural heterogeneity in Prada limestone. The decrease on P-wave velocity reflects microstructural changes produced during heating, specially between 400 ºC and 500 ºC, which indicates an increase in the number and size of fissures for that interval of temperatures, for both light and dark grey textures. Although the effects of rapid cooling lead to increased thermal damage (Kim et al. 2014; Mallet et al. 2014; Kumari et al. 2018), the cooling of Prada limestones was carried out at a slow rate: in a first step at a rate of 1 to 5 ºC/min to 300 ºC inside the furnace, and later under ambient conditions up to room temperature. Otherwise, microstructural changes could be mainly explained by internal stress concentrations resulting from anisotropic thermal expansion of the calcite (Lion et al. 2005; Malaga-Starzec et al. 2006). However the differing evolution of open porosity, P- and S-wave velocities between textures at 400 and 500 ºC is remarkable (Figure 3.7), and so further additive mechanisms must be contributing on the thermal damage on the dark grey texture.

Firstly, the variation of physical properties with temperature is attributed in certain cases to the decomposition of clay minerals cementing particles or filling micropores (Zhang and Lv 2020). Results in Table 3.2 are inconclusive and do not permit to ensure the transformation of clay compounds in the range of tested temperatures, apart from the amount of clay mineral contents is low according to the values of Al_2O_3 (Table 3.2). Regarding to water content in clays, heating could lead to pore-pressure build-up when clay is organized in a continuous phase (as layers or pockets) that significantly affects the material features (Delage et al. 2000; Sultan et al. 2002; Gens et al. 2011). Indeed, for temperatures up to 200 ºC the loss of water is the main influencing factor on the thermal damage of limestones (Zhang and Lv 2020), as the high-pressure vapour escaping from the rock sample induces the generation and expansion of micro-fractures (Meng

et al. 2020). TG-DTA-DSC and TG-DTA-MS tests on dark grey samples allowed concentrate between 100 and 200 ºC the removal of water adsorbed on mineral surfaces and in clay minerals. However, such range of temperatures is far from 400 and 500 ºC, where different thermal damage between textures was registered. Thus, we do not consider clay mineral decomposition, nor the loss of water, a reason for a greater thermal damage on the dark grey samples.

The presence of quartz on dark grey samples could also cause thermal damage in limestones by the mineral phase transition. Rocks containing quartz experiment a sudden microcracking and volume increase at the phase transition between 550 and 600 ºC, with a strong peak at 573 ºC (Van der Molen 1981; Glover et al. 1995), but such mechanism cannot explain different thermal damage between textures in the range of temperatures tested (T<500 ºC). Following with the different mineral composition between textures, thermal coefficient of calcite (1.4×10^{-5} ºC^{-1}) is less than a half than that of clay (3.4×10^{-5} ºC^{-1}) or quartz (3.3×10^{-5} ºC^{-1}) (Belmokhtar et al. 2017). Local thermal stress concentrations occur between mineral particles of different nature, due to mismatch in thermal expansion coefficients, thus increasing microcracking. Such effect has been reported in limestones by different authors (Liu and Xu 2013; Zhang et al. 2017b; Villarraga et al. 2018; Yang et al. 2019), and the range of temperatures of 400 to 500 °C configures a threshold for thermal cracking (Meng et al. 2020). Thus, microscale destructuring process induced by differential thermal expansion of the mineral components contribute to differences between textures when heated. Moreover, an initial micro-fissuring in the intact dark grey samples lead to greater coalescence and growth of fissures when heated, and so contributes on a greater thermal damage.

Nevertheless, existing research on thermal damage in limestones reports to microcracking, fracturing and splitting in the samples, but not to explosive events of such violence as that observed in our research. Thus, there must be additional mechanisms triggering the explosion of certain samples between 400 and 500 ºC, and such mechanisms must contribute, among those discussed above, on a greater thermal damage in the dark texture in terms of open porosity and ultrasound velocity variation. For all above, we will discuss the role of organic matter and the presence of pyrite.

Coloration constitutes a visible difference between textures forming Prada limestones. That difference seems to be caused by a greater content on organic matter in the dark grey texture, in view of the results from the potassium permanganate method: samples showed six times more organic matter. Moreover, the presence of organic matter is related to the presence of pyrites (FeS_2), which is common in continental margin sediments: these marine anoxic conditions enable bacterial sulphate reduction from organic matter that later reacts with detrital iron minerals in the sediment to form pyrite (Berner 1970, 1982). Observations using SEM confirmed framboidal pyrite structures in the group of dark grey samples, whose presence in organic matter can be a result of microbial activity (Sawlowicz 2000; Shawar et al. 2018).

XRD characterisation confirmed the presence of pyrite in the dark texture, and that was corroborated with EDX analysis on the framboidal minerals. Presence of iron and sulphur was established in the chemical composition (Table 3.2). Therefore, a greater content of pyrites in the dark texture established an additional difference between varieties.

TG-DTA-DSC-MS analysis over dark grey samples showed three different stages (Figure 3.4) representing different chemical processes. Stage I (100 < T <200 °C) corresponded to sample dehydration, involving removal of water adsorbed by the microporosity of mineral surfaces and in clay minerals. Stage II (400 < T <600 ºC) took place between 400-600 ºC and involved two different chemical processes: TG-MS curves displayed the presence of CO_2 and H_2O from 400 to 600 ºC, which is consistent with a thermal oxidation of organic matter (Galbács et al. 1998; Cuypers et al. 2002; Boyle 2004) that can be represented as $CH_2O_{(OM)} + O_2 \rightarrow CO_2 + H_2O$. SO_2 was detected between 405 and 535 ºC, showing a pronounced peak at 460 ºC, which is consistent with thermal oxidation of pyrites (Hong and Fegley 1997; Gazulla et al. 2009), which can be represented as $2FeS_{2\ (pyrite)} + 11/2O_2 \rightarrow Fe_2O_{3\ (hematite)} + 4SO_2$. Finally, stage III (T > 600 ºC) coincides with initial stages in the decomposition of inorganic carbonate and can be written as $CaCO_{3\ (calcite)} \rightarrow CaO + CO_2$.

EDX analysis on dark grey samples after thermally-treated at 500 ºC showed a clear increase in oxygen accompanied by a decrease in sulphur, and chemical results (Table 3.2) showed a decrease in sulphide content, which is consistent with pyrite oxidation. Moreover, thermal oxidation of pyrites produces hematite, which was confirmed by XRD results. The range of temperatures for hematite formation can be described by means of colorimetry analysis: the process of reddening limestone rocks by oxidative conditions during thermal treatment has been experimentally proven and associated with the apparition of hematite (González-Gómez et al. 2015). Indeed, a tendency towards reddish tones was visually appreciated between 400 ºC and 500 ºC (Figure 3.8), and numerically confirmed in view of CIELAB a* values (Figure 3.8e), which is consistent with the range of temperatures for thermal oxidation of pyrites. For all the above, in view of the results obtained using different techniques, it can be confirmed that an oxidation process of pyrites takes place, releasing SO_2, when dark grey samples forming Prada limestone are heated from 400 ºC.

However, XRD, chemical characterisation, and framboids observed using SEM for samples heated to 500 ºC revealed that pyrite transformation was incomplete for the test conditions of temperature and time. This must be related to a lack of oxygen in the pore space. Available oxygen in pores depends on the gas diffusion coefficient, which decreases in porous materials as porosity and pore size decreases (Currie 1960). MIP results showed that dark grey limestone is a low-porosity rock with dual microstructure, which leads to poorly connected small pores. Such tortuosity strongly affects availability for gaseous transport (Benavente and Pla 2018). Consequently, air diffusion, and particularly the presence of O_2, must be limited in dark grey samples, which explains the incomplete oxidation of pyrites. However, different conditions of volume, interstitial water

content, and air exposure time, would enable greater O_2 penetration throughout the rock and enable more efficient oxidation. An additional factor contributing to reduce the gas diffusion coefficient in the rock was described by Hu et al. (2006), who stated that the direct oxidation process leads to inward diffusion of oxygen due to the pore-blocking effect of the formation of ferric/ferrous compounds.

The release of SO_2 from 400 ºC leads to an increase in pore pressure. Moreover, thermal oxidation of organic matter, which releases CO_2 and H_2O specially from above 420 ºC, could contribute to increase the pore-pressure. In addition, the presence of CO_2 from organic matter and calcite decomposition speeds up the thermal oxidation of the pyrite (Lv et al. 2015; Zhang et al. 2019), which leads to a more violent chemical reaction. The DSC curve showed that thermal oxidation of pyrites and organic matter are both exothermic reactions which locally accelerate the thermal oxidation of pyrite (Figure 3.4). The increasing presence of SO_2, CO_2, and H_2O within closed pores may cause an expansion of the rock, and so an accelerated fissuring. The observed behaviour is closely related to the initial number and distribution of micro-fissures, identified on dark samples using MIP, and their two-dimensional shape, which causes a stress concentration in their tips (Griffits 1920). Consequently, the heating of the pyrite-bearing limestone causes a nonlinear decay in physical properties, also observed in other mechanisms of physical and durability decay (Smith et al. 2008; Martínez-Martínez et al. 2013; Benavente et al. 2018). Catastrophic decay in rock integrity is a nonlinear process that dark limestones might suffer, where the initial microcracks may grow and begin to coalesce. Smith et al. (2008) argued that this situation constitutes the critical threshold for macroscopic rock integrity decay. When this critical threshold is exceeded, microcracks turn into cracks and grow rapidly. The increase in porosity may accelerate the decay in physical properties until the ultimate failure is reached."

During heating of the samples, we registered the sound of multiple impacts inside the furnace. Such impacts occurred instantly and were violent enough to be clearly heard in the laboratory. After opening the furnace, exploded samples showed a total lack of structure and its fragments were spread over the furnace, even embedded in the furnace walls as a result of the explosion. Consequently, we undoubtedly identified that sound with an explosive event, since it cannot be confused with fracturing or splitting of the samples. Additionally, we reported the exact temperatures at the moment of that explosion: 390 ºC in the centre of the sample and 438 ºC on its surface. Considering that the SO_2 generation curve starts at 405º C and peak is at 460 ºC, temperatures in the sample were compatible with the rising branch of the curve. Consequently, the release of SO_2 must have been taking place within the sample at an accelerated rate. Additionally, there are more indicators of that event, since produced SO_2 was released throughout the room immediately after the explosive event, detaching a strong smell that made necessary the use of gas extraction means and forced us to leave the room. The release of SO_2 above a narrow range of temperatures would cause a peak in pore pressure that, jointly with a structure of micro-fissures in the dark texture, would cause a violent fracturing of the material. For all above, we associate the documented explosive phenomenon to SO_2 production

rather than oxidation of organic matter for the next reasons: (i) oxidation of pyrites evolves in a narrower temperature range than organic matter; and (ii) the peak release of SO_2 occurs at lower temperatures (above 460 ºC) than organic matter (above 520 ºC). Moreover, explosive behaviour similar to that described in this work are not described in the existing scientific literature on the thermal effects on carbonate rocks containing organic matter (Yavuz et al. 2010; Andriani and Germinario 2014; González-Gómez et al. 2015). Consequently, thermal oxidation of pyrites has a greater contribution in the explosive phenomenon than organic matter oxidation.

Regarding the thermal damage suffered by the dark texture in terms of open porosity and ultrasound wave velocity variation, the partial contribution of the pore overpressure and gas release caused by the thermal oxidation of pyrites on the total thermal damage is difficult to evaluate. However, we cannot ignore this process because the release curve of SO_2 has been identified, and their negative effects observed (i.e. the explosion of certain samples). Summarizing, in this work we describe a new thermo-chemical process to explain the observed thermal damage on dark texture limestones from Prada formation based on the thermal oxidation of pyrites, jointly with further factors identified in this research (i.e. differential thermal expansion of the mineral components and initial micro-fissuring in the intact rock).

Finally, a 40 % of the dark samples did not undergo visible damage after heat treatment although they suffered thermal damage after heat treatment according to the variation of their physical properties (Figure 3.6). Prada limestone presents a great chemical and textural heterogeneity that varies within and between samples. Hence, pyrite content and initial micro-fissure and pore structure (that determines the gas transport and the oxidation reaction efficiency) would induce a particular explosive potential to each sample. Although our results are definitive and are based on evidences, further investigations would be necessary to quantitatively relate pyrite content and initial micro-fissure with explosive potential to each sample. Nevertheless, heterogeneity hinders any systematic investigation because of chemical and textural test are destructive, and therefore are not compatible with the need to count with intact samples to monitor their explosive behaviour during heating process. Despite of such difficulties, only a systematic study would be fully conclusive.

3.5. Conclusions

Prada limestone, formed by dark and light grey varieties, was subjected to temperatures of 105, 300, 400 and 500 ºC. We have observed two effects of different intensity when heating the dark texture above 400 ºC, not reported in the light grey texture: (a) the explosion of certain samples; and (b) a greater thermal damage in terms of open porosity and ultrasound wave velocity variation. The influence of the specific features of the dark texture on such thermal effects have been discussed and the derived conclusions are listed below:

1. Two textures from Prada limestone have been characterised: a dark grey texture with micro-porosity and microcracks, bearing quartz, clay, organic matter and pyrites, and a light grey texture with greater pore size and few microcracks, and little or no presence of such mineral components.
2. Thermal damage on Prada Limestone could be mainly explained by internal stress concentrations resulting from anisotropic thermal expansion of the calcite. However, the differing evolution of open porosity, P- and S-wave velocities between textures at 400 and 500 ºC is explained by differences on their mineral and textural composition.
3. Different thermal damage between textures could be partly explained by microscale destructuring process induced by differential thermal expansion of the rock-forming minerals, and an original micro-fissuring in the intact dark grey samples leading to greater coalescence and growth of fissures. Effects from clay thermal decomposition, water loss and quartz phase transition have been also reasoned and discarded. Such mechanisms cannot explain the explosive events observed between 400 and 500 ºC
4. The sound of multiple impacts was registered inside the furnace during the heating process of the samples. This process was instantly and violent enough to be clearly heard in the laboratory room. Furthermore, after opening the furnace, exploded samples showed a total lack of structure and their fragments were spread over the furnace, even embedded in the furnace walls as a result of the explosion. We undoubtedly associated that sound with an explosive event that cannot be confounded with fracturing or splitting on rocks.
5. The heating of dark texture samples revealed two thermal reactions involving gas release: thermal oxidation of pyrites (FeS2) releasing SO_2 from 400 to 520 ºC, and thermal oxidation of organic matter releasing H_2O and CO_2 from 400 to 600 ºC. Temperatures for rock explosion are compatible with the rising branch of the SO_2 release curve, that would cause a peak in pore pressure that combined with the micro-fissured structure of the dark texture, would cause violent fracturing of the material.
6. We relate the explosive phenomenon to SO_2 production rather than oxidation of organic matter for different reasons: oxidation of pyrites evolves in a narrower temperature range than organic matter, and the peak release of SO_2 occurs at lower temperatures (above 460 ºC) than organic matter (above 520 ºC). Moreover, SO_2 was released throughout the laboratory immediately after the explosive event.
7. Total thermal damage on the dark texture is attributed to thermal oxidation of pyrites, jointly with further factors identified in this research (i.e. differential thermal expansion of the mineral components and initial micro-fissuring in the intact rock).

8. Although results are definitive and are based on evidences, further investigations would be necessary to quantitatively relate pyrite content and initial microfissure with explosive potential to each sample. Despite of difficulties derived from great chemical and textural heterogeneity that varies within and between samples, only a systematic study would be fully conclusive.

The practical relevance of the observed phenomenon in underground infrastructures and mining engineering works is critical, since temperatures greater than 400 ºC could lead to explosive phenomenon on pyrite-bearing limestones, involving mass fracturing, rock integrity loss and strength decay on mining works and underground infrastructures. In addition, SO_2 released into the atmosphere as a result of thermal oxidation of pyrites has a harmful effect on health (ATSDR 1998) of people involved on mining or underground construction or works, users of tunnels or emergency intervention teams in case of a fire event. Additionally, SO_2 can react with other atmospheric chemical elements forming acid compounds (sulphurous or sulphuric acid) that corrode metals, concrete, limestone, and other materials (Kumar and Imam 2013), shortening underground structures life and increasing maintenance costs.

Chapter 4. Thermal effects on the drilling performance of a limestone: relationships with physical and mechanical properties

Authors:	Víctor Martínez-Ibáñez, María Elvira Garrido, Carlos Hidalgo Signes, Aniello Basco, Tiago Miranda, Roberto Tomás		
Status:	Manuscript published		
Journal:	Applied Sciences, 2021		
DOI	https://doi.org/10.3390/app11073286		
JCR IF (2019)	2.474		
	JCR Category	Ranking	Quartile
	Multidisciplinary Chemistry,	*88/177*	*Q2*
	Multidisciplinary Engineering	*63/155*	*Q2*
	Applied Physics	*32/91*	*Q2*
	Multidisciplinary Materials Science	*161/314*	*Q3*
Presentation:	Post-print (Author version)		

Abstract

This work evaluates the effect of high temperatures and cooling methods on the drillability of Prada limestone. Samples from boreholes drilled during the design stage of the Tres Ponts Tunnel in the Catalan south Pyrenean zone (Spain) were subjected to temperatures of 105, 200, 300, 400, and 600 °C, and then cooled at a slow rate or by quenching. Sievers' J-value (SJ) and brittleness (S_{20}) were determined on thermally treated samples, and the drilling rate index (DRI) was calculated for each temperature. The results show that thermal treatment implied a sustained increase in the drillability of the rock of up to 40% at 600 °C and a change in the drillability category (from medium to high). At 600 °C, SJ and S_{20} tripled and doubled, respectively, the initial values obtained for the intact rock. The results were inconclusive about the influence of the cooling method on the drilling performance of Prada limestone for the tested range of temperatures. The substantial improvement observed in the drillability of Prada limestone when heated, measured in terms of DRI, could help in the development of novel thermally assisted mechanical excavation methods. Additionally, strong correlations between drillability variables (i.e., SJ and S_{20}) and physical and mechanical variables of Prada limestone (i.e., P- and S-wave velocities, uniaxial compression strength, elastic modulus, and Poisson's ratio) are proposed. Correlations will help make preliminary predictions of drillability based on properties such as uniaxial compression strength and ultrasound wave velocities.

Keywords

rock drillability; drilling rate index (DRI); thermal treatment; temperature; limestone; correlations

4.1. Introduction

Modern mechanical excavation strongly depends on the efficiency of the means involved to optimise investment costs, and so rock features must be considered (Yetkin et al. 2016). Prior to excavation, the type and performance of excavation machinery (i.e., hydraulic breakers, roadheaders, shear-loaders, TBMs, drilling rigs, and cutting bits) must be determined. The influence of rock properties on drillability has been discussed by various authors. Yaşar et al. (2011) experimented on cement mortar (an analogue for natural rock samples) and found that uniaxial compression strength (UCS) strongly influenced the efficiency of the drilling process in terms of specific energy increases and penetration rate decreases. Yarali and Kahraman (2011) used 32 different rock types and found a strong relation between the drilling rate index (DRI) and the brittleness expressed as the area under the curve of the compressive strength-tensile strength (Altindag 2010). In addition, good linear correlations were found between DRI and UCS, Brazilian tensile strength (BTS), shore scleroscope hardness, and axial and diametral point load strength (PLT) (Yarali and Soyer 2011, 2013). Saeidi et al. (2014) studied 38 in situ drillings in porphyry andesite, limestone, and sandstone, and found that the UCS of rock, the vertical pressure on bit, and bit rotational speed were the most significant parameters in the penetration rate for rotary drilling. Özfirat et al. (2016) experimented on 42 rocks of different types and found that DRI showed strong correlations with UCS and BTS. Yetkin et al. (2016) used schist samples and found a strong relationship between DRI, UCS, BTS, Schmidt hardness (SH), instantaneous cutting rate (ICR), unit weight, rock mass rating (RMR), and the Cerchar abrasiveness index (CAI). Capik et al. (2017) used 43 samples from different types of rocks and determined that DRI decreased with increasing UCS, PLT, BTS, and SH, and that DRI increased with apparent porosity and void ratios. More recently, Yenice (2019) found better predictions of DRI from UCS and BTS for hard rocks (UCS > 100 MPa) than for soft rocks.

Elastic and plastic deformations occur during drilling, and for that reason the effects of elastic properties have also been studied in terms of drilling aspects by different authors. Jamshidi et al. (2013) used artificial neural networks to estimate UCS and elastic modulus (using operational drilling parameters from oil wells in Iran as inputs) and determined that both UCS and elastic modulus are strongly correlated with operational drilling parameters, although UCS showed the best coefficients of determination (demonstrating that UCS has a greater effect in drilling performance than elastic modulus). Ataei et al. (2015) studied 11 drilling sites from a mine in Iran and showed a good relationship between drilling rate (DR) and UCS, P-, and S- wave velocities. Su et al. (2016) experimented on samples from nine different rocks and found a strong correlation between DRI and UCS. Although correlation between DRI and elastic modulus was poor, a correlation between Sievers' J-value (SJ) and elastic modulus was found.

Previous research evidence shows that mechanical and physical properties strongly determine the drilling performance of rocks, and such properties show the dramatic variations with temperature and cooling method that condition the drillability of thermally treated rocks. Thermal effects on the physical, mineralogical, and mechanical properties of rocks are of interest to researchers. Moreover, the degree of thermal damage strongly depends on the type of rock, and more than a quarter of the studies on the thermal response of rocks are specifically focused on limestones (Martinho and Dionísio 2020). Lion et al. (2005) observed a decrease in UCS even at low temperatures ($T < 250$ °C). Yavuz et al. (2010) described a marked decrease in bulk density, P-wave velocity, and effective porosity at 400 °C. Franzoni et al. (2013) reported an increase in open porosity, as well as water absorption and reduction in mechanical properties when heating limestones up to 400 °C, as a consequence of the anisotropic thermal deformation of calcite crystals. Brotóns et al. (2013) reported an increased variation in the physical and mechanical features of carbonate rocks when cooled by water immersion. Andriani and Germinario (2014) observed a clear reduction in uniaxial compression strength (UCS) from 500 °C on calcareous and dolomitic rocks from Apulia in Italy, with temperatures above 600 °C usually marking a dramatic decline in UCS (Mao et al. 2009; Sengun 2014). Beck et al. (2016) explored colourimetry to determine thermal damage in buildings and described a trend of limestone to redden (later confirmed in Prada limestone and related to oxidation of iron compounds) (Martínez-Ibáñez et al. 2021a). Natural limestone becomes lighter in appearance with increasing temperature (Ozguven and Ozcelik 2013; Martínez-Ibáñez et al. 2021a). Zhang et al. (2017b) determined that from 200 to 500 °C porosity and pore size rapidly increase, and from 500 to 600 °C UCS, elastic modulus, Poisson's ratio, and hardness decreased. Later, Zhang and Lv (2020) described a strong relationship between mineral content and thermal damage in limestones (China). Martínez-Ibáñez et al. (2021a) described a significant contribution of the thermal oxidation of pyrites in the explosive behaviour and thermo-chemical damage of Prada limestone from 400 °C. Martínez-Ibáñez et al. (2021b) identified micro-structural changes produced by high temperatures and cooling methods in Prada limestone, and related them with severe variations in the physical and mechanical features of this type of rock. Such dramatic changes are mainly explained by the anisotropic expansion of calcite (Lion et al. 2005; Malaga-Starzec et al. 2006), and by other physicochemical processes such as the mismatch in thermal expansion coefficients between mineral particles (Belmokhtar et al. 2017) and the quartz phase transition (Van der Molen 1981; Glover et al. 1995). The greater thermal damage in water-cooled samples is due to tensile stresses that nucleate cracks (Mallet et al. 2014).

Current drilling methods are based on mechanical abrasion, and this produces substantial drill bit wearing and low rates of penetration in hard rocks, resulting in high drilling costs (Kubik 2006; Sigfusson and Uihlein 2015). Therefore, researchers aim to improve drilling performances using emerging drilling technologies, and one alternative approach is to thermally assist conventional rotary drilling by heating the rock. Rossi et al. (2018) explored the feasibility of thermally assisted drilling using a flame jet to achieve high

local heating rates, and determined a drop of 30% in UCS for temperatures up to 600 °C. Jamali et al. (2019) used high powered laser technology to decrease rock strength, drilling strength, and fracture toughness at rates of 60% in granite and 30% in sandstone. Rossi et al. (2020d) studied a combined thermo-mechanical drilling (CTMD) using a flame jet and stated that the thermal treatment of rocks causes extensive thermally induced cracks in granite and sandstone, which significantly enhances the penetration performance of cutting tools. Later, Rossi et al. (2020a, b, c) implemented this technology in the field and demonstrated an increase in the removal performance in hard rocks by up to a factor of three when compared to conventional drilling methods, and concluded that integration of thermal assistance to conventional rotary drilling constitutes an interesting approach to facilitate the drilling process.

DRI (Bruland 2000) is among the most used testing methods to determine the drillability characteristics of rock. NTNU/SINTEF registered as trademark the DRI test (Dahl et al. 2010), which is assessed on the basis of two laboratory tests, the brittleness value (S_{20}) test (von Matern and Hjelmér 1943) and Sievers' J-value (SJ) miniature drill test (Sievers 1950). In this study, SJ and S_{20} tests were performed on thermally treated samples from two boreholes drilled during the design stage of the Tres Ponts Tunnel in Prada limestone to determine drilling rate index (DRI) variation with temperature. Thermal treatment effects on Prada limestone drillability would help improve the efficiency of mechanical excavation. Prediction of penetration rates for rotary drill rigs is of great importance in mine and tunnelling scheduling (Sievers 1950; Hartman 1959; Kahraman et al. 2003; Hoseinie et al. 2009). Using prediction equations enable selecting the drilling rig type best suited for certain conditions (Kahraman 1999). We explore correlations to predict the SJ and S_{20} of thermally treated limestone from P- and S-wave velocities, UCS, elastic modulus, and Poisson's ratio. Such correlations would help make preliminary predictions of the variation in SJ, S_{20}, and DRI of Prada limestone from: (a) other properties whose determination is quicker and easier; (b) non-destructive laboratory tests (i.e., ultrasound wave velocity); or (c) from more common test procedures (e.g., the uniaxial compressive test).

4.2. Materials and methods

Prada limestone is a Lower Cretaceous formation located in the Serra de Prada, a range of mountains in the southern Pyrenees (Lleida province, Spain). Rock samples were taken from two horizontal boreholes drilled during the design stage of the Tres Ponts Tunnel, which is planned to be entirely excavated from Prada limestone in the municipalities of Organyà and Fígols, close to a narrowing of the Segre river as it passes next to the Serra de Prada, in an area known as the Congost de Tres Ponts. The tunnel will be oriented north-south on the C-13 road, measures 1273 m in length, and its maximum depth from the ground surface will be of 285 m. Figure 4.1 shows the area of study including the Serra de Prada, Congost de Tres Ponts, the Tres Ponts Tunnel, and the position and spatial coordinates of the two horizontal boreholes.

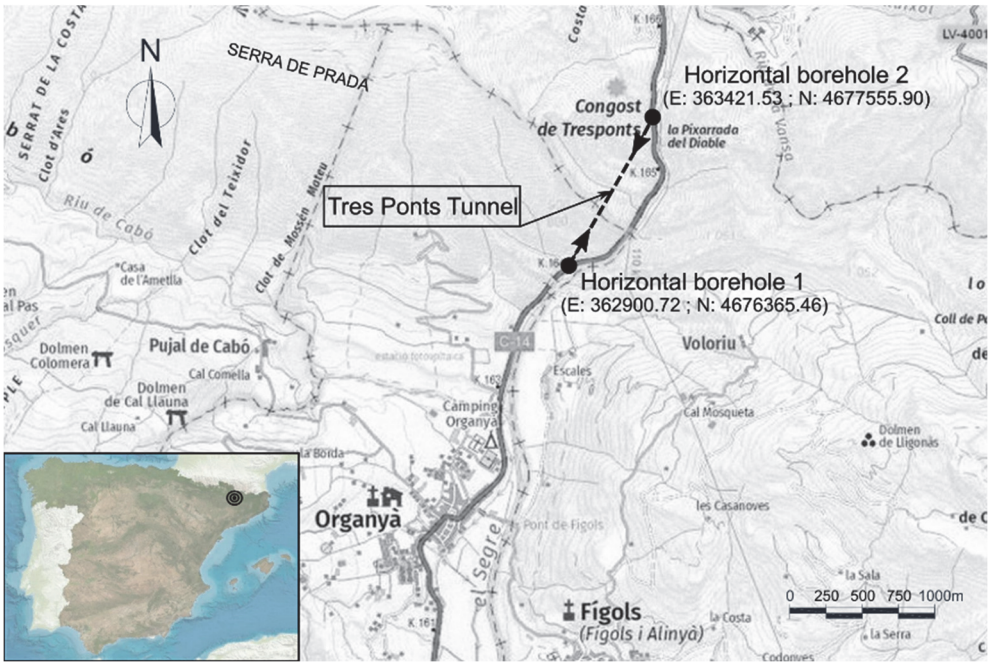

Figure 4.1. Location of the Tres Ponts Tunnel in the Congost de Tresponts area. Borehole coordinates are expressed in meters in the UTM 31N/ETRS 89 reference system. Image modified from Institut Cartogràfic i Geològic de Catalunya (www.icc.cat).

Samples were very homogeneous and only presented changes in the grey tone and very thin veins of calcite (Figure 4.2). The effects of high temperatures in textural, physical, and mechanical features from the Prada formation were described in previous research (Martínez-Ibáñez et al. 2021b). A dark grey fraction from Prada limestone exhibited an increased thermal damage and explosive behaviour when heated to above 400 °C, and this is related to an increase in the pore pressure caused by SO_2 released during the thermal oxidation of pyrites (Martínez-Ibáñez et al. 2021a). Due to such different effects produced by the thermal treatment, the dark grey fraction was separated from the rest of samples and was not considered in this research.

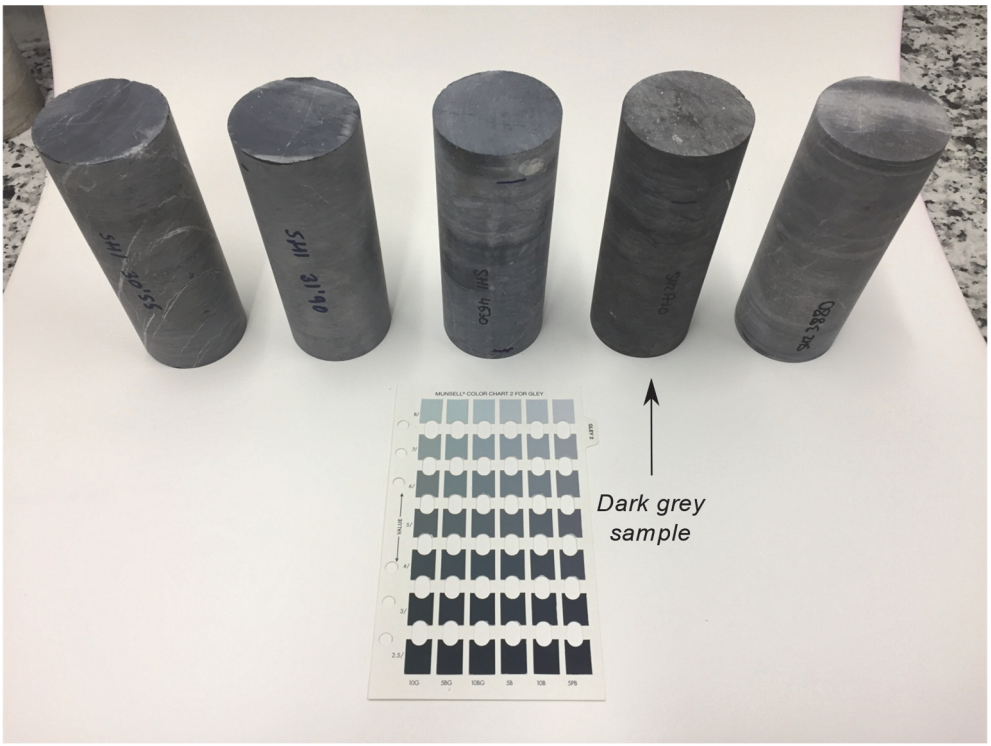

Figure 4.2. Changes in the grey tone and very thin veins of calcite observed in the intact samples. A dark grey texture was separated from the rest of samples and does not form part of this research.

Optical microphotographs (Figure 4.3) enabled Prada limestone to be identified as a grainstone or biosparite with abundant bioclasts, where cement is abundant and mainly consists of crystalline mosaics of calcite spar that fill the interparticle porosity. Micritic matrix is minor and irregularly distributed, and discontinuities are abundant and consist of fissures, calcite veins, and a small number of stylolites. Some angular and sub-angular grains of monocrystalline quartz, and sub-rounded grains of iron sulphides dispersed in the rock matrix appeared in a minor proportion.

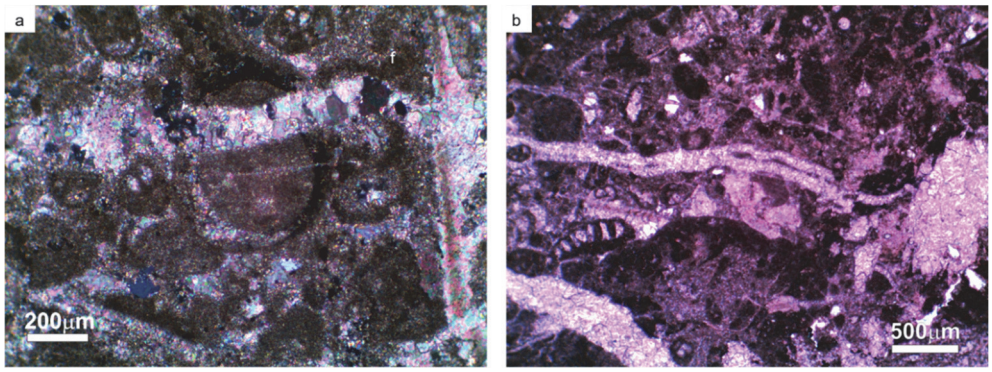

Figure 4.3. Optical microphotographs of intact Prada limestone. Bioclasts and micritic matrix cut by calcite veins (a). Detail of molluscs (b). Microphotographs were taken under parallel-nicols.

A temperature of 105 °C was applied to a total of 110 samples to remove moisture and these are considered references for the determination of intact rock properties. The average initial values for physical and mechanical properties of the intact rock are summarised in Table 4.1. Subsequently, five groups of 20 samples were separated and heated in an electric furnace at a slow rate (a gradient of 5 °C/s was applied) to target temperatures of 200, 300, 400, 500, and 600 °C. Target temperatures were then maintained for one hour. Heated specimens at each target temperature were then separated into two groups of five samples and cooled by one of two methods: (i) at a slow rate to room temperature of 21 °C; or (II) by quenching through water immersion, according to the procedure described by Brotóns et al. (2013). Temperatures inside the furnace were monitored with a PicoLog 6 data logger. Figure 4.4 illustrates the number of laboratory tests performed for each temperature and the number of samples used in this research methodology.

Table 4.1. Reference values for intact samples heated at 105 °C.

Parameter	Min.	Max.
Dry unit weight, ρ_d (kN/m^3)	26.59	27.09
Open porosity, n_e (%)	0.67	1.75
P-wave velocity, V_p (km/s)	5.30	5.41
S-wave velocity, vs. (km/s)	2.63	2.67
Uniaxial compressive strength, σ_{ci} (MPa)	140.86	188.40
Elastic modulus, E (GPa) (from mechanical tests)	71.15	84.23
Poisson's ratio, ν (from mechanical tests)	0.26	0.36

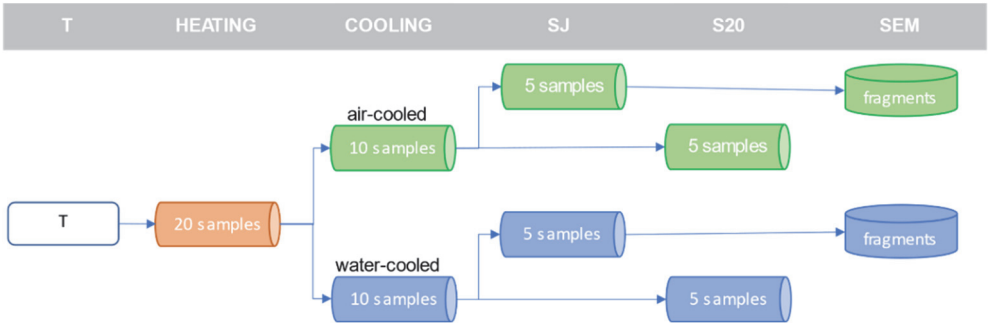

Figure 4.4. Methodological scheme of the laboratory tests and the number of samples tested. The tests performed at each temperature (T) are: Siever's J drillability value (SJ); brittleness value (S_{20}); and microstructure by scanning electron microscopy (SEM).

Optical and scanning electron microscopy (SEM) in backscattered electron mode was used to study the petrographic features of representative samples from Prada limestone. Sample surfaces were polished with alumina and diamond powder; the finest abrasive used was a 0.4 μm diamond powder. Uncovered polished surfaces were studied in a Hitachi S-3000 N variable pressure SEM working in a low vacuum, and salt tested surfaces were analysed in a high vacuum SEM in secondary electron mode.

Sievers' J-miniature drill test measures rock surface hardness or resistance to indentation. Figure 4.5a shows the laboratory equipment used in this research to determine SJ value according to Bruland (2000), which is defined as the measured drillhole depths after 200 revolutions of the 8.5 mm miniature drill bit (Figure 4.5b) acting with a vertical load of 20 kg. A total of 55 samples (five samples from each temperature and cooling method) were chosen to perform Sievers' J-miniature drill test. The test was repeated five times on each rock sample, and the Sievers' J-value was calculated as the mean value of the depth of the miniature drill holes, measured in 1/10 mm according to Bruland (2000).

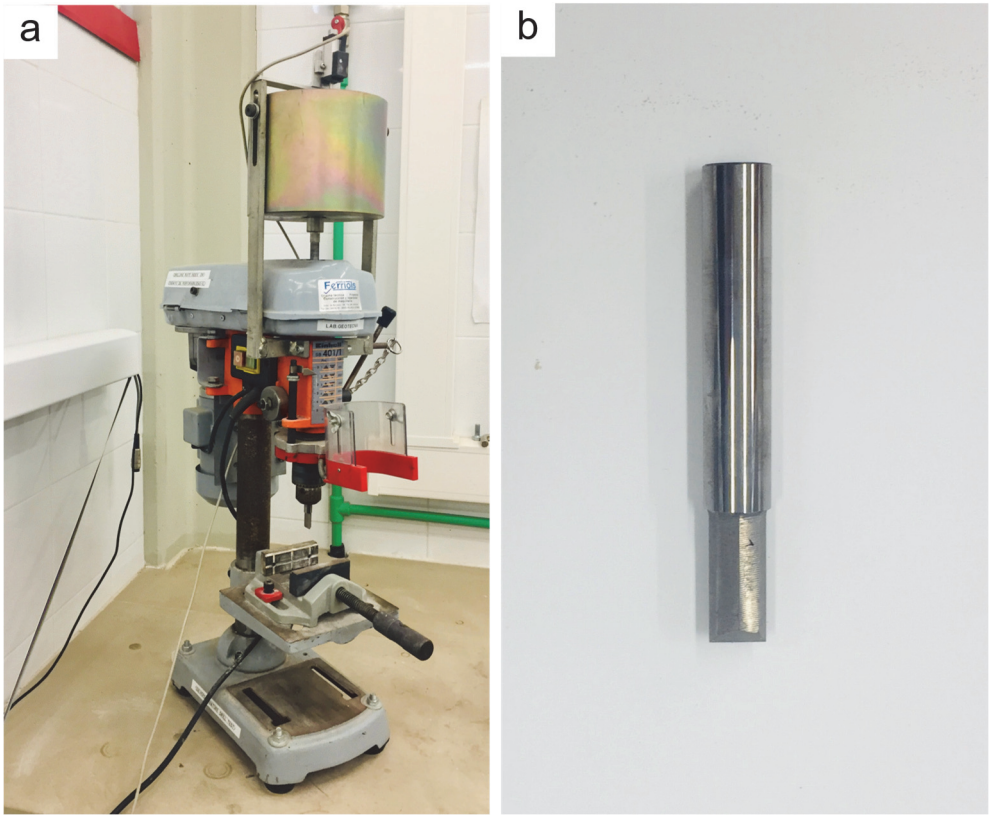

Figure 4.5. Laboratory equipment for Sievers' J-miniature drill test (a) and miniature drill bit (b) used in this research.

The brittleness test gives a good measure of the rock brittleness or the ability of the rock to resist crushing by repeated impacts. The test was conducted according to Bruland (2000), so a total of 500 g of aggregate in the fraction 11.2–16.0 mm was prepared from each sample. The aggregate was then crushed by 20 impacts in the mortar and then the value S_{20} was expressed as the percentage of material passing through the 11.2 mm sieve (Figure 4.6). The test was conducted on 55 samples (five samples from each temperature and cooling method), and the brittleness S_{20} value for each temperature was taken as the mean value of the samples tested.

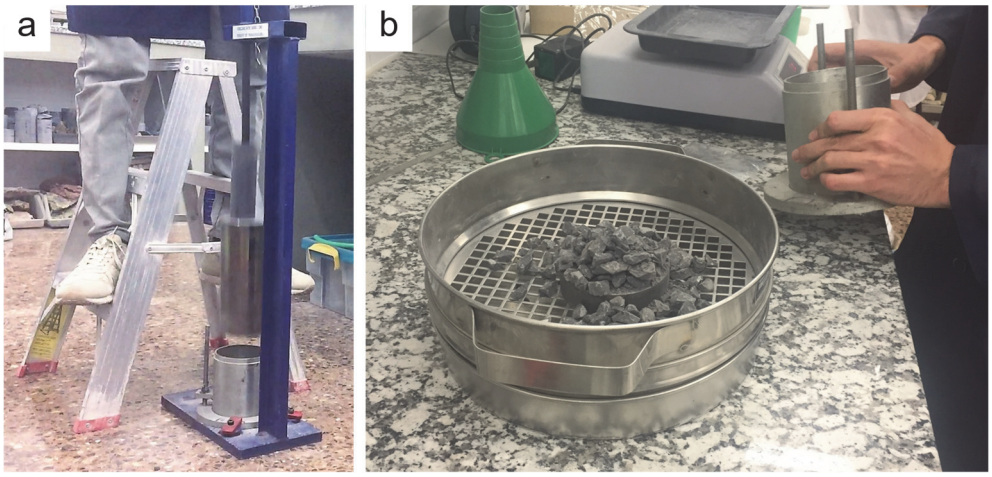

Figure 4.6. Crushing of the aggregate in the mortar (a) and determination of the percentage of material passing through the 11.2 mm sieve (b).

4.3. Results

4.3.1. Effects of temperature on the micro- and macro-structural features

Variations in the micro- and macro-structural features of Prada limestone with temperature were already documented in detail in previous research (Martínez-Ibáñez et al. 2021b), where SEM and MIP analyses refer to thermal treatment as a cause for dramatic micro-structural changes in Prada limestone in terms of porosity and micro-crack growth and coalescence. New SEM performed in this study confirms the presence of trans-granular fissures and porosity when heated to 400 °C (Figure 4.7a), and well-formed and connected fissures developed at 600 °C (Figure 4.7b), both in water-cooled samples. The macro-structural effects of temperature involve visible fissure growth, splitting, and cracking (Figure 4.8). Such effects were noticeable from 400 °C and were more severe with increasing temperature.

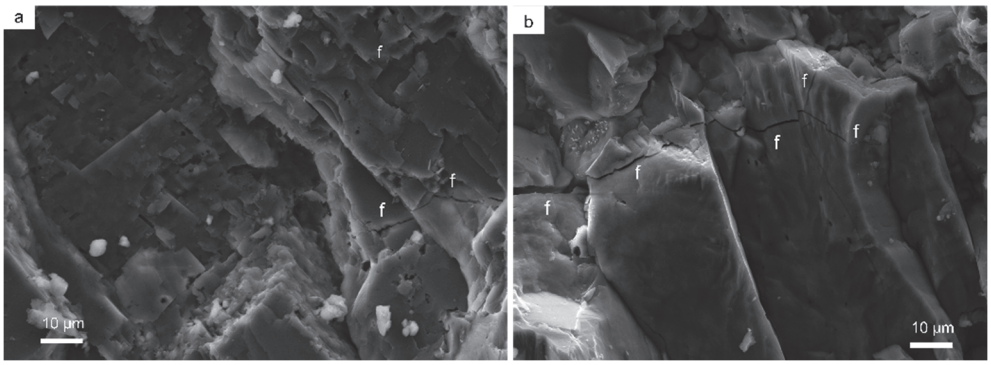

Figure 4.7. SEM images showing fissures (f) for samples heated to 400 °C (a) and 600 °C (b) and then water-cooled. An increase of 2000× was used for all figures.

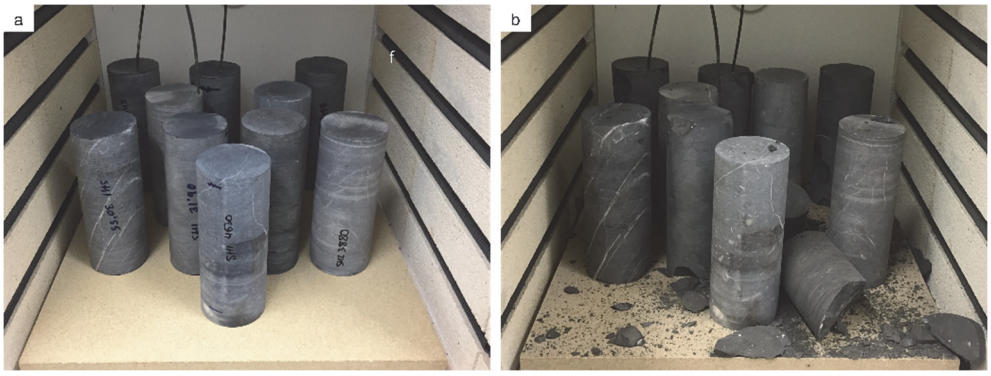

Figure 4.8. Samples before (a) and after (b) heated to 600 °C. Effects of temperature involve visible fissure growth, splitting, and cracking.

4.3.2. Drillability variation with temperature

Mean and standard deviation numerical values of SJ and S_{20} are depicted in Table 4.2 and evolution for the different temperatures are represented in Figure 4.9. The results show significant values of standard deviation at certain temperatures related to the perceived slight variations in the visual appearance of samples (i.e., changes in the grey tone and presence of very thin calcite veins).

Table 4.2. Variation with temperature of Siever's J miniature drillability test (SJ), brittleness test (S_{20}), and drilling rate index (DRI) final value and for air- and water-cooled samples.

Temperature (°C)	Air-Cooled Samples				Water-Cooled Samples			
	SJ(1/10 mm)	S_{20} (%)	DRI	Class	SJ (1/10 mm)	S_{20} (%)	DRI	Class
105	11.35 ± 4.41	42.77 ± 10.94	44	Medium	11.35 ± 4.41	42.77 ± 10.94	44	Medium
200	14.92 ± 6.27	45.12 ± 8.40	49	Medium	5.73 ± 0.71	39.23 ± 6.02	39	Low
300	10.30 ± 7.05	44.23 ± 7.41	45	Medium	14.66 ± 5.97	41.73 ± 7.26	45	Medium
400	17.29 ± 10.66	49.45 ± 5.67	52	Medium	14.56 ± 9.02	48.16 ± 2.18	50	Medium
500	16.34 ± 10.70	55.84 ± 6.07	59	High	21.88 ± 5.60	57.71 ± 4.74	62	High
600	30.13 ± 11.32	56.43 ± 4.44	62	High	23.60 ± 9.81	55.89 ± 9.87	62	High

SJ for air-cooled samples showed little variation up to 500 °C, and then we observed a sudden increase at 600 °C that tripled the initial mean values of the intact rock. Water-cooled samples showed a constant increase with temperature except for a marked local decrease at 200 °C. Final mean values at 600 °C doubled the initial values of the intact rock. Values of S_{20} for air-cooled samples were almost constant up to 300 °C. Values then increased for 400 °C and 500 °C, and remained constant at 600 °C (where a final mean value of 1.3 times that for intact rock was reached). Slight differences were registered between air- and water-cooled samples up to 400 °C where water-cooled samples showed lower values especially at 200 °C. For higher temperatures, trends were almost equal for both cooling methods.

Values of SJ and S_{20} were combined to obtain a final DRI value for each temperature (Figure 4.9c), and this enabled classification of the drillability of Prada limestone (Table 4.2) according to Bruland (2000). DRI increased with temperature, and this implied a change in the drillability category at 500 °C (from medium to high) for both cooling methods. Decreases in the DRI could be observed at 200 °C for water-cooled samples, which is consistent with the recorded variations in SJ and S_{20}. No relevant differences could be observed between cooling methods for the highest temperatures.

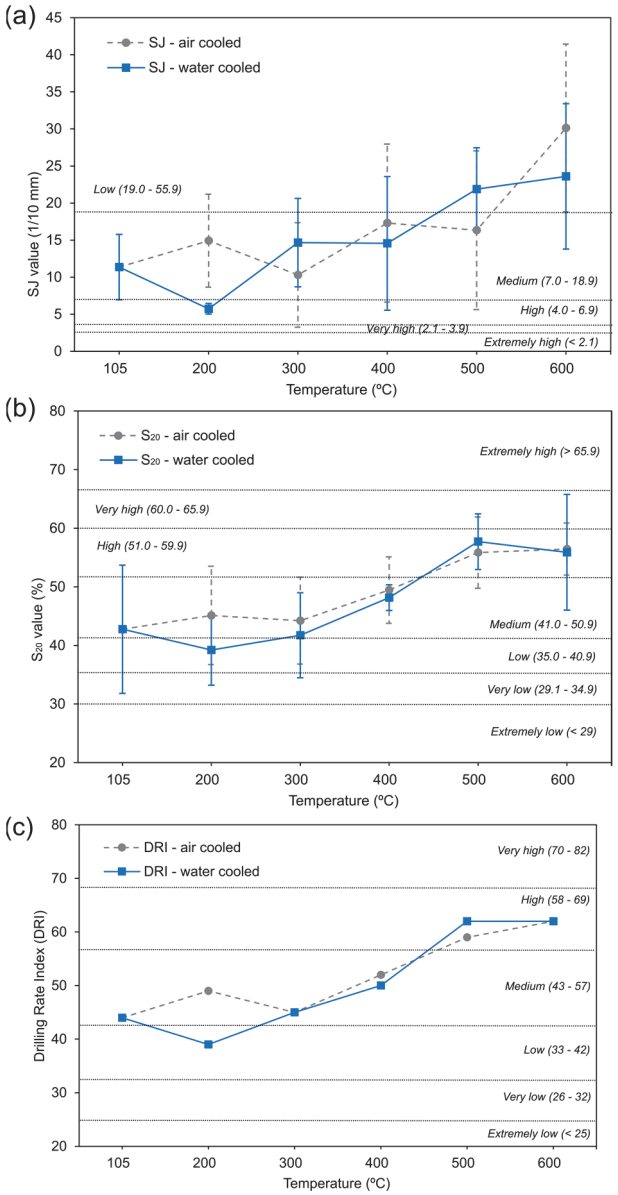

Figure 4.9. Variation with temperature of Siever's J miniature drillability SJ (a), brittleness S_{20} (b), and drilling rate index (c) for air- and water-cooled samples. Categories have been represented for Sj and S_{20} according to Dahl et al. (2012), and for DRI according to Bruland (2000).

4.3.3. Correlations between parameters

Correlations have been proposed in this work to predict the variation in the drillability with temperature from variations in the physical and mechanical properties for both air and water-cooled samples. Properties correlated in this study are obtained from different fragments within the same samples, which prevents providing pairs of values for the same fragments. This is because drillability tests performed here are destructive, and therefore it is not possible to make other tests such UCS on the same rock specimens. In other words, since DRI and UCS tests are destructive, for each temperature they are performed using different fragments (whose values are averaged and then correlated). Thus, regression curves are calculated using the mean values of each property determined at each temperature in line with other authors (Nasseri et al. 2007; Yenice 2019; Martínez-Ibáñez et al. 2021b) since the pairs of correlated values of each sample that define the scatter cannot be considered for adjusting such functions. Different correlation functions exist between SJ, S_{20}, and other physicomechanical parameters of the intact rock, but they do not refer to thermally treated samples. This research novelty explores the variation in SJ and S_{20} with temperature, and their correlation with other physicomechanical features in a thermally treated rock. To provide the most accurate predictions of drillability parameters for making preliminary decisions about the drilling process (e.g., drilling rig type and excavation process), we propose correlations to explore the best fitting functions based on coefficients of determination (Table 4.3), and we evaluate their suitability based on residuals and relative errors (Table 4.4). We also discuss if correlations can provide reference values for the drillability features of thermally treated rocks, and so we consider valid those correlations providing coefficients of determination greater than 0.80 and relative errors smaller than 10%.

Table 4.3. Coefficients of determination (R^2) for simple regression curves studied to predict SJ and S_{20} from mechanical and normalised (N) physical parameters (UCS, elastic modulus, Poisson's ratio, P- and S-wave velocities).

Cooling method	Parameter	R^2 for SJ Predictions				R^2 for S_{20} Predictions			
		Linear	Exponential	Logarithmic	Power	Linear	Exponential	Logarithmic	Power
Air	UCS	0.74	0.79	0.87	0.89	0.71	0.73	0.69	0.70
	Elastic modulus	0.56	0.61	0.55	0.59	0.96	0.96	0.93	0.92
	Poisson's ratio	0.76	0.77	0.86	0.84	0.90	0.89	0.84	0.83
	P-wave velocity	0.65	0.64	0.69	0.66	0.92	0.91	0.90	0.89
	S-wave velocity	0.74	0.71	0.77	0.72	0.89	0.88	0.86	0.84
Water	UCS	0.63	0.43	0.72	0.51	0.69	0.67	0.77	0.75
	Elastic modulus	0.76	0.66	0.78	0.64	0.80	0.79	0.85	0.84
	Poisson's ratio	0.85	0.69	0.80	0.62	0.90	0.89	0.83	0.81
	P-wave velocity	0.80	0.62	0.82	0.63	0.88	0.87	0.89	0.88
	S-wave velocity	0.82	0.64	0.81	0.62	0.91	0.90	0.88	0.86

Table 4.4. Average residuals and relative errors for predictions of SJ and S_{20} from physical and mechanical variables at the highest temperatures (400, 500, and 600 °C).

Cooling Method	Parameter	SJ Predictions		S_{20} Predictions	
		Average Residuals (1/10 mm)	Average Relative Errors (%)	Average Residuals (1/10 mm)	Average Relative Errors (%)
Air	UCS	1.48	6.97	3.15	5.84
	Elastic modulus	5.04	23.70	0.93	1.71
	Poisson's ratio	1.99	9.35	1.69	3.10
	P-wave velocity	4.31	20.26	1.58	2.93
	S-wave velocity	3.68	17.33	1.65	3.37
Water	UCS	0.90	4.48	2.87	5.33
	Elastic modulus	2.23	11.16	2.95	5.34
	Poisson's ratio	1.05	5.26	1.99	3.72
	P-wave velocity	0.19	0.96	1.96	3.64
	S-wave velocity	0.39	1.97	2.04	4.28

In general, the best fitting functions for SJ were logarithmic, while linear functions showed best results for S_{20} correlations for most parameters and cooling methods (Table 4.3). Coefficients of determination were higher in the case of S_{20} predictions for almost all regression functions and parameters.

The best correlation functions derived from Table 4.3 have been plotted to discuss trends. Thus, predictions from mechanical variables (UCS, elastic modulus, and Poisson's ratio) are represented for SJ in Figure 4.10 and for S_{20} in Figure 4.11. Predictions from physical variables (P- and S-wave velocities) are depicted in Figure 4.12 for SJ and in Figure 4.13 for S_{20}. Residuals have been also plotted as the differences between values measured in laboratory tests and predicted from regression functions. To evaluate the quality of predictions, absolute residuals and relative errors have been represented for the average temperatures where DRI exhibited greatest variation (400, 500, and 600 °C) (Table 4.4).

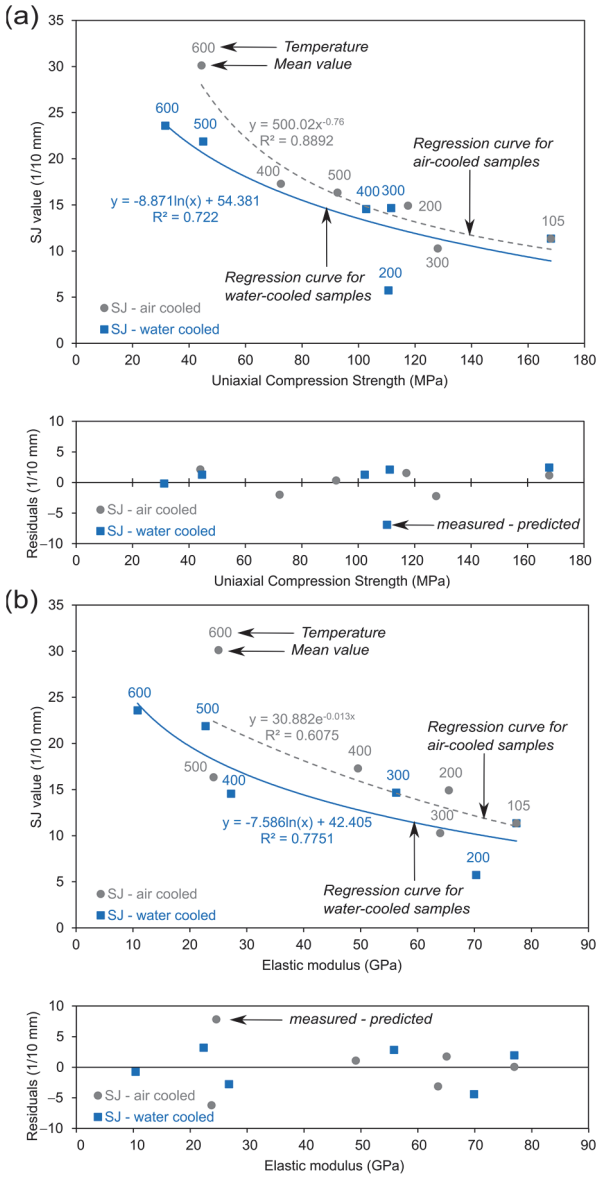

Figure 4.10. Cont.

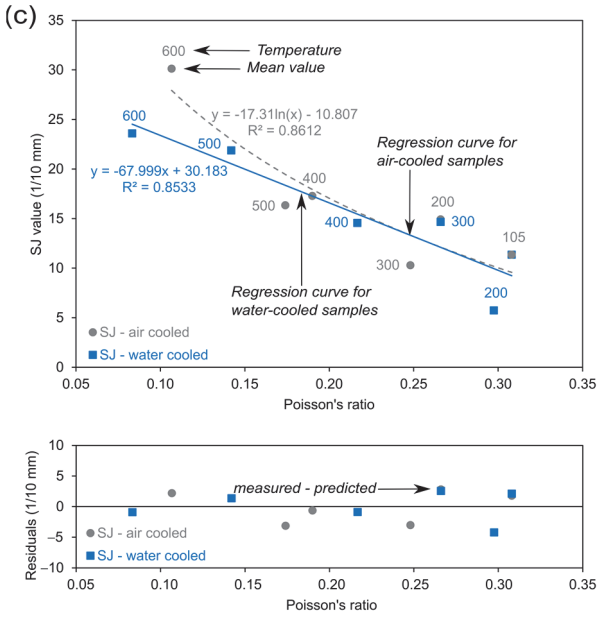

Figure 4.10. Correlations between variation of SJ and: (a) UCS; (b) elastic modulus; and (c) Poisson's ratio for air- and water-cooled samples.

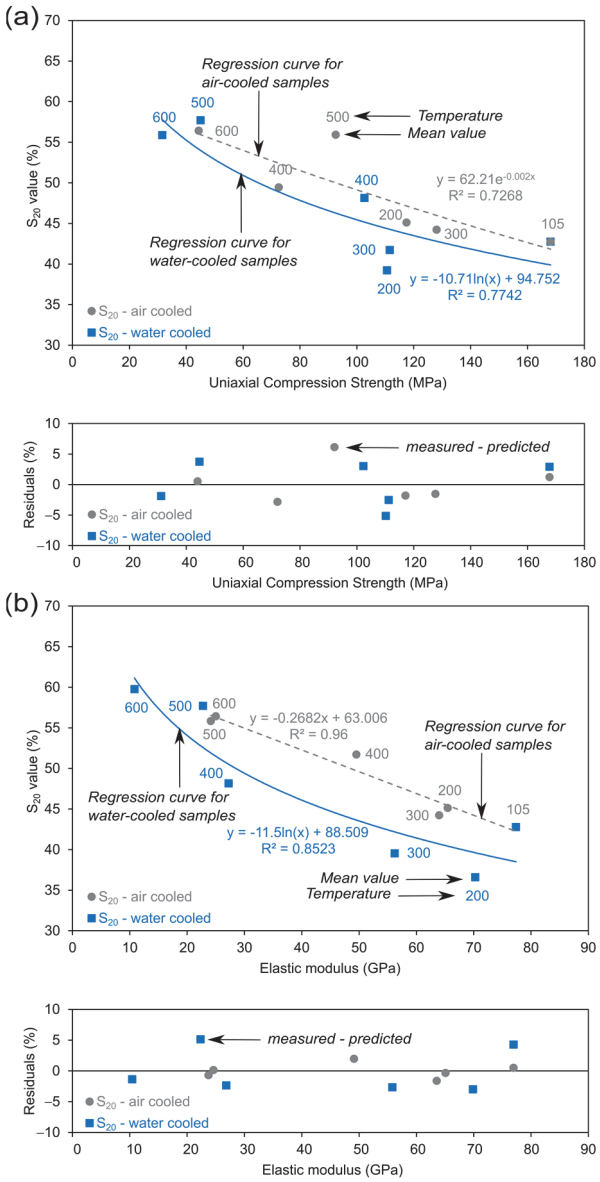

Figure 4.11. Cont.

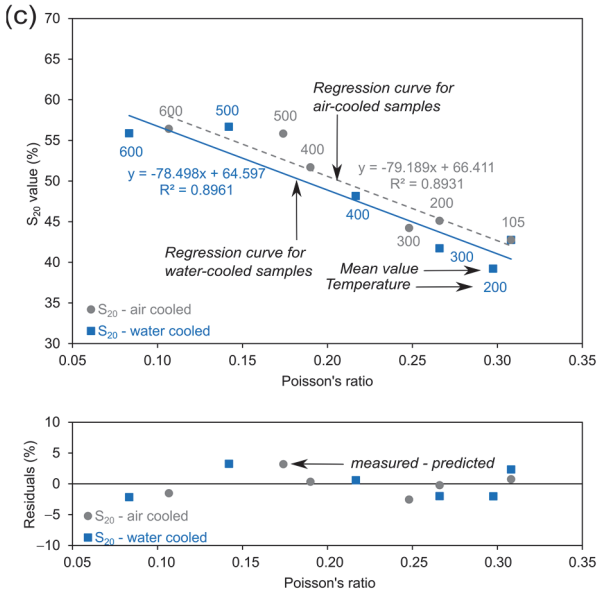

Figure 4.11. Correlations between variation of S_{20} and: (a) UCS; (b) elastic modulus; and (c) Poisson's ratio for air- and water-cooled samples.

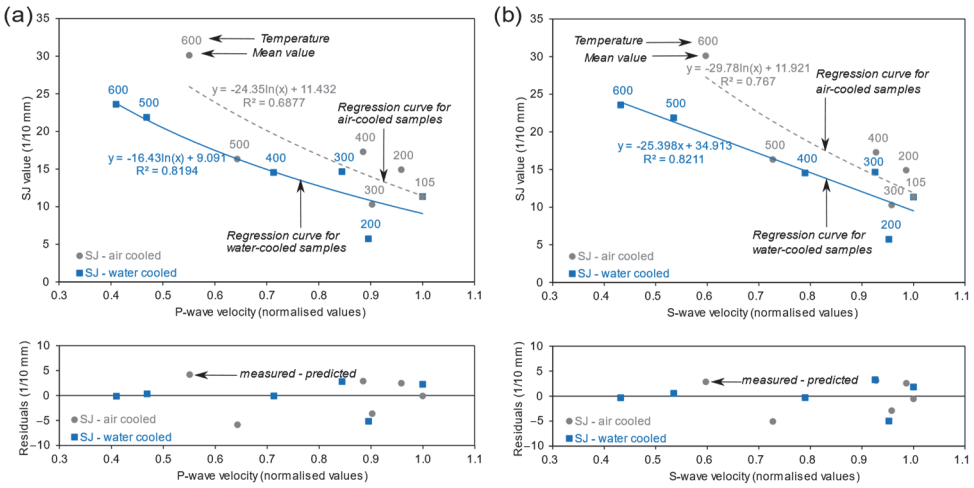

Figure 4.12. Correlations between variation of SJ and (a) P- wave velocity; and (b) S-wave velocity for air- and water-cooled samples.

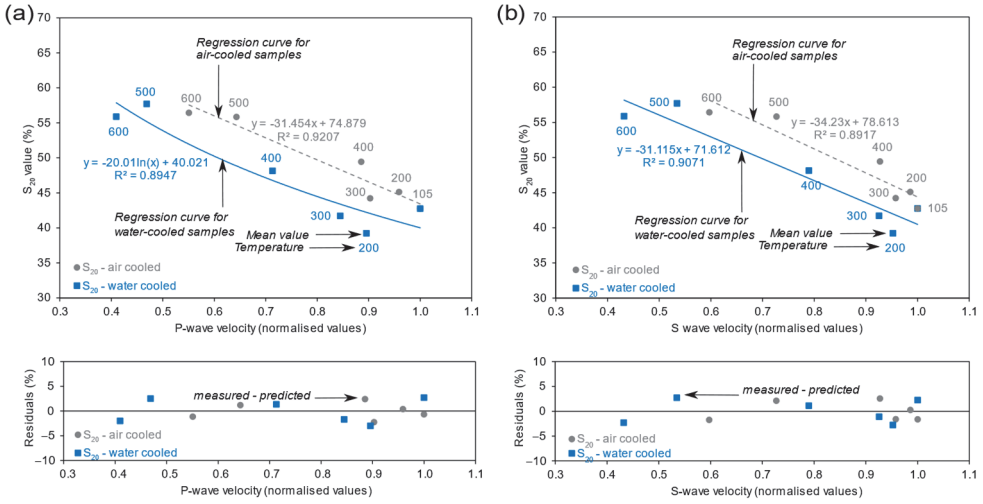

Figure 4.13. Correlations between variation of S_{20} and P- (a) and S-wave velocity (b) for air- and water-cooled samples.

4.4. Discussion

Decay in mechanical (UCS, elastic modulus, and Poisson's ratio) and physical (P- and S-wave velocities) properties were accompanied with a general increase in the Siever's J-value and in the brittleness S_{20} value that, together with the DRI index, point to a sustained increase in Prada limestone drillability.

DRI, SJ, and S_{20} values for the Prada intact limestone (before thermal treatment) have been compared with three types of intact limestones studied by Yarali and Soyer (2011). Although those limestones presented high, or very high, drillability categories, a lower DRI in Prada limestone (DRI = 44 corresponding to a 'medium drillability' class) is attributed to a greater UCS. Indeed, a linear correlation between UCS and DRI was proposed by Yarali and Soyer (2013) for intact limestones. This type of correlation has proven an excellent prediction of DRI from UCS for intact Prada limestone (UCS = 168.09 MPa; DRI = 43.71). In the case of SJ, we obtained a value of 11.35 ± 4.41 1/10 mm for the intact Prada limestone, and this corresponds to medium surface hardness, or resistance to indentation, according to the classes proposed by Dahl et al. (2012). In the case of S_{20} we obtained a value of 42.77 ± 10.94% for the intact rock and this is consistent with a medium rock brittleness, or the ability to be crushed by repeated impacts, also according to Dahl et al. (2012).

Thermal treatment resulted in a total increase of 40% in the DRI of Prada limestone at 600 °C, with no significant differences between cooling methods for the studied range of temperatures. Research is scarce on the variation of DRI with temperature, and so results cannot be compared with other lithologies. Research is scarce on the variation of

DRI with temperature and so results cannot be compared with other existing experiences. Methodologies and variables considered in the existing research on thermally assisted drilling differ greatly from those presented in our research. Rossi et al. (2018) reported a drop of 30% in the UCS of sandstone and granite for temperatures at 600 °C when using a flame jet to achieve high local heating rates, and UCS is strongly related to the drillability of the rock (Jamshidi et al. 2013; Ataei et al. 2015; Su et al. 2016). Although such a decrease in drillability is in the same range as that observed in our research, the lithologies and heating rates (20 °C/s) are very different. Jamali et al. (2019) applied high powered laser technology and performed scratch tests to indirectly measure reductions in rock strength, drilling strength, and fracture toughness at rates of 60% in granite and 30% in sandstone, but such results cannot be directly compared to the DRI reduction observed in our research, because the achieved temperatures and applied heating rates cannot be deduced. A decrease in the DRI with temperature for water-cooled samples coincided with a marginal porosity and a volume decrease at 200 °C (Martínez-Ibáñez et al. 2020). This effect is related to the closure of pores and fissures by thermal dilation of calcite (Yavuz et al. 2010; Fioretti et al. 2018) and is a factor that hinders penetration (Rossi et al. 2020d). Thus, closure of pores and fissures is behind a decrease in thermal drilling performance at low temperatures for water-cooled samples.

SJ and S_{20} represent different effects in a rotary-percussive drilling process, since the impact action of the bit is expressed by S_{20}, whereas thrust and rotation match with the SJ value (Su et al. 2016), and so we study their respective variations with temperature separately. Temperature influence is remarkable because for the highest temperature of 600 °C, SJ tripled and S_{20} doubled the initial values of the intact Prada limestone. The category of brittleness, or the ability to be crushed by repeated impacts (measured by S_{20}), varied with temperature from medium to high, and rock surface hardness or resistance to indentation (represented by SJ) varied from medium to low (both in the scale of Dahl et al.). We attribute this effect to the increase of porosity and the propagation and coalescence of micro fissures due to thermal treatment. That is noticeable in the case of S_{20}, where the trend is consistent with microstructural changes due to thermal treatment (Martínez-Ibáñez et al. 2021b). Incipient trans-granular fissures and porosity developed when heated to 400 °C match a gentle increase in S_{20}. At 500 °C the pore-sizes increase and fissures were larger and more connected, in agreement with a marked increase in crushability by repeated impacts represented by S_{20}

It is noteworthy that at 600 °C, SJ values were smaller for water-cooled samples, and S_{20} values were equal for both cooling methods. These results contradict the general observed trend of greater decay in mechanical and physical parameters when cooling with water for the studied range of temperatures. Finally, the variation on DRI with temperature almost copied that for S_{20}, and so variation with temperature of DRI is more influenced by S_{20} than by SJ.

We have explored different correlations to predict the variation in the drillability with temperature from variations in the physical and mechanical properties. In this study,

those correlations providing coefficients of determination greater than 0.80 and relative errors smaller than 10% have been considered. Logarithmic functions were predominant for SJ predictions, and the best correlations at high temperatures were found from UCS and Poisson's ratio for all cooling methods, and from P- and S-wave velocities for water-cooled samples. SJ predictions from UCS showed good values of relative error for the highest temperatures, but a low coefficient of determination was measured for water-cooled samples, although it strongly improved when skipping UCS value at 200 °C (R^2 = 0.99). This good correlation with UCS can be explained as vertical pressure on the bit and bit rotational speed (represented by SJ value), which have proven to be the most significant parameters in the penetration rate for rotary drilling (Saeidi et al. 2014). In addition, SJ represents surface hardness (Dahl et al. 2012), and therefore good correlations with UCS and other tests measuring surface hardness in the intact rock, such as Schmidt hardness test (Sabatakakis et al. 2008; Yarali and Soyer 2013), have been observed. Su et al. (2016) stated that elastic or plastic deformations affect rotary drilling, and this explains correlations with deformational parameters obtained in our research. Correlation with elastic modulus was weaker than with UCS, which is consistent with conclusions from other researchers (Jamshidi et al. 2013; Su et al. 2016). Finally, good correlations with P- and S-wave velocities were previously reported in existing research (Ataei et al. 2015) being higher for water-cooled samples in this case study. Coefficients of determination and residuals were remarkably better for S_{20} predictions and linear functions were predominant, providing good predictions for all variables and cooling methods. Correlations with UCS were the weakest when compared with the other parameters. It should be pointed out here that Dahl et al. (2012) explained this result by the fact that S_{20} and UCS are two very different test methods for determining the strength properties of rock, since S_{20} is determined by applying repeated impacts on the sample material, causing crushing of the sample material, while UCS is performed by applying load on the sample, at a relatively slow constant rate, until failure occurs.

The correlations between SJ and S_{20} with physical and mechanical parameters in thermally treated rocks derived from this work showed greater coefficients of determination than those reported for intact rocks by most authors (Jamshidi et al. 2013; Ataei et al. 2015; Su et al. 2016). The reason could be related to the fact that the increase in thermal damage in the rock (in terms of porosity and micro crack growth and coalescence), especially at certain temperatures, proportionally affects all the studied properties from Prada limestone. An increase in the micro-fissures leads to an increase in the ability to indent represented by SJ, and a drop in the rock resistance to crushing represented by S_{20}. In other words, variability in the studied properties from Prada limestone is caused by common thermal damage phenomena. Indeed, thermal treatment induces thermal decay on limestones, and that is triggered by well-known processes such as the decomposition of clay minerals cementing particles or filling micropores (Zhang and Lv 2020). For temperatures of up to 200 °C, the loss of water is the main influencing factor in the

thermal damage of limestones (Zhang and Lv 2020) due to high-pressure vapour escaping from the rock sample that causes the generation and coalescence of micro-fractures (Meng et al. 2020).

Quartz-bearing limestones experiment a dramatic microcracking and volume increase at the phase transition between 550 and 600 °C, with a strong peak at 573 °C (Van der Molen 1981; Glover et al. 1995). Local thermal stress concentrations and microcracking occur due to mismatches in thermal expansion coefficients of different mineral particles (Liu and Xu 2013; Zhang et al. 2017b; Villarraga et al. 2018; Yang et al. 2019), especially in the range of temperatures between 400 and 500 °C (Meng et al. 2020); and thermal oxidation of pyrites leads to a dramatic increase in pore-pressure on pyrite-bearing limestones, resulting in increased thermal damage and explosive behaviour (Martínez-Ibáñez et al. 2021a). All these processes affect rock integrity and cause a continuous and gradual decay in physical and mechanical properties of rock with temperature — with some threshold temperatures marking changes in the general trend (Meng et al. 2020). For all the above, it can be stated that strong correlations between physical, mechanical, and drillability variables in thermally treated Prada limestone can be explained by a common pattern of change in features due to thermal damage processes.

Consequently, the strong correlations observed between UCS and SJ, and between P- and S-wave velocities and S_{20}, enable quick and easy evaluations to be made of the variation with temperature in drillability based on the variation of such mechanical and physical properties for supporting tunnel excavations. Furthermore, these results open the door to the development of drilling and excavation equipment based on the concept of thermal treatments for improving the tunnel excavation performance.

4.5. Conclusions

In our study, samples from Prada limestone were heated to temperatures of 105, 200, 300, 400, 500, and 600 °C and then cooled at a slow rate in air, or by quenching in water. The rocks significantly increased in surface hardness, resistance to indentation (measured by Siever's J value), and in brittleness (measured by the brittleness S_{20} value). These measurements combined with the evidence from the DRI index, point to a sustained increase in rock drillability. Variation in drillability with temperature were compared with decay in mechanical (UCS, elastic modulus and Poisson's ratio) and physical (P- and S-wave velocity) properties of Prada limestone. The derived conclusions of our study are listed below:

1. DRI increased with temperature, implying a change in the drillability category at 500 °C (from medium to high) and a total increase of 40% at 600 °C, with no significant differences between cooling methods in the studied range of temperatures.
2. A decrease in DRI at 200 °C for water-cooled samples is explained by the closure of pores and fissures at that temperature.

3. Temperature influence is remarkable, as SJ tripled and S_{20} doubled at 600 °C the initial values for intact rock. An increase in micro-fissures leads to an increase in the ability to indent represented by SJ, and a drop in resistance to crushing represented by S_{20}.
4. DRI trend almost copied that for S_{20}, so thermal variation in DRI is more influenced by S_{20} than by SJ.
5. We investigated correlations to predict the variation of SJ and S_{20} with temperature from variations in the physical and mechanical properties, and we reported strong correlations between most of the studied variables. The common explanation for these correlations is that variation of the studied properties with temperature is caused by a common thermal damage phenomenon (increase in porosity and micro cracking growth and coalescence) that strongly affects all considered geomechanical parameters.

In summary, a substantial improvement in the drillability of the rock when heated, measured in terms of DRI value increase, can help improve the efficiency of mechanical excavation. Additionally, the obtained correlations enable quick and easy evaluations of drillability based on basic geomechanical parameters (such as UCS and P- and S-velocities) to support the Tres Ponts Tunnel excavations.

Chapter 5. Discussion

The present PhD thesis has raised several research questions regarding the thermal behaviour of Prada limestone and the derived consequences on the Tres Ponts Tunnel. To cope with them, samples from Prada limestone were thermally treated and variation in chemical composition and microstructure, physical, mechanical, and drilling properties were analysed. The following sections discuss in detail the results and answer the issues raised that led to this research.

5.1. Research Question Q1

What are the micro and macro-structural effects of high temperatures in Prada limestone?

To answer this question, samples were heated to 105, 200, 300, 400, 500 and 600 ºC, then cooled using one of two methods to simulate various modes of fire intervention: air- or water-cooling. Observation through SEM and MIP techniques pointed to dramatic micro-structural changes in Prada limestone. Thus, samples heated to 300 ºC showed an increase in the size of micro-fissures when compared with intact rock (Figure 2.3) and pores developed with a lack of connections (retained mercury was maximum at that temperature). Incipient trans-granular fissures and porosity developed when heated to 400 ºC (Figure 2.2a, b). At 500 ºC the pore-size increased and fissures were larger and more connected (Figure 2.2c) as was previously reported by other authors (Chen et al. 2009) especially for the water-cooled samples (Figure 2.2d). Well-formed and connected fissures developed at 600 ºC for both cooling methods (Figure 2.2e, f), and pores

exhibited a wide range of sizes (Figure 2.3) that are more connected than at lower temperatures (retained mercury was minimum).

Such thermal damage described above is caused by various physicochemical mechanisms. Thermochemical damage involves specific chemical reactions, such as thermal decomposition of calcite, but that effect is discarded in Prada limestone: the proportion of calcite remained almost constant (Table 2.2), and that is explained because the maximum temperature in this study (600 ºC) was lower than that for carbonate dissociation from 700 to 900 ºC (Ferrero and Marini 2001). In certain cases, thermal damage causes the decomposition of clay minerals cementing particles or filling micropores (Zhang and Lv 2020), but in this research the content of oxides remained almost unchanged with temperature (Table 2.2) and so that effect is discarded. Finally, the loss of water is the main influencing factor on the thermal damage of limestones for temperatures up to 200 ºC (Zhang and Lv 2020), as the high-pressure vapour escaping from the rock sample induces the generation and expansion of micro-fractures (Meng et al. 2020). Nevertheless, no significant micro-textural changes developed for temperatures up to 200 ºC in Prada limestone. For these reasons, thermal decomposition of calcite, clay mineral decomposition, and the loss of water, do not explain the thermal damage observed in Prada limestone.

Anisotropic expansion of calcite is the main cause of thermal cracking in carbonate rocks heated at a slow rate (Lion et al. 2005; Malaga-Starzec et al. 2006). A variable presence of quartz in Prada limestone was observed through SEM (Figure 3.3), and rocks containing quartz experience a sudden microcracking and volume increase at the phase transition between 550 and 600 ºC, with a strong peak at 573 ºC (Van der Molen 1981; Glover et al. 1995), and this is consistent with severe micro-cracking in Prada limestone at 600 ºC. Additionally, the thermal coefficient of calcite (1.4×10^{-5} ºC^{-1}) is less than a half than that of clay (3.4×10^{-5} ºC^{-1}) or quartz (3.3×10^{-5} ºC^{-1}) (Belmokhtar et al. 2017), and so a mismatch in thermal expansion coefficients between mineral particles led to local thermal stress concentrations, thus increasing microcracking (Liu and Xu 2013; Zhang et al. 2017b; Villarraga et al. 2018; Yang et al. 2019), especially from 400 ºC (Meng et al. 2020). Thus, anisotropic expansion of calcite, and mismatches in thermal expansion coefficients between mineral particles and quartz phase transition explain the micro textural changes observed in Prada limestone in the range of temperatures between 400 and 600 ºC. Greater damage observed in water-cooled samples at 500 ºC is attributed to the effect of rapid cooling (quenching) that leads to such tensile stresses that nucleate cracks (Kim et al. 2014; Mallet et al. 2014).

To discuss the accuracy of the results, standard deviations were compared with other authors for variables such as UCS (Sengun 2014) and the elastic modulus (González-Gómez et al. 2015). The obtained accuracy is considered normal for a natural material such as the studied rock, where changes in the grey tone and a variable presence of calcite veins are typical (Figure 1.2), and this contrasts with manufactured materials whose composition and texture is controlled. For these reasons, trends are described in view of

mean values, and local variations are dismissed in some cases when standard deviation is high.

The effects of thermal treatment at temperatures up to 400 ºC refer to a gentle increase in open porosity (Figure 2.4) and a decrease in ultrasound wave velocities (Figure 2.6), and that was also reported in limestones by other authors (Yavuz et al. 2010; Andriani and Germinario 2014; Sengun 2014; Yang et al. 2019). That is consistent with an increase in the size of pores and micro-fissures observed through MEP (Figure 2.3) and SEM (Figure 2.2a, b). P- and S- wave velocities showed lower values for water-cooled samples, and that points to greater thermal damage in the rock when cooling samples at a rapid rate. Elastic modulus and Poisson's ratio (Figure 2.9) also showed a slow decay in this range of temperatures, what was previously reported by other authors (Yavuz et al. 2010; Sengun 2014). This is because of a gradual increase in porosity and micro-fissures that ease the deformation in the rock (Figure 2.8). It is noteworthy that at 300 ºC water-cooled samples exhibited an increase in open porosity that was followed by an evident decrease in the elastic modulus. UCS showed a steady decrease at 200 ºC (Figure 2.7) and that could be attributed to intra-granular micro-fissures and is in line with other authors (Lion et al. 2005), although SEM observations were inconclusive at that temperature. Consequently, structural resistance within the Tres Ponts Tunnel may be affected from the first stages of a fire.

Micro-structural changes at 500 ºC involved larger fissures (Figure 2.2c, d) and the effects are clear: samples exhibited a sharp increase in open porosity (Figure 2.4) and a marked decrease in P- and S-wave velocities (Figure 2.6). Elastic modulus and Poisson's ratio exhibited decreasing trends in this range of temperatures (Figure 2.9). Fissures were more connected in water-cooled samples (Figure 2.2d) and that caused a steep drop in the UCS (Figure 2.7). Values in all physical and mechanical variables point to greater decay in the rock when cooling samples at a rapid rate. At 600 ºC open porosity and ultrasound wave velocities showed a continuing trend after the abrupt changes observed at 500 ºC, and elastic modulus and Poisson's ratio exhibited decreasing values or stabilization. Coalescence of microfissures in air-cooled samples involved an abrupt decrease in UCS. It is remarkable that values at 600 ºC showed greater variations for water-cooled samples for most parameters, and this indicates greater thermal damage when cooling samples at a rapid rate and in line with other authors (Brotóns et al. 2013). Total mean variation at 600 ºC for air- and water-cooled samples (respectively) was 382 % and 568 % in open porosity; – 45% and – 59% in P-wave velocity; – 40% and – 57% in S-wave velocity; – 74% and – 81% in UCS; – 68% and – 86 % in elastic modulus; – 65% and – 73% in Poisson's ratio. Higher temperatures than 600 ºC led to samples losing their integrity due to mass cracking and that prevented testing.

Dark grey samples represent a small fraction of the total Prada limestone. Such samples exhibited a greater variation in open porosity and ultrasound wave velocities than reported above when heated from 400 ºC, and even certain dark samples showed an explosive behaviour and release of sulphurous gas. How the samples were studied

separatedly and the causes and mechanisms for such different thermal behaviour will be discussed in Research Question 2.

5.2. Research Question Q2

What mechanisms are behind thermal damage and explosive behaviour registered in a dark fraction of the Prada limestones?

Intact Prada limestone shows a bluish grey colour, and a variable grade of lightness between samples: from light bluish grey (5B 6/1) to dark bluish grey (5B 3/1) according to Munsell colour chart (Figure 1.2c). Dark grey samples exhibited a greater variation in open porosity and ultrasound wave velocities from 400 ºC (Figure 3.7), and even certain dark samples showed an explosive behaviour (Figure 3.6) and released sulphurous gas. To determine the causes and mechanisms behind such differentiated behaviour, two varieties of Prada limestones were separated: a dark grey texture, bearing quartz and clay minerals, pyrites, and organic matter, and a light grey texture with minor or nonexistent presence of such components (Table 3.2). Samples were heated to temperatures of 105, 300, 400 and 500 ºC, and the thermal behaviour of both textures was compared.

Physicochemical mechanisms behind thermal damage in Prada limestone were discussed in Research Question Q1, and involve anisotropic expansion of calcite, and mismatches in thermal expansion coefficients between mineral particles and quartz phase transition. Although the presence of quartz was greater in the dark grey texture, different thermal damage between textures was found in the range from 400 and 500 ºC, and that is far from quartz phase transition. Thus, content in quartz cannot explain different thermal damage between textures. Clay minerals were present in a greater proportion in the dark grey fraction, and so microscale destructuring processes induced by differential thermal expansion of the mineral components contributes to differences between textures. SEM enabled the discovery of differences in the micro-structure of the intact samples: the dark grey texture showed micro-porosity and microcracks, while the light grey samples showed greater pore size and few microcracks (Figure 3.3). An initial micro-fissuring in the intact dark grey samples leads to greater coalescence and growth of fissures when heated, and so contributes on a greater thermal damage. Thus, an initial greater proportion in clay minerals, as well as microcracks, contribute to greater thermal damage in the dark texture. Nevertheless, certain dark grey samples exploded between 400 and 500 ºC, and therefore there must be additional mechanisms triggering such violent behaviour. Such mechanisms must contribute, among those discussed above, to a greater variation in open porosity and ultrasound wave velocities. Hence, discussion will focus on the differing content of organic matter and pyrites between textures.

The presence of organic matter (Table 3.2) explains the dark grey tone and the presence of pyrite. Thus, marine anoxic conditions existing in continental margin sediments enable bacterial sulphate reduction from organic matter. Sulphate then reacts with detrital iron minerals in the sediment to form pyrites (Fe_2S) (Berner 1970, 1982).

Chemical analyses determined a greater content in iron and sulphide in the dark grey texture (Table 3.2). XRD confirmed the presence of pirites and SEM enabled direct observation of framboidal pyrite structures (Figure 3.3c). Therefore, a greater content in organic matter and pyrites in the dark texture established an additional difference between varieties.

TG-DTA-DSC-MS enabled the identification of three different thermochemical processes in the dark grey texture (Figure 3.4). Stage I (100 < T <200 ºC) involved dehydration of water adsorbed by the microporosity of mineral surfaces and in clay minerals. Stage II (400 < T <600 ºC) covers two different chemical processes. The release of CO_2 and H_2O from 400 to 600 ºC is consistent with thermal oxidation of organic matter, represented as $CH_2O_{(OM)} + O_2 \rightarrow CO_2 + H_2O$ (Galbács et al. 1998; Cuypers et al. 2002; Boyle 2004). SO_2 was detected from 405 to 535 ºC, and exhibited a sharp peak at 460 ºC and this is consistent with thermal oxidation of pyrites (Hong and Fegley 1997; Gazulla et al. 2009) and is represented as $2FeS_{2\ (pyrite)} + 11/2O_2 \rightarrow Fe_2O_{3\ (hematite)} + 4SO_2$. Finally, stage III (T > 600 ºC) represents the initial decomposition stages of inorganic carbonate and can be written as $CaCO_{3\ (calcite)} \rightarrow CaO + CO_2$. Hence, thermal oxidation of pyrites, releasing SO_2 and forming hemathite, takes place when dark grey samples forming Prada limestone are heated above 400 ºC. Additional techniques enabled confirming the chemical reactions mentioned above, such as EDX and chemical analysis, that determined a reduction in oxygen, sulphur, and sulphide at 500 ºC (Table 3.2). Hematite (Fe_2O_3) was confirmed through XRF and using colorimetry analysis, as limestones exhibit a process of reddening when heated under oxidative conditions (González-Gómez et al. 2015). Indeed, a tendency towards reddish tones was visually appreciated between 400 ºC and 500 ºC and numerically confirmed in view of CIELAB a* values (Figure 3.8). However, pyrite transformation was incomplete for the test conditions of temperature and time, in view of chemical composition and XRD at 500 ºC. This must be related to a lack of available oxygen in pores that depends on the gas diffusion coefficient (Currie 1960). Such gas diffusion coefficient strongly depends on the porosity and pore size (Benavente and Pla 2018), and dark grey Prada limestone is a low-porosity rock with dual microstructure that leads to poorly connected small pores in view of MIP (Figure 3.5). In addition, the formation of ferric/ferrous compounds in the oxidation process has a pore-blocking effect (Hu et al. 2006). The release of SO_2 in the pyrite oxidation process, together with thermal oxidation of organic matter which releases CO_2 and H_2O from 400 ºC, leads to an increase in pore pressure, causes an expansion of rock, and so an accelerated fissuring. This process is accelerated by the presence of CO_2 from organic matter and calcite decomposition that speeds up the thermal oxidation of the pyrite (Lv et al. 2015; Zhang et al. 2019) which leads to a more violent chemical reaction. The observed behaviour is closely related to the initial number and distribution of micro-fissures, identified on dark samples using MIP, and their two-dimensional shape, which causes a stress concentration in their tips (Griffits 1920).

During heating of the samples, we clearly heard the sound of multiple violent impacts inside the furnace. Moreover SO_2 was released throughout the room immediately after

the explosive event, detaching a strong smell that made necessary the use of gas extraction means. After opening the furnace, exploded samples showed a total lack of structure and its fragments were spread over the furnace, even embedded in the furnace walls as a result of the explosion (Figure 3.6). Lectures from thermocouples in the exact moment of that explosion were of 390 ºC in the centre of the sample and 438 ºC on its surface, and that is compatible with the rising branch of the SO_2 generation curve, that starts at 405ºC and exhibit its peak at 460 ºC. The release of SO_2 above a narrow range of temperatures would cause a peak in pore pressure that, jointly with a structure of micro-fissures in the dark texture, would cause a violent fracturing of the material. Thermal oxidation of pyrites has a greater contribution in the explosive phenomenon than organic matter oxidation, since release of SO_2 evolves in a narrower temperature range than CO_2 and H_2O. Moreover peak SO_2 occurs at a temperature that is compatible with the registered explosive event (above 460 ºC), while peak for organic matter oxidation takes place at higher temperatures (above 520 ºC). Moreover the existing research on the thermal effects on carbonate rocks containing organic matter relate to splitting and cracking events (Yavuz et al. 2010; Andriani and Germinario 2014; González-Gómez et al. 2015), but not refer to explosive events of such violence as described in this work. The total thermal damage on dark grey samples, in terms of open porosity and ultrasound wave velocity variation (Figure 3.7), is explained by the partial contribution of the pore overpressure and gas release caused by the thermal oxidation of pyrites and organic matter, jointly with further factors identified in this research such as differential thermal expansion of the mineral components and initial micro-fissuring in the intact rock.

Finally, a 40 % of the dark samples did not undergo visible damage after heat treatment, although they experimented a greater variation in their physical properties when compared to the light grey texture. This is because pyrite content and initial micro-fissure and pore structure would induce a particular explosive potential to each sample. Further investigations would be necessary to quantitatively relate pyrite content and initial micro-fissure with explosive potential to each sample. Nevertheless, that is difficult because chemical and textural test are destructive, and therefore are not compatible with the need to count with intact samples to monitor their explosive behaviour when heated.

5.3. Research Question Q3

Could temperature and cooling methods improve the drilling of Prada limestone?

To determine the thermal effects on the drillability of Prada limestone, thermally treated samples from Research Question Q1 were used. A dark grey fraction from Prada limestone described in Research Question Q2 is not included in this research. Prada limestone before being thermally treated exhibits a medium surface drillability or resistance to indentation (SJ of 11.35 ± 4.41 1/10 mm), a medium rock brittleness that can be crushed by repeated impacts (S_{20} of 42.77 ± 10.94 %), and a medium drillability (DRI of 44), according to classes proposed by Dahl et al. (2012).

Temperature influence in the drilling performance of Prada limestone is noteworthy. At 500 ºC the category of brittleness varied from medium to high, rock surface hardness varied from medium to low, and drillability varied from medium to high. At 600º C, S_{20} doubled, SJ tripled, and DRI increased by 40 % from the initial values of the intact limestone. That is attributed to microstructural changes derived from the thermal treatment of Prada limestone, whose causes and mechanisms have been extensively discussed in this PhD dissertation in Research Questions Q1 and Q2. Thus, the increase in the number and density of micro-fissures leads to an ease in the ability to indentation represented by SJ, and a drop in the strength of rock to resist crushing represented by S_{20}. A decrease in the SJ, S_{20}, and DRI at 200 ºC for water-cooled samples coincided with a marginal decrease in porosity (Figure 2.4) and volume (Figure 2.5), and this is related to the closure of pores and fissures by thermal dilation of calcite (Yavuz et al. 2010; Fioretti et al. 2018). No significant differences between cooling methods were observed in the DRI at the highest temperatures of 500 and 600 ºC (Figure 4.9c). That is different from results discussed in Research Question Q1, where a greater decay was highlighted in mechanical and physical parameters when cooling with water. It is noteworthy that the DRI trend almost copied that for S_{20}, and so variation in DRI with temperature is more influenced by S_{20} than by SJ. Summarizing, the temperature improves the drillability of Prada Limestone. In contrast, the effect of the cooling method is not significant.

5.4. Research Question Q4

Do significant correlations exist between properties in the thermally treated Prada limestone? Would correlations be useful to indirectly predict the final values of strength, elasticity, and drillability after a fire in the Tres Ponts Tunnel affecting Prada limestone?

ANOVA and simple regression analyses were conducted to explore if the natural position of samples have a significant influence in the variability of rock properties presented in Research Question 1. The dark fraction from Prada limestone presented in Research Question Q2 is not included in this research. Results enabled discarding such influence (Table 2.4, Figure 2.11). Consequently, laboratory results can be compared between various samples, and conclusions can be generalised throughout the Tres Ponts Tunnel. Moreover, correlations can be proposed to indirectly obtain reference values for the rock affected by temperature. It was also confirmed that temperature and cooling methods are factors with statistical significance, and this is coherent with that experimentally proven and discussed in Research Question Q1. Simple regression functions were chosen because they configure a simple and quick method to provide good predictions for intact carbonate rocks (Yasar and Erdogan 2004). In this study, correlations are considered of good quality when coefficiens of determination are greater than 0.80 and mean relative errors for the highest temperatures (400, 500 and 600 ºC) are smaller than 10 %.

UCS predictions for air-cooled samples exhibited poor coefficients of determination that varied between 0.65 and 0.69 (Figure 2.12), and high relative errors for the highest temperatures of between 23 and 30 % (calculated from Table 2.6), with slight differences between predictors. Correlations improved for water-cooled samples, and exhibited coefficients of determination from 0.88 to 0.97 (Figure 2.12), and relative errors of between 13 and 17 % (calculated from Table 2.6). The best-fitting results were obtained when using P-wave velocity and volume as predictors. Although predictions improved for water-cooled samples, the relative errors are still high. Elastic modulus predictions showed excellent coefficients of determination that varied from 0.91 to 0.96 for all cooling methods (Figure 2.13). The average residuals for the highest temperatures were between 10 and 17 % for air-cooled samples, and from 20 to 27 % for water-cooled samples (calculated from Table 2.7), and so the relative errors are still considered high. The best-fitting results were obtained when using open porosity as a predictor, for all cooling methods. Correlations presented in this research enable predicting mechanical and deformational parameters from non-destructive tests on limestone affected by high temperatures, but relative errors are high (greater than 10 %) in most cases, and predictions of UCS in air-cooled samples showed weak correlations (coefficient of determination lower than 0.80). For these reasons, predicted values have to be used carefully and only to provide quick indicative values to make the initial decisions after a tunnel fire.

SJ predictions for air-cooled samples exhibited a range of coefficients of determination between 0.61 and 0.89 (Figure 4.10, Figure 4.12), and of relative errors for the highest temperatures of between 7 and 24 % (Table 4.4). Predictions for water-cooled samples showed coefficients of determination from 0.72 to 0.85 (Figure 4.10, Figure 4.12), and relative errors of between 1 and 11 % (Table 4.4). UCS showed a good predictor for SJ, and this is because good correlations exist between UCS and surface hardness for the intact rock (Sabatakakis et al. 2008; Yarali and Soyer 2013). Good correlations also exist between SJ and elastic modulus for the water-cooled samples, and this is because elastic deformations affect rotary drilling (Su et al. 2016), although such correlation was weaker than with UCS (Jamshidi et al. 2013; Su et al. 2016). Finally, good correlations with ultrasound wave velocities exist, and that was previously revealed in existing research (Ataei et al. 2015). In this research such correlations are higher for water-cooled samples, and this represents a direct relation between the thermal damage in the rock, represented by ultrasound wave velocity variation, and the ability to indent represented by SJ. For S_{20} predictions, air-cooled samples showed coefficients of determination that varied from 0.73 and 0.96 (Figure 4.11, Figure 4.13), and relative errors for the highest temperatures of between 2 and 6 % (Table 4.4). Predictions for water-cooled samples exhibited coefficients of determination from 0.77 to 0.91 (Figure 4.11, Figure 4.13), and relative errors of between 4 and 5 % (Table 4.4). Thus, S_{20} predictions were better than that for SJ, for almost all predictors and cooling methods, except for correlations from UCS. That is because S_{20} and UCS are two very different test methods (Dahl et al. 2012), since S_{20} represents the ability to be crushed by repeated impacts that is determined by

crushing of the sample material by repeated impacts, while UCS is performed by applying load on the sample at a relatively slow constant rate, until failure occurs. Consequently, the strong correlations observed between UCS and SJ, and between P- and S-wave velocities and S_{20}, enable us to easily perform quick evaluations of the variation in the drillability with temperature to support tunnel excavations.

Correlations between most physical, mechanical, and drilling features in the thermally-treated Prada limestone are stronger than reported for intact rocks (Jamshidi et al. 2013; Ataei et al. 2015; Su et al. 2016). Such strong correlations represent a common pattern of change in the rock features, and this is a result of thermal damage in the rock. Thus, increasing porosity and micro crack growth and coalescence, especially for certain temperatures and cooling methods, proportionally affects all the studied properties from Prada limestone. The physicochemical mechanisms behind such thermal damage have been extensively discussed in this PhD dissertation in Research Questions Q1 and Q2, and involve the anisotropic expansion of calcite, mismatch in thermal expansion coefficients between mineral particles, quartz phase transition, and thermal oxidation of pyrite and organic matter.

Chapter 6. Conclusions

The present Chapter summarises the main conclusions of this research. These have been grouped according to the research questions stated in the objectives of this PhD thesis. This work has opened new lines of research that will be also presented in this chapter.

6.1. Effects of high temperatures on the physical and mechanical properties of Prada limestone

This research provides an in-depth insight into the micro- and macro-structural changes induced by temperature in the properties of Prada limestone. The main conclusions are listed below:

1. Micro-structural changes are explained by various physicochemical mechanisms such as the anisotropic expansion of calcite, mismatch in thermal expansion coefficients between mineral particles, and quartz phase transition. A greater thermal damage in water-cooled samples is due to tensile stresses that nucleate cracks.
2. Up to 400 ºC, increase in open porosity and decrease in ultrasound wave velocities are consistent with growth of pores and micro-fissures. That is also linked to progressive decrease in elastic modulus. P- and S- wave velocities showed lower values for water-cooled samples, which indicates a greater thermal damage fot such cooling method. UCS showed a steady decrease in this range of temperatures and so strength in Prada may be affected from the first stages of a fire.

3. At 500 ºC, samples exhibited a sharp increase in open porosity and a marked decrease in P- and S-wave velocities due to larger fissures. Water-cooled samples showed more connected fissures and that caused a steep drop in the UCS. Samples showed greater decay in all variables if cooled with water.
4. At 600 ºC, coalescence of microfissures in air-cooled samples involved an abrupt decrease in UCS. Final values at 600 ºC showed greater variation for water-cooled samples for most parameters.
5. Total mean variation at 600 ºC for air- and water-cooled samples was of 382 % and 568 % in open porosity; – 45% and – 59% in P-wave velocity; – 40% and – 57% in S-wave velocity; - 74% and – 81% in UCS; - 68% and -86 % in elastic modulus; - 65% and – 73% in Poisson's ratio. Samples lost their integrity over 600 ºC and that prevented further testing.
6. Dark grey samples represent a small fraction of the total Prada limestone. These samples exhibited a greater variation in open porosity and ultrasound wave velocities than reported above when heated from 400 ºC, and certain dark samples showed an explosive behaviour and release of sulphurous gas. These dark grey samples were studied separatedly and conclusions are presented in the next section.

The obtained results enable the evaluation of the degree of damage in this limestone if it is affected by a fire in the Tres Ponts Tunnel and the subsequent determination of the new physical and mechanical properties of this rock after a fire event. This information will help in planning intervention protocols for emergency response teams, predicting times available for evacuation, evaluating safety conditions during post-fire inspections, as well estimating the extent of the damage and the time needed for repair.

6.2. Thermal damage mechanisms on pyrite-bearing Prada limestones

In this research, two negative effects of different intensity are identified when heating a dark texture from Prada limestone over 400 ºC. Firstly, the explosion of certain samples releasing SO_2 and secondly, a greater thermal damage in terms of open porosity and ultrasound wave velocity variation. The main derived conclusions from this research are:

1. Two varieties of Prada limestones are compared: a dark grey texture, bearing quartz and clay minerals, pyrites and organic matter; and a light grey texture with minor or no presence of such components.
2. Thermochemical analysis of the dark texture revealed two thermal reactions involving gas release: thermal oxidation of pyrites (FeS_2) releasing SO_2 from 400 to 520 ºC, and thermal oxidation of organic matter releasing H_2O and CO_2 from 400 to 600 ºC.
3. The explosion of certain samples and the release of sulphurous gas in the room are compatible with temperatures in the rising branch of SO_2 release, between 405 and 406 ºC. That would cause a peak in pore pressure that, jointly with a

structure of micro-fissures in the dark texture, would cause a violent fracturing of the material.

4. Thermal oxidation of pyrites has a greater contribution in the explosive phenomenon than organic matter oxidation, as the release of SO_2 occurs in a narrower temperature range than organic matter, and peak SO_2 occurs at a temperature that is compatible with the explosive event.
5. Total thermal damage on dark grey samples is explained by the partial contribution of the pore overpressure and gas release caused by the thermal oxidation of pyrites and organic matter, jointly with further factors such as mismatch in the thermal expansion coefficients of rock-forming minerals and initial micro-fissuring in the intact rock.
6. Some 40 % of the dark samples did not undergo visible damage after heat treatment. Although results are definitive and based on evidence, further investigations would be necessary to quantitatively relate pyrite content and initial micro-fissure with explosive potential to each sample.

Effects described above have critical implications in underground infrastructures and mining engineering works, since temperatures greater than 400 ºC could lead to explosive phenomenon, involving mass fracturing, rock integrity loss, and strength decay. Moreover, SO_2 released into the atmosphere has a harmful effect on the health (ATSDR 1998) of people exposed. Additionally, SO_2 can form corrosive acid compounds (Kumar and Imam 2013) that shorten infrastructure life and increase maintenance costs.

6.3. Thermal effects on the drilling performance of Prada limestone

In this research a substantial improvement in the drillability of rock has been observed when heated, measured in terms of DRI. The derived conclusions of this research are listed below:

1. At 500 ºC, the category of brittleness varied from medium to high, rock surface hardness varied from medium to low, and the drillability varied from medium to high. At 600º C, S_{20} doubled, SJ tripled, and DRI increased by 40 % the initial values of the intact limestone.
2. Improvement in drillability is attributed to increase in porosity and growth and propagation of fissures with temperature. A decrease in the SJ, S_{20} and DRI at 200 ºC for water-cooled samples coincided with a marginal decrease in porosity and volume, and this is related to the closure of pores and fissures by thermal dilation of calcite.

3. No significant differences between cooling methods were observed in the DRI at the highest temperatures of 500 and 600 ºC, and this is different from observed in mechanical and physical parameters (which exhibited greater variation when cooled with water).
4. The DRI trend almost copied that for S_{20}, and so variation in DRI with temperature is more influenced by S_{20} than by SJ.
5. The dark fraction from Prada limestone discussed in Research Question Q2 is not included in this research.

Modern mechanical excavation strongly depends on the efficiency of the means involved to optimise investment costs. The effects of thermal treatment on Prada limestone drillability would help improve the efficiency of mechanical excavation.

6.4. Prediction of mechanical parameters in Prada limestone using correlations

Correlations between physical, mechanical, and drillability features discussed in research questions Q1 and Q3 are exlored to evaluate if strength and deformational features can be predicted in Prada limestone affected by high temperatures. The main derived conclusions from this research are:

1. ANOVA and simple regression analyses enabled discarding a significant influence of the position of the natural sample in the variability of physical and mechanical properties, therefore results can be compared between various samples, conclusions can be generalised throughout the tunnel, and correlations between parameters can be explored.
2. Predictions for elastic modulus were more accurate than those for UCS, with small differences between predictors and cooling methods. Calculated values of UCS after thermal treatment were better for water-cooled samples, especially when using P-wave velocity as a predictor.
3. Relative errors for the highest temperatures were greater than 10 % in most cases, and so predicted strength and deformational values have to be used carefully and only to provide quick indicative values to make the initial decisions after a tunnel fire.
4. UCS showed a good predictor for SJ, for all cooling methods, and the elastic modulus and ultrasound wave velocities also exhibited good correlations in water-cooled samples. S_{20} predictions were better than that for SJ for almost all predictors and cooling methods, except for correlations from UCS.
5. The obtained correlations facilitate quick evaluations of drillability based on basic geomechanical parameters as UCS and P- and S-velocities to support the Tres Ponts Tunnel excavations.
6. Correlations between most physical, mechanical, and drilling features in the thermally-treated Prada limestone are stronger than reported for intact rocks,

because thermal damage processes in the rock strongly affect all features in Prada limestone.

7. The dark fraction from Prada limestone discussed in Research Question Q2 is not included in this research.

The use of correlations would enable predicting the strength and deformational features from other parameters whose determination from non-destructive tests is quicker and easier. Additionally, correlations facilitate quick evaluations of drillability based on basic geomechanical parameters to support the Tres Ponts Tunnel excavations.

6.5. Future lines

To estimate the extent of the thermal damage in Prada limestone, it would be necessary to perform a numeric simulation of heat penetration through the lining and rock mass. To so do, it is critical to understand the variation in the thermal conductivity of thermally-treated Prada limestones. It has been long recognized that thermal conductivity varies inversely with temperature (Birch and Clark 1940), and this was observed specifically for low-porosity limestones by Zhang and Lv (2020). For sedimentary rocks the most controlling factor on thermal conductivity is porosity (Çanakci et al. 2007; Dalla Santa et al. 2020): as air has lower conductivity than minerals, an increase on porosity leads to a high proportion of air in the material and a decrease in thermal conductivity (Clauser and Huenges 1987). For these reasons, dramatic increases in porosity registered in Prada limestone must be connected with appreciable drops in thermal conductivity. A new line has been opened at the Department of Geological and Geotechnical Engineering of the Universitat Politècnica de València to explore this issue. Preliminary tests have been performed by means of a Modified Transient Plane Source (MTPS) as it provides a non-invasive, quick, and precise method when compared with other steady-state laboratory alternatives. Laboratory tests point to a decay in thermal conductivity in the thermally-treated samples. Results derived from this research have been presented to *ISRM International Symposium - EUROCK 2021* (article accepted).

A future line should be focused on the study of high-temperature in the shear strength of the rock matrix and joints. Moreover, it is of interest to study the stress-strain response from triaxial tests to simulate the stress levels really present in the inner contour of the tunnel, which would be more representative than those obtained from UCS tests. To cover the needs for both research lines, a coordinated project entitled 'Impact of wildfires on rockfall occurrence, prediction and mitigation (FireRock)' has been proposed to the Spanish Ministry of Science and Innovation.

In this PhD dissertation it has been stated that further investigations would be necessary to quantitatively relate pyrite content and initial micro-fissuring with the explosive potential of each sample. A research methodology has to be conceived considering that chemical and textural tests are destructive, and therefore incompatible with the need for intact samples to monitor explosive behaviour during heating process. It would be useful

to extend the study to other limestone formations bearing pyrites, such as the Herbers formation, which has also shown explosive behaviour in preliminary tests conducted at the Department of Geological and Geotechnical Engineering of the Universitat Politècnica de València. Numerical models would be of great help for fully understanding the mechanisms of growth and coalescence of pores and fissures due to the different mechanisms identified in this study such as the thermal oxidation of pyrites, anisotropic expansion of calcite, mismatch in thermal expansion coefficients between mineral particles, and quartz phase transition.

Finally, this PhD thesis is focused on the DRI because it is among the most used testing methods to determine the drillability characteristics of rock. However, it would be of great interest to explore the variation with temperature of other parameters to evaluate the drillability of rock, such as the Brazilian Tensile Strength, shore scleroscope hardness, axial and diametral point load strength, and the Cerchar abrasiveness index. This would enable advancing a future index to rate rock mass after exposure to high temperatures.

References

Aboutaleb S, Behnia M, Bagherpour R, Bluekian B (2018) Using non-destructive tests for estimating uniaxial compressive strength and static Young's modulus of carbonate rocks via some modeling techniques. Bull Eng Geol Environ 77:1717–1728. https://doi.org/10.1007/s10064-017-1043-2

Altindag R (2010) Assessment of some brittleness indexes in rock-drilling efficiency. Rock Mech Rock Eng 43:361–370. https://doi.org/10.1007/s00603-009-0057-x

Andriani GF, Germinario L (2014) Thermal decay of carbonate dimension stones: fabric, physical and mechanical changes. Environ Earth Sci 72:2523–2539. https://doi.org/10.1007/s12665-014-3160-6

Armaghani DJ, Tonnizam Mohamad E, Momeni E, et al (2016) Prediction of the strength and elasticity modulus of granite through an expert artificial neural network. Arab J Geosci 9:48. https://doi.org/10.1007/s12517-015-2057-3

Ataei M, KaKaie R, Ghavidel M, Saeidi O (2015) Drilling rate prediction of an open pit mine using the rock mass drillability index. Int J Rock Mech Min Sci 73:130–138. https://doi.org/10.1016/j.ijrmms.2014.08.006

ATSDR (1998) Public Health Statement - Sulfur Dioxide CAS#: 7446-09-5. ATSDR - Public Heal Statement

Aydin A (2014) Upgraded ISRM suggested method for determining sound velocity by ultrasonic pulse transmission technique. Rock Mech Rock Eng 47:255–259. https://doi.org/10.1007/s00603-013-0454-z

Bamonte P, Gambarova PG, Nafarieh A (2016) High-temperature behavior of structural and non-structural shotcretes. Cem Concr Compos 73:42–53. https://doi.org/10.1016/j.cemconcomp.2016.06.009

Baykasoğlu A, Güllü H, Çanakçi H, Özbakir L (2008) Prediction of compressive and tensile strength of limestone via genetic programming. Expert Syst Appl 35:111–123. https://doi.org/10.1016/j.eswa.2007.06.006

Beck K, Janvier-Badosa S, Brunetaud X, et al (2016) Non-destructive diagnosis by colorimetry of building stone subjected to high temperatures. Eur J Environ Civ Eng 20:643–655. https://doi.org/10.1080/19648189.2015.1035804

Behnia D, Ahangari K, Moeinossadat SR (2017) Modeling of shear wave velocity in limestone by soft computing methods. Int J Min Sci Technol 27:423–430. https://doi.org/10.1016/j.ijmst.2017.03.006

Belmokhtar M, Delage P, Ghabezloo S, Conil N (2017) Thermal Volume Changes and Creep in the Callovo-Oxfordian Claystone. Rock Mech Rock Eng 50:2297–2309. https://doi.org/10.1007/s00603-017-1238-7

Benavente D, Martinez-Martinez J, Cueto N, et al (2018) Impact of salt and frost weathering on the physical and durability properties of travertines and carbonate tufas used as building material. Environ Earth Sci 77:147. https://doi.org/10.1007/s12665-018-7339-0

Benavente D, Pla C (2018) Effect of pore structure and moisture content on gas diffusion and permeability in porous building stones. Mater Struct Constr 51:1–14. https://doi.org/10.1617/s11527-018-1153-8

Berner RA (1985) Sulphate reduction, organic matter decomposition and pyrite formation. Philos Trans R Soc London Ser A, Math Phys Sci 315:25–38. https://doi.org/10.1098/rsta.1985.0027

Berner RA (1982) Burial of organic carbon and pyrite sulfur in the modern ocean; its geochemical and environmental significance. Am J Sci 282:451–473. https://doi.org/10.2475/ajs.282.4.451

Berner RA (1970) Sedimentary pyrite formation. Am J Sci 268:1–23. https://doi.org/10.2475/ajs.268.1.1

Birch AF, Clark H (1940) The thermal conductivity of rocks and its dependence upon temperature and composition. Am J Sci 238:529–558. https://doi.org/10.2475/ajs.238.8.529

Boyle J (2004) A comparison of two methods for estimating the organic matter content of sediments. J Paleolimnol 31:125–127. https://doi.org/10.1023/B:JOPL.0000013354.67645.df

Brotóns V, Tomás R, Ivorra S, Alarcón JC (2013) Temperature influence on the physical and mechanical properties of a porous rock: San Julian's calcarenite. Eng Geol 167:117–127. https://doi.org/10.1016/j.enggeo.2013.10.012

Bruland A (2000) Hard Rock Tunnel Boring Vol. 8 - Drillability - Test Methods. Doctoral thesis. Norwegian University of Science and Technology (NTNU Trondheim)

Çanakci H, Demirboğa R, Burhan Karakoç M, Şirin O (2007) Thermal conductivity of limestone from Gaziantep (Turkey). Build Environ 42:1777–1782. https://doi.org/10.1016/j.buildenv.2006.01.011

Capik M, Yilmaz AO, Yasar S (2017) Relationships between the drilling rate index and physicomechanical rock properties. Bull Eng Geol Environ 76:253–261. https://doi.org/10.1007/s10064-016-0991-2

CETU (2005) Comportement au feu des tunnels routiers. Ministère de l'Équipement, des Transports, de l'Aménagement du territoire, du Tourisme et de la Mer. Direction des routes, France

Cevik A, Sezer EA, Cabalar AF, Gokceoglu C (2011) Modeling of the uniaxial compressive strength of some clay-bearing rocks using neural network. Appl Soft Comput 11:2587–2594. https://doi.org/10.1016/j.asoc.2010.10.008

Chen L, He J, Chao J, Qin B (2009) Swelling and breaking characteristics of limestone under high temperatures. Min Sci Technol 19:503–507. https://doi.org/10.1016/S1674-5264(09)60094-6

Cheng H, Liu Q, Zhang S, et al (2014) Evolved gas analysis of coal-derived pyrite/marcasite. J Therm Anal Calorim 116:887–894. https://doi.org/10.1007/s10973-013-3595-0

CIE (1977) CIE Recommendations on Uniform Color Spaces, Color-Difference Equations, and Metric Color Terms. Color Res Appl 2:5–6. https://doi.org/doi:10.1002/j.1520-6378.1977.tb00102.x

Clauser C, Huenges E (1987) Thermal Conductivity of Rocks and Minerals. In: Methods in Experimental Physics. pp 271–302

Crosby ZK, Gullett PM, Akers SA, Graham SS (2018) Characterization of the mechanical behavior of salem limestone containing thermally-induced microcracks. Int J Rock Mech Min Sci 101:54–62. https://doi.org/10.1016/j.ijrmms.2017.11.002

Currie JA (1960) Gaseous diffusion in porous media Part 1. - A non-steady state method. Br J Appl Phys 11:314–317. https://doi.org/10.1088/0508-3443/11/8/302

Cuypers C, Grotenhuis T, Nierop KGJ, et al (2002) Amorphous and condensed organic matter domains: the effect of persulfate oxidation on the composition of soil/sediment organic matter. Chemosphere 48:919–931. https://doi.org/10.1016/S0045-6535(02)00123-6

Dahl F, Bruland A, Jakobsen PD, et al (2012) Classifications of properties influencing the drillability of rocks, based on the NTNU/SINTEF test method. Tunn Undergr Sp Technol 28:150–158. https://doi.org/10.1016/j.tust.2011.10.006

Dahl F, Grøv E, Bruland A, Nilsen B (2010) Trademarking the NTNU / SINTEF drillability test indices. Tunnels Tunn Int June:44–46

Dalla Santa G, Galgaro A, Sassi R, et al (2020) An updated ground thermal properties database for GSHP applications. Geothermics 85:101758. https://doi.org/10.1016/j.geothermics.2019.101758

Dehghan S, Sattari G, Chehreh Chelgani S, Aliabadi M (2010) Prediction of uniaxial compressive strength and modulus of elasticity for Travertine samples using regression and artificial neural networks. Min Sci Technol 20:41–46. https://doi.org/10.1016/S1674-5264(09)60158-7

Delage P, Sultan N, Cui YJ (2000) On the thermal consolidation of Boom clay. Can Geotech J 37:343–354. https://doi.org/10.1139/cgj-37-2-343

Fairhurst C, Hudson JA (1987) International society for rock mechanics commission on testing methods. Int J Rock Mech Min Sci Geomech Abstr 24:53. https://doi.org/10.1016/0148-9062(87)91231-9

Ferreira APG, Farage MCR, Barbosa FS, et al (2014) Thermo-hydric analysis of concrete-rock bilayers under fire conditions. Eng Struct 59:765–775. https://doi.org/10.1016/j.engstruct.2013.11.033

Ferrero AM, Marini P (2001) Technical note: Experimental studies on the mechanical behaviour of two thermal cracked marbles. Rock Mech Rock Eng 34:57–66. https://doi.org/10.1007/s006030170026

Fioretti G, Mazzoleni P, Acquafredda P, Andriani GF (2018) On the technical properties of the Carovigno stone from Apulia (Italy): physical characterization and decay effects by means of experimental ageing tests. Environ Earth Sci 77:17. https://doi.org/10.1007/s12665-017-7201-9

Franklin J (1979) Suggested methods for determining water content, porosity, density absorption and related properties and swelling and slake- durability index properties. Int J Rock Mech Min Sci 16:141–156

Franzoni E, Sassoni E, Scherer GW, Naidu S (2013) Artificial weathering of stone by heating. J Cult Herit 14:e85–e93. https://doi.org/10.1016/j.culher.2012.11.026

Galbács G, Kántor T, Moens L, Dams R (1998) Mass spectrometric studies of thermal decomposition products of reference materials for use in solid sampling atomic spectrometry. Spectrochim Acta Part B At Spectrosc 53:1335–1346. https://doi.org/10.1016/S0584-8547(98)00177-3

García Senz J (2002) Cuencas extensivas del cretácico inferior en los Pirineos centrales, formación y subsecuente inversión. Universitat de Barcelona

Gautam PK, Verma AK, Maheshwar S, Singh TN (2016) Thermomechanical Analysis of Different Types of Sandstone at Elevated Temperature. Rock Mech Rock Eng 49:1985–1993. https://doi.org/10.1007/s00603-015-0797-8

Gazulla MF, Gómez MP, Orduña M, et al (2009) Sulfur Determination in Geological Samples Based on Coupled Analytical Techniques: Electric Furnace-IC and TGA-EGA. Geostand Geoanalytical Res 33:71–84. https://doi.org/10.1111/j.1751-908X.2008.00902.x

Gens A, Vaunat J, Garitte B, Wileveau Y (2011) In situ behaviour of a stiff layered clay subject to thermal loading: observations and interpretation. In: Stiff Sedimentary Clays. Thomas Telford Ltd, London, pp 123–144

Glover PWJ, Baud P, Darot M, et al (1995) α/β phase transition in quartz monitored using acoustic emissions. Geophys J Int 120:775–782. https://doi.org/10.1111/j.1365-246X.1995.tb01852.x

Gokceoglu C, Zorlu K (2004) A fuzzy model to predict the uniaxial compressive strength and the modulus of elasticity of a problematic rock. Eng Appl Artif Intell 17:61–72. https://doi.org/10.1016/j.engappai.2003.11.006

Gómez-Tena MP, Machí C, Gilabert J, Zumaquero E (2014) Methodologies for the detection and quantification of pyrite in clay raw materials. Congr Mund La Calid Del Azulejo Y Del Paviment Ceram Qualicer

González-Gómez WS, Quintana P, May-Pat A, et al (2015) Thermal effects on the physical properties of limestones from the Yucatan Peninsula. Int J Rock Mech Min Sci 75:182–189. https://doi.org/10.1016/j.ijrmms.2014.12.010

Griffits AA (1920) The phenomena of rupture and flow in solids. Masinovedenie 221:163–195. https://doi.org/10.1098/rsta.1921.0006

Hansen JP, Jensen LS, Wedel S, Dam-Johansen K (2003) Decomposition and oxidation of pyrite in a fixed-bed reactor. Ind Eng Chem Res 42:4290–4295. https://doi.org/10.1021/ie030195u

Hartman HL (1959) Basic Studies of Percussion Drilling. Min Eng 11:68–75

Heuze FE (1983) High-temperature mechanical, physical and Thermal properties of granitic rocks— A review. Int J Rock Mech Min Sci Geomech Abstr 20:3–10. https://doi.org/10.1016/0148-9062(83)91609-1

Hong Y, Fegley B (1997) The kinetics and mechanism of pyrite thermal decomposition. Berichte der Bunsengesellschaft für Phys Chemie 101:1870–1881. https://doi.org/10.1002/bbpc.19971011212

Hoseinie SH, Ataei M, Osanloo M (2009) A new classification system for evaluating rock penetrability. Int J Rock Mech Min Sci 46:1329–1340. https://doi.org/10.1016/j.ijrmms.2009.07.002

Hu G, Dam-Johansen K, Wedel S, Hansen JP (2006) Decomposition and oxidation of pyrite. Prog Energy Combust Sci 32:295–314. https://doi.org/10.1016/j.pecs.2005.11.004

Ingason H (2012) Fire dynamics in tunnels. In: Handbook of Tunnel Fire Safety. ICE Publishing, pp 273–307

ITA (2004) Guidelines for structural fire resistance for road tunnels

Jamali S, Wittig V, Börner J, et al (2019) Application of high powered Laser Technology to alter hard rock properties towards lower strength materials for more efficient drilling, mining, and Geothermal Energy production. Geomech Energy Environ 20:100112. https://doi.org/10.1016/j.gete.2019.01.001

Jamshidi E, Arabjamaloei R, Hashemi A, et al (2013) Real-time Estimation of Elastic Properties of Formation Rocks Based on Drilling Data by Using an Artificial Neural Network. Energy Sources, Part A Recover Util Environ Eff 35:337–351. https://doi.org/10.1080/15567036.2010.495971

Kahraman S (1999) Rotary and percussive drilling prediction using regression analysis. Int J Rock Mech Min Sci 36:981–989. https://doi.org/10.1016/S0148-9062(99)00050-9

Kahraman S, Bilgin N, Feridunoglu C (2003) Dominant rock properties affecting the penetration rate of percussive drills. Int J Rock Mech Min Sci 40:711–723. https://doi.org/10.1016/S1365-1609(03)00063-7

Keski-Rahkonen O, Holmlund C, Loikkanen P, et al (1986) Two full scale pilot fire experiments in a tunnel, Research R. Espoo: VTT Technical Research Centre of Finland. Valtion teknillinen tutkimuskeskus. Tutkimuksia

Kim K, Kemeny J, Nickerson M (2014) Effect of Rapid Thermal Cooling on Mechanical Rock Properties. Rock Mech Rock Eng 47:2005–2019. https://doi.org/10.1007/s00603-013-0523-3

Koca MY, Ozden G, Yavuz AB, et al (2006) Changes in the engineering properties of marble in fire-exposed columns. Int J Rock Mech Min Sci 43:520–530. https://doi.org/10.1016/j.ijrmms.2005.09.007

Kubik M (2006) The Future of Geothermal Energy. Massachusetts Institute of Technology, Idaho

Kumar P, Imam B (2013) Footprints of air pollution and changing environment on the sustainability of built infrastructure. Sci Total Environ 444:85–101. https://doi.org/10.1016/j.scitotenv.2012.11.056

Kumari WGP, Ranjith PG, Perera MSA, Chen BK (2018) Experimental investigation of quenching effect on mechanical, microstructural and flow characteristics of reservoir rocks: Thermal stimulation method for geothermal energy extraction. J Pet Sci Eng 162:419–433. https://doi.org/10.1016/j.petrol.2017.12.033

Leitner A (2001) The fire catastrophe in the Tauern Tunnel: experience and conclusions for the Austrian guidelines. Tunn Undergr Sp Technol 16:217–223. https://doi.org/10.1016/S0886-7798(01)00042-6

Li Z, Wong LNY, Teh CI (2017) Low cost colorimetry for assessment of fire damage in rock. Eng Geol 228:50–60. https://doi.org/10.1016/j.enggeo.2017.07.006

Lion M, Skoczylas F, Ledésert B (2005) Effects of heating on the hydraulic and poroelastic properties of bourgogne limestone. Int J Rock Mech Min Sci 42:508–520. https://doi.org/10.1016/j.ijrmms.2005.01.005

Liu S, Xu J (2013) Study on dynamic characteristics of marble under impact loading and high temperature. Int J Rock Mech Min Sci 62:51–58. https://doi.org/10.1016/j.ijrmms.2013.03.014

Lv W, Yu D, Wu J, et al (2015) The chemical role of CO2 in pyrite thermal decomposition. Proc Combust Inst 35:3637–3644. https://doi.org/10.1016/j.proci.2014.06.066

Malaga-Starzec K, Åkesson U, Lindqvist JE, Schouenborg B (2006) Microscopic and macroscopic characterization of the porosity of marble as a function of temperature and impregnation. Constr Build Mater 20:939–947. https://doi.org/10.1016/j.conbuildmat.2005.06.016

Mallet C, Fortin J, Guéguen Y, Bouyer F (2014) Evolution of the crack network in glass samples submitted to brittle creep conditions. Int J Fract 190:111–124. https://doi.org/10.1007/s10704-014-9978-9

Mao X-B, Zhang L, Li T, Liu H (2009) Properties of failure mode and thermal damage for limestone at high temperature. Min Sci Technol 19:290–294. https://doi.org/10.1016/S1674-5264(09)60054-5

Martínez-Ibáñez V, Benavente D, Hidalgo Signes C, et al (2021a) Temperature-Induced Explosive Behaviour and Thermo-Chemical Damage on Pyrite-Bearing Limestones: Causes and Mechanisms. Rock Mech Rock Eng 54:219–234. https://doi.org/10.1007/s00603-020-02278-x

Martínez-Ibáñez V, Garrido ME, Hidalgo Signes C, Tomás R (2021b) Micro and macro-structural effects of high temperatures in Prada limestone: Key factors for future fire-intervention protocols in Tres Ponts Tunnel (Spain). Constr Build Mater 286:122960. https://doi.org/10.1016/j.conbuildmat.2021.122960

Martínez-Ibáñez V, Garrido ME, Signes CH, Tomás R (2020) Indirect Evaluation of Strength for Limestones Subjected to High Temperatures. In: ISRM International Symposium - EUROCK 2020. Trondheim, Norway

Martínez-Martínez J, Benavente D, Gomez-Heras M, et al (2013) Non-linear decay of building stones during freeze–thaw weathering processes. Constr Build Mater 38:443–454. https://doi.org/10.1016/j.conbuildmat.2012.07.059

Martinho E, Dionísio A (2020) Assessment Techniques for Studying the Effects of Fire on Stone Materials: A Literature Review. Int J Archit Herit 14:275–299. https://doi.org/10.1080/15583058.2018.1535008

Meng Q-B, Wang C-K, Liu J-F, et al (2020) Physical and micro-structural characteristics of limestone after high temperature exposure. Bull Eng Geol Environ 79:1259–1274. https://doi.org/10.1007/s10064-019-01620-0

Nasseri MHB, Schubnel A, Young RP (2007) Coupled evolutions of fracture toughness and elastic wave velocities at high crack density in thermally treated Westerly granite. Int J Rock Mech Min Sci 44:601–616. https://doi.org/10.1016/j.ijrmms.2006.09.008

Nordlund E, Zhang P, Dineva S, et al (2014) Impact of fire on the stability of hard rock tunnels in Sweden. Stockholm

Özfırat MK, Yenice H, Şimşir F, Yaralı O (2016) A new approach to rock brittleness and its usability at prediction of drillability. J African Earth Sci 119:94–101. https://doi.org/10.1016/j.jafrearsci.2016.03.017

Ozguven A, Ozcelik Y (2013) Investigation of some property changes of natural building stones exposed to fire and high heat. Constr Build Mater 38:813–821. https://doi.org/10.1016/j.conbuildmat.2012.09.072

Pei L, Blöcher G, Milsch H, et al (2018) Thermo-mechanical Properties of Upper Jurassic (Malm) Carbonate Rock Under Drained Conditions. Rock Mech Rock Eng 51:23–45. https://doi.org/10.1007/s00603-017-1313-0

PIARC (2016) Experience with significant incidents in road tunnels

PIARC (1999) Fire and smoke control in road tunnels

Pospíšil J, Hrdý J, Hrdý J (2007) Basic methods for measuring the reflectance color of iron oxides. Optik (Stuttg) 118:278–288. https://doi.org/10.1016/j.ijleo.2006.03.020

Prochazka PP, Peskova S (2008) The Influence of Elevated Temperatures on Tunnel Linings. In: Proceedings of the Ninth International Conference on Computational Structures Technology. Civil-Comp Press

Rabat, Tomás R, Cano M (2020a) Evaluation of mechanical weakening of calcarenite building stones due to environmental relative humidity using the vapour equilibrium technique. Eng Geol 278:105849. https://doi.org/10.1016/j.enggeo.2020.105849

Rabat, Tomás R, Cano M, Miranda T (2020b) Impact of water on peak and residual shear strength parameters and triaxial deformability of high-porosity building calcarenite stones: Interconnection with their physical and petrological characteristics. Constr Build Mater 262:120789. https://doi.org/10.1016/j.conbuildmat.2020.120789

Ranjith PG, Viete DR, Chen BJ, Perera MSA (2012) Transformation plasticity and the effect of temperature on the mechanical behaviour of Hawkesbury sandstone at atmospheric pressure. Eng Geol. https://doi.org/10.1016/j.enggeo.2012.09.007

Rossi E, Jamali S, Saar MO, Rudolf von Rohr P (2020a) Field test of a Combined Thermo-Mechanical Drilling technology. ModeI: Thermal spallation drilling. J Pet Sci Eng 190:107005. https://doi.org/10.1016/j.petrol.2020.107005

Rossi E, Jamali S, Schwarz D, et al (2020b) Field test of a Combined Thermo-Mechanical Drilling technology. Mode II: Flame-assisted rotary drilling. J Pet Sci Eng 190:106880. https://doi.org/10.1016/j.petrol.2019.106880

Rossi E, Jamali S, Wittig V, et al (2020c) A combined thermo-mechanical drilling technology for deep geothermal and hard rock reservoirs. Geothermics 85:101771. https://doi.org/10.1016/j.geothermics.2019.101771

Rossi E, Kant MA, Madonna C, et al (2018) The Effects of High Heating Rate and High Temperature on the Rock Strength: Feasibility Study of a Thermally Assisted Drilling Method. Rock Mech Rock Eng 51:2957–2964. https://doi.org/10.1007/s00603-018-1507-0

Rossi E, Saar MO, Rudolf von Rohr P (2020d) The influence of thermal treatment on rock–bit interaction: a study of a combined thermo–mechanical drilling (CTMD) concept. Geotherm Energy 8:16. https://doi.org/10.1186/s40517-020-00171-y

Sabatakakis N, Koukis G, Tsiambaos G, Papanakli S (2008) Index properties and strength variation controlled by microstructure for sedimentary rocks. Eng Geol 97:80–90. https://doi.org/10.1016/j.enggeo.2007.12.004

Saeidi O, Torabi SR, Ataei M, Rostami J (2014) A stochastic penetration rate model for rotary drilling in surface mines. Int J Rock Mech Min Sci 68:55–65. https://doi.org/10.1016/j.ijrmms.2014.02.007

Sawlowicz Z (2000) Framboids: From their origin to application. Pr Mineral 88:1–58

Seehra MS, Jagadeesh MS (1981) A comparative study of the properties of marcasite and pyrite. AIP Conf Proc 70:448–448. https://doi.org/10.1063/1.32915

Sengun N (2014) Influence of thermal damage on the physical and mechanical properties of carbonate rocks. Arab J Geosci 7:5543–5551. https://doi.org/10.1007/s12517-013-1177-x

Sharma LK, Vishal V, Singh TN (2017) Developing novel models using neural networks and fuzzy systems for the prediction of strength of rocks from key geomechanical properties. Measurement 102:158–169. https://doi.org/10.1016/j.measurement.2017.01.043

Shawar L, Halevy I, Said-Ahmad W, et al (2018) Dynamics of pyrite formation and organic matter sulfurization in organic-rich carbonate sediments. Geochim Cosmochim Acta 241:219–239. https://doi.org/10.1016/j.gca.2018.08.048

Sievers H (1950) Die Bestimmung des Bohrwiderstandes von Gesteinen. In: Glückauf. Glückauf G.M.B.H, Essen, pp 776–784

Sigfusson B, Uihlein A (2015) 2014 JRC Geothermal Energy Status Report. European Union, Petten (The Netherlands)

Singh R, Umrao RK, Ahmad M, et al (2017) Prediction of geomechanical parameters using soft computing and multiple regression approach. Measurement 99:108–119. https://doi.org/10.1016/j.measurement.2016.12.023

Singh R, Vishal V, Singh TN, Ranjith PG (2013) A comparative study of generalized regression neural network approach and adaptive neuro-fuzzy inference systems for prediction of unconfined compressive strength of rocks. Neural Comput Appl 23:499–506. https://doi.org/10.1007/s00521-012-0944-z

Singh V., Singh D, Singh T. (2001) Prediction of strength properties of some schistose rocks from petrographic properties using artificial neural networks. Int J Rock Mech Min Sci 38:269–284. https://doi.org/10.1016/S1365-1609(00)00078-2

Sippel J, Siegesmund S, Weiss T, et al (2007) Decay of natural stones caused by fire damage. Geol Soc London, Spec Publ 271:139–151. https://doi.org/10.1144/GSL.SP.2007.271.01.15

Sirdesai NN, Singh A, Sharma LK, et al (2017) Development of novel methods to predict the strength properties of thermally treated sandstone using statistical and soft-computing approach. Neural Comput Appl 31:1–27. https://doi.org/10.1007/s00521-017-3233-z

Sirdesai NN, Singh A, Sharma LK, et al (2018) Determination of thermal damage in rock specimen using intelligent techniques. Eng Geol 239:179–194. https://doi.org/10.1016/j.enggeo.2018.03.027

Smith AG, Pells PJ (2009) Discussion of the paper "Impact of fire on Tunnels in Hawkesbury Sandstone" by Smith and Pells [Tunnelling and Underground Space Technology 23 (2008) 65-74]. Tunn Undergr Sp Technol 24:112–114. https://doi.org/10.1016/j.tust.2008.05.001

Smith AG, Pells PJN (2008) Impact of fire on tunnels in Hawkesbury sandstone. Tunn Undergr Sp Technol 23:65–74. https://doi.org/10.1016/j.tust.2006.11.003

Smith BJ, Gomez-Heras M, McCabe S (2008) Understanding the decay of stone-built cultural heritage. Prog Phys Geogr Earth Environ 32:439–461. https://doi.org/10.1177/0309133308098119

Sonmez H, Gokceoglu C, Medley EW, et al (2006) Estimating the uniaxial compressive strength of a volcanic bimrock. Int J Rock Mech Min Sci 43:554–561. https://doi.org/10.1016/j.ijrmms.2005.09.014

Sonmez H, Tuncay E, Gokceoglu C (2004) Models to predict the uniaxial compressive strength and the modulus of elasticity for Ankara Agglomerate. Int J Rock Mech Min Sci 41:717–729. https://doi.org/10.1016/j.ijrmms.2004.01.011

Su O, Sakız U, Akçın NA (2016) Effect of elastic and strength properties of rocks during blasthole drilling. ISRM Int Symp - EUROCK 2016 217–221. https://doi.org/10.1201/9781315388502-36

Sultan N, Delage P, Cui YJ (2002) Temperature effects on the volume change behaviour of Boom clay. Eng Geol 64:135–145. https://doi.org/10.1016/S0013-7952(01)00143-0

UNE-EN-103204 U-E (2019) Determinación del contenido de materia orgánica oxidable de un suelo por el método del permanganato de potasio

Van der Molen I (1981) The shift of the α-β transition temperature of quartz associated with the thermal expansion of granite at high pressure. Tectonophysics 73:323–342. https://doi.org/10.1016/0040-1951(81)90221-3

Verron H, Sterpenich J, Bonnet J, et al (2019) Experimental Study of Pyrite Oxidation at 100 °C: Implications for Deep Geological Radwaste Repository in Claystone. Minerals 9:427. https://doi.org/10.3390/min9070427

Villarraga CJ, Gasc-Barbier M, Vaunat J, Darrozes J (2018) The effect of thermal cycles on limestone mechanical degradation. Int J Rock Mech Min Sci 109:115–123. https://doi.org/10.1016/j.ijrmms.2018.06.017

von Matern N, Hjelmér A (1943) Försök med pågrus ("Tests with Chippings"). Statens väginstitut, Stockholm

Xu ZX, Wang Q, Fu XQ (2015) Thermal stability and mechanism of decomposition of emulsion explosives in the presence of pyrite. J Hazard Mater 300:702–710. https://doi.org/10.1016/j.jhazmat.2015.07.069

Yagiz S, Sezer EA, Gokceoglu C (2012) Artificial neural networks and nonlinear regression techniques to assess the influence of slake durability cycles on the prediction of uniaxial compressive strength and modulus of elasticity for carbonate rocks. Int J Numer Anal Methods Geomech 36:1636–1650. https://doi.org/10.1002/nag.1066

Yang J, Fu L-Y, Zhang W, Wang Z (2019) Mechanical property and thermal damage factor of limestone at high temperature. Int J Rock Mech Min Sci 117:11–19. https://doi.org/10.1016/j.ijrmms.2019.03.012

Yarali O, Kahraman S (2011) The drillability assessment of rocks using the different brittleness values. Tunn Undergr Sp Technol 26:406–414. https://doi.org/10.1016/j.tust.2010.11.013

Yarali O, Soyer E (2011) The effect of mechanical rock properties and brittleness on drillability. Sci Res Essays 6:1077–1088. https://doi.org/10.5897/SRE10.1004

Yarali O, Soyer E (2013) Assessment of relationships between drilling rate index and mechanical properties of rocks. Tunn Undergr Sp Technol 33:46–53. https://doi.org/10.1016/j.tust.2012.08.010

Yasar E, Erdogan Y (2004) Correlating sound velocity with the density, compressive strength and Young's modulus of carbonate rocks. Int J Rock Mech Min Sci 41:871–875. https://doi.org/10.1016/j.ijrmms.2004.01.012

Yaşar E, Ranjith PG, Viete DR (2011) An experimental investigation into the drilling and physico-mechanical properties of a rock-like brittle material. J Pet Sci Eng 76:185–193. https://doi.org/10.1016/j.petrol.2011.01.011

Yavuz H, Demirdag S, Caran S (2010) Thermal effect on the physical properties of carbonate rocks. Int J Rock Mech Min Sci 47:94–103. https://doi.org/10.1016/j.ijrmms.2009.09.014

Yenice H (2019) Determination of Drilling Rate Index Based on Rock Strength Using Regression Analysis. An Acad Bras Cienc 91:1–10. https://doi.org/10.1590/0001-3765201920181095

Yesiloglu-Gultekin N, Gokceoglu C, Sezer EA (2013) Prediction of uniaxial compressive strength of granitic rocks by various nonlinear tools and comparison of their performances. Int J Rock Mech Min Sci 62:113–122. https://doi.org/10.1016/j.ijrmms.2013.05.005

Yetkin ME, Özfırat MK, Yenice H, et al (2016) Examining the relation between rock mass cuttability index and rock drilling properties. J African Earth Sci 124:151–158. https://doi.org/10.1016/j.jafrearsci.2016.09.025

Zhang C-L, Conil N, Armand G (2017a) Thermal effects on clay rocks for deep disposal of high-level radioactive waste. J Rock Mech Geotech Eng 9:463–478. https://doi.org/10.1016/j.jrmge.2016.08.006

Zhang F, Zhao J, Hu D, et al (2018) Laboratory Investigation on Physical and Mechanical Properties of Granite After Heating and Water-Cooling Treatment. Rock Mech Rock Eng 51:677–694. https://doi.org/10.1007/s00603-017-1350-8

Zhang W, Lv C (2020) Effects of mineral content on limestone properties with exposure to different temperatures. J Pet Sci Eng 188:106941. https://doi.org/10.1016/j.petrol.2020.106941

Zhang W, Sun Q, Zhu S, Wang B (2017b) Experimental study on mechanical and porous characteristics of limestone affected by high temperature. Appl Therm Eng 110:356–362. https://doi.org/10.1016/j.applthermaleng.2016.08.194

Zhang X, Kou J, Sun C (2019) A comparative study of the thermal decomposition of pyrite under microwave and conventional heating with different temperatures. J Anal Appl Pyrolysis 138:41–53. https://doi.org/10.1016/j.jaap.2018.12.002

Zorlu K, Gokceoglu C, Ocakoglu F, et al (2008) Prediction of uniaxial compressive strength of sandstones using petrography-based models. Eng Geol 96:141–158. https://doi.org/10.1016/j.enggeo.2007.10.009